Thermodynamic, dynamic and structural properties of liquid and supercritical matter

by

Dmitry Bolmatov

A report presented for the examination

for the transfer of status to the degree of

Doctor of Philosophy of the University of London

Thesis Supervisor

Dr Konstantin Trachenko

Centre for Condensed Matter and Materials Physics

School of Physics and Astronomy

Queen Mary, University of London

Mile End Road, London, E1 4NS

United Kingdom

August 2013

Abstract

Among three basic states of matter (solid, liquid, gas), liquids are least understood from the theoretical point of view. The perceived difficulty is that interactions in a liquid are both strong and system-specific, implying that the energy strongly depends on the liquid type and that, therefore, liquid energy can not be calculated in general form. In this thesis, a phonon theory of liquids is developed where this problem is avoided. Central to the thesis is a development an alternative to calculating liquid energy and heat capacity. The proposed phonon theory of liquids covers both classical and quantum regimes and accounts for the contribution of anharmonicity and thermal expansion to liquid energy and heat capacity. Within the framework of the phonon theory of liquids a good agreement of calculated and experimental heat capacity of liquids, including helium, noble, metallic, molecular and hydrogen-bonded network liquids in a wide range of temperature and pressure is demonstrated.

It was also found that in the very wide pressure range 5 MPa-500 MPa liquid helium near melting temperature is both solid-like and quantum.

The thermodynamic properties of the supercritical state are studied, which lead to discovery that specific heat shows a crossover between two different dynamic regimes of the low-temperature rigid liquid and high-temperature non-rigid supercritical fluid. A theory of heat capacity above the crossover is formulated, and good agreement between calculated and experimental data for rare-gas supercritical liquids is obtained. The relationship between power exponents of heat capacity and viscosity in the supercritical region is derived. The thermodynamic properties are explained by the temperature behaviour of the maximal length of the longitudinal phonons that can exist in the supercritical system and that is not sensitive to system details.

We also introduce a new idea that enables a unified description of all three states of matter. A generic form of an interacting phonon Hamiltonian with ground state configurations minimising the potential is introduced. Symmetry breaking leads to emergence of energy gaps of shear excitations as a consequence of the Goldstone theorem, and readily results in the emergence of energy spectra of solid, liquid and gas phases.

Acknowledgements

This Ph.D. thesis has greatly benefited from comments and suggestions of several people. First of all, I would like to thank my supervisor, Dr. Kostya Trachenko, whose professional knowledge and willingness to help were supportive during the process of making this scientific research. It has been an honor to be his first Ph.D. student. Kostya has given me the freedom to pursue various projects without objection.

I also acknowledge my fellow colleagues at Queen Mary and other institutions for their inspiration and the lively discussions we had, in particular: Vadim Brazhkin, Andrei Sapelkin, Martin Dove, Ben Still, Chung-Yu Mou, Sergey Bastrukov, Neil Ashcroft, Roald Hoffmann, Ben Widom, Oleg Teryaev, Hsiu-Hau Lin, Daw-Wei Wang, Sanjaye Ramgoolam, David Dunstan, Alan Drew, Bill Gillin, Bill Spence, Yu. D. Fomin, V. N. Ryzhov, Dominic Carter.

Special thanks to Garry Efimov and Vladimir S. Melezhik for their support and guidance during my first steps in theoretical physics.

Finally, my warmest thanks goes to my beloved parents for their exceptional support and excellent assistance during my whole life.

Declaration

I hereby declare that this thesis is my own work and effort and is result of collaboration with Kostya Trachenko, Vadim Brazhkin, Yu. D. Fomin, V. N. Ryzhov and Edvard Musaev. The material presented further describes results of publications and unpublished papers. Where other sources of information have been used, they have been acknowledged. This thesis has not been submitted previously in whole or in part for a degree examination at this or any other institution.

Contents

CHAPTER 1

INTRODUCTION

1.1 Invitation to the Topic

In an amusing story about student teaching experience, Granato recalls his persistent fear of a potential student question about liquid specific heat. Noting that such a question was never asked over many years by a total of 10,000 students, Granato observes that this possibly reflects an important deficiency of our standard teaching method that fails to mention unsolved problems in physics, both in lectures and textbooks [1].

The classical description of the structure and dynamics of liquids, in comparison with the solid and gas phases, is relatively incomplete. The fundamental difficulty is that the liquid state lacks any idealized abstraction such as the ideal gas or perfect solid, which can later form a basis for theoretical refinement. Unlike the solid or the gas where either configurational or kinetic processes dominate the description, in the liquid state we are confronted with the full and general statistical problem in which there are both dynamical and configurational contributions to the total energy. Approximation, if not judicious, will lead to a description of either high-density gases or disordered high-temperature solids. Indeed, at one time considerable effort was devoted to the representation of liquids in these terms [2], but it is now known that fluids do not have a simple interpolated status between gas and solid, although features of both the adjacent phases can be detected. It appears that a direct statistical mechanical approach is necessary, and this forms the foundation of the modern theory of liquids to be developed in this thesis.

The ultimate objective of a statistical description of matter is to relate the macroscopic observables to the details of the structure and intermolecular potential operating between particles in the assembly. Whilst we have no satisfactory liquid theory to form a basis model, assemblies of *idealized particles* interacting through some simple model interaction have an important theoretical status, even if the results are not immediately comparable to real physical system. The simple forms of interaction generally considered are hard spheres, Lennard-Jones, etc., and whilst no more than caricatures of realistic interactions they do allow a welcome simplification in analysis. The advent of powerful computers is complementary to experiments: it is now perfectly feasible to

simulate system of ~ 100000 particles interacting through these idealized interactions. Indeed, the computer schemes have now adopted such a central role that they represent a buffer between theory and experiment, and current theoretical developments are about equally preoccupied with both simulated and real data. In many respects the simulations are preferable in that the wealth of microscopic data relating to molecular trajectories and distributions is far greater and more direct than that obtainable by conventional experiment.

1.2 Solids, Liquids and Gases: Distinctions and Similarities

The ability of liquids and solids to form a free bounding surface obviously distinguishes them from gases which will diffusively fill the accessibly volume. Indeed, the coefficients of self-diffusion of liquids ($\sim 10^{-5}$ cm^2 s^{-1}) and solids ($\sim 10^{-9}$ cm^2 s^{-1}) are orders of magnitude below that of the gas. On the other hand, the viscosities of gases and liquids are some thirteen orders of magnitude lower than those of solids, and this we may easily understand in terms of the molecular process of momentum exchange. Flow in a solid consists primarily in rupturing of bonds and propagation of dislocations and imperfections. The resistance of a solid to a sustained shear stress is therefore understood in configurational terms and, as usual in a solid, potential contributions dominate. In a liquid there is both molecular transport and configurational readjustment and the flow process is characterized by both configurational and kinetic processes, whilst in a gas the flow is understood purely in terms of kinetic transport. It is in this limited sense that liquids have an interpolated status between gas and solid.

Whilst a qualitative description enables us to characterize some of the features of a solid, liquid and gaseous phases, what it does not tell us is why three states of matter exist, and why indeed we do not have one single phase whose features are simply characterized by the temperature. The essential feature we also need to mention here is the *geometric* one concerning the packing of particles–the above description appealed only to the dynamic features of the assembly–known to be independent of structure. Geometric considerations are largely irrelevant at gas densities, though the finite size of the molecular core does modify the ideal gas law as, for example, in Van der Waals' equation of state. At liquid and solid densities geometric packing of spheres and the entropy differences between ordered and disordered arrangements intervenes to effect a lowering of the free energy through a modification of molecular order. This is a purely thermodynamic argument, and takes no account of molecular processes involved in the phase transition.

1.3 Theories of the Liquid State

There is no theory of the liquid state based on a simple model, similar to theories of solid and gaseous states are known. Theories of liquid have been discussed at different levels. Many properties of a liquid may be calculated from the hypothesis that the interatomic forces and energies in a classical liquid are dominated by the sum of pair interactions. That is if three or more atoms are close together in a liquid, the energy of the system is the sum of the energies obtained by taking the atoms in pairs. Thus "three-body" or higher-order forces can be neglected and such a "pair theory" of the liquid state, expressions for the equation of state, for instance, can be readily obtained in perturbative approaches but not for strong interactions [3].

A great deal of work has been published on calculations of the quantities that appear in these equations and from which numerical (P, V, T) values are obtained to compare with experiment. Sometimes in the literature, the phrase "theory of liquids" is used solely to describe a particular version of such calculations, and in this sense there are many theories of liquids. Thus the "pair theory of liquids" means the attempt to derive expressions for all liquid properties (equilibrium, transport, macroscopic and microscopic) on the basis of the pair approximation. There are substantial difficulties in using these expressions to obtain accurate numerical predictions of almost all properties, so that the pair theory has not yet been adequately tested. A full test of the pair theory should indicate where it is able to predict experimental data adequately and where it fails to do so. In some cases (the most important of which are the diffusion and viscosity coefficients) the pair theory has not been developed to the point where rigorous expressions may be derived. In these cases approximate expressions (based on a model which is used in addition to the pair theory) are commonly employed.

Thus the models are used in two ways: to obtain mathematical expressions for physical quantities and to obtain numerical estimates for the functions appearing in these expressions. It is important to distinguish between these two uses of models. It is also relevant to distinguish between cases where a single hypothesis (e.g. the pair approximation) has been used and cases where a model is required in addition to the hypothesis.

The analytical, numerical, and experimental study of properties of fluids is a well-established discipline of statistical mechanics. The theory of ionic solutions has been one of the most important and fundamental problems in statistical physics throughout the last century. There is general agreement that the Debye-Hückel (DH) theory was a revolution in the understanding of the properties of homogeneous ionic solutions (electrolytes). The theory of electrolyte solutions has been the object of a huge number of scientific results during the 20th century and last decade [4–6], due to the great

amount of applications in the most diverse areas of basic and applied research [7–10]. Progress in this field has been possible predominantly because of an adequate knowledge of the interionic interactions. The formalisms of electrostatics, statistical mechanics and hydrodynamics have been successfully applied to situations where the long-range Coulombic interactions prevail over solvent-solvent, ion-solvent or short-ranged ion-ion forces.

One of the earliest efforts to evaluate the ionic distribution functions was undertaken by Debye and Hückel in their classical paper of 1923 [11]. Their results were extremely influential, mainly because more elaborate liquid state theories were not developed until the 1960s and 1970s and a common approach to electrolytes and non-electrolytes was not possible. DH results are now recognized as the universally valid limiting law for ionic thermodynamic quantities at infinite dilution. The importance of DH formalism is still enormous nowadays, when it continues to be the theoretical basis of most practical applications, particularly in physics of liquids, solid-state plasmas, astrophysics and nuclear reactor physics.

Debye and Hückel introduced a model of ionic solutions where the ions are treated as ionic point charges which interact by means of a Coulomb potential in a uniform dielectric background. They assumed that the ions are distributed according to an exponential distribution law (Boltzmann distribution) characteristic of a system in thermal equilibrium with a heat reservoir (the solvent). The key concept in DH theory is the ionic atmosphere, a spatial separation of charge made up of mobile ions which balance the charge of the central ion, that allows the understanding of the particular ordering inside the bulk solution. The spatial range of correlations itself is determined by the size of this charge inhomogeneity.

A great number of attempts to go beyond the Debye-Hückel theory have been reported, based on avoiding the linearization of the Poisson-Boltzmann equation [12], the introduction of ionic pairing [13], or the existence of structures in the dense regime of an ionic solution [14]. Integral equation techniques have also been used to obtain the pair correlation functions from the Ornstein-Zernike equation: the mean spherical approximation [15], its thermodynamically consistent generalization [16], or their improvements based on cluster resummation techniques, the optimized random phase approximation [17]. Other integral equation techniques have been tested with success, such as the Percus-Yevick type equation [18], the hypernetted chain equation [19], and path integral approaches [20, 21]. Nevertheless, a liquid energy and heat capacity was not calculated in a general analytical form in the above approaches.

1.4 Methods of Studying the Liquid State

Microscopic studies of the liquid state involve processes of a number of types including X-ray scattering and neutron diffraction. From experiments on the scattering of X-rays or neutrons by the liquid it is possible to derive the radial distribution function $g(r)$, the significance of which is that, if we concentrate upon a particular atom at the origin, the average number of atoms to be found within a thin spherical shell of radii r and $r+dr$ is $4\pi r^2 dr g(r)$. Within the pairwise interaction approximation, if $u(r)$ is a potential energy of two atoms at a distance r apart, it is easily seen that the total energy of the liquid is

$$E = \frac{3}{2}Nk_{\mathrm{B}}T + 2\pi N\rho \int_0^\infty r^2 u(r)g(r)dr \tag{1.4.1}$$

where ρ is the density, k_{B} is the Boltzmann constant and N is the number of atoms. Since the total energy of the liquid may be deduced from the latent heat of vaporization and the equation of state of the gas, this provides us with an empirical method of obtaining both the potential and kinetic energies at all temperatures. The broad features of the liquid structure were established by the early X-ray analysis experiments of Keesom and Taconis (1938) and Reekie (1940, 1947).

1.5 Liquid Heat Capacity

Heat capacity of matter is considered to be its most important property because it holds information about system's degrees of freedom as well as the regime in which the system operates, classical or quantum. While physicists have a good theoretical understanding of the heat capacity of both solids and gases, a general theory of the heat capacity of liquids has always remained elusive. Apart from being an awkward hole in our knowledge of condensed-matter physics, heat capacity – the amount of heat needed to change a substance's temperature by a certain amount – is a technologically relevant quantity that would be important to predict. Physicists had been reluctant to develop a theory because the relevant interactions in a liquid are both strong and specific to that liquid, which, it was felt, would make it challenging to develop a general way of calculating heat capacity.

Experimental data from many elemental liquids show that their constant-volume heat capacity C_V, decreases with temperature, from about $3k_{\mathrm{B}}N$, k_{B} is the Boltzmann constant and N is the number of particles, at the melting point to $2k_{\mathrm{B}}N$ at high temperature [22, 23]. The decrease of C_V is also seen in many complex liquids [24]. This behaviour is not understood in a consistent framework similar to those that exist for

solid and gas phases.

Most calculations of liquid energy E, approach a liquid from the gas phase, and calculate the potential energy in addition to the gas kinetic energy, giving $E = K+U$, where K is a kinetic energy of an ideal gas and U is the potential energy of interatomic interaction [25–27]. The simplest treatment assumes the case of a dilute system with only pair interactions. Assuming that the interactions are weak (except at short separations), the high-temperature expansion gives the system described by the Van der Waals equation [25]. While this approach can describe a dense gas or weakly interacting fluids, it is not adequate for real liquids. For example, C_V of the Van der Waals is equal to that of an ideal gas [25], in contrast to the experimental results. The improved calculations of U employ higher-order particle correlations [28]. The results, however, are not straightforward to use for numerical estimates and require the knowledge of correlation functions as well as the properties of interatomic interactions.

A distinctly different, and less common, approach to discuss the energy and heat capacity of a liquid is to include the strong interactions from the outset, by approaching a liquid from the solid phase. The temperature-dependent term of the energy of a solid is given by the phonon energy. In an isotropic solid (glass) all vibrations can be represented by one longitudinal and two transverse waves. In classical case, this gives the heat capacity of C_V, he Dulong-Petit law.

In this approach, Brillouin modified the solid-like result [29], $C_V = 3k_{\mathrm{B}}N$, by assuming that a liquid does not support transverse waves, and encountered an interesting contradiction. The total energy of the harmonic solid is $E = \left(\frac{k_{\mathrm{B}}TN}{2} + \frac{k_{\mathrm{B}}TN}{2}\right) + 2\left(\frac{k_{\mathrm{B}}TN}{2} + \frac{k_{\mathrm{B}}TN}{2}\right) = 3k_{\mathrm{B}}TN$, where the first and the second term give the energy of longitudinal and transverse vibrations, respectively, and $\frac{k_{\mathrm{B}}TN}{2}$ is the mean potential or kinetic energy. This formula is based on the application of the equipartition theorem, which states that energy is shared equally amongst all energetically accessible degrees of freedom of a system, and for a harmonic oscillator results in the equality of potential and kinetic energies. If a liquid loses two transverse vibrations, their potential terms vanish, but kinetic terms remain, and the liquid energy becomes $E = \left(\frac{k_{\mathrm{B}}TN}{2} + \frac{k_{\mathrm{B}}TN}{2}\right) + 2\left(\frac{k_{\mathrm{B}}TN}{2}\right) = 2k_{\mathrm{B}}TN$, giving $C_V = 2k_{\mathrm{B}}N$. This contradicted the experimental result that liquid heat capacity at the melting point is about the same as that of crystals, $C_V = 3k_{\mathrm{B}}N$.

C_V was also studied in molecular dynamics simulations, with liquid Al as a case study [30]. Similar to the experiment, the decrease of heat capacity with temperature was observed, and was interpreted as the progressive loss of liquid shear resistance. The idea that a liquid loses two transverse vibrational modes was also used by Landau to calculate the energy of phonon excitations in a quantum liquid at very low temperature.

This gives the result that the temperature-dependent energy term of a liquid is three times smaller than that in a harmonic solid, reflecting the fact that only one longitudinal mode is preserved [25]. More recently, liquid heat capacity has been discussed on the basis of alternative mechanisms, including the consideration of liquid potential energy landscape with inter-valley motions [23].

In this thesis, we propose that energy and heat capacity of liquids can be understood on the basis of their solid-like elastic properties. In particular, we discuss how the idea of relaxation time τ can be used to describe liquid vibrational states by approaching them from the solid phase.

1.6 Thesis Layout

In chapter I, we discuss that liquids have similarities and distinctions with adjacent phases, therefore they do not have a simple interpolated status between gas and solid states, although features of both the adjacent phases can be detected. Many properties of a liquid may be calculated from the hypothesis that the interatomic forces and energies in a classical liquid are dominated by the sum of pair interactions. Nevertheless, a liquid energy and heat capacity was not calculated in general analytical form in 20th century.

In Chapter II, we review classical approach to liquids and develop it by accounting for the contribution of anharmonicity and thermal expansion to liquid energy and heat capacity. We subsequently compare theoretical calculations to the experiments results of 5 commonly discussed liquids, and find a good agreement by fitting only physically meaningful parameters. We discuss and compare the proposed theory to previous approaches.

Heat capacity is well understood in gases and solids but not in the third state of matter, liquids, and is not discussed in physics textbooks as a result. The perceived difficulty is that interactions in a liquid are both strong and system-specific, implying that the energy strongly depends on the liquid type and that, therefore, liquid energy can not be calculated in general form. In Chapter III, we develop a phonon theory of liquids in the quantum regime where this problem is avoided. The theory covers both classical and quantum regimes. We demonstrate good agreement of calculated and experimental heat capacity of 21 liquids, including noble, metallic, molecular and hydrogen-bonded network liquids in a wide range of temperature and pressure.

The investigation of the properties of helium has been one of the most prolific endeavors since its discovery. In Chapter IV, in the framework of the phonon theory of liquids by taking into account liquid non-static shear rigidity we study an internal energy and heat capacity of compressed liquid ^{4}He. We demonstrate good agreement of

calculated and experimental heat capacity of liquid helium at elevated pressures and supercritical temperatures. We show that helium remains a quantum liquid at elevated pressures for a wide range of temperature supporting both longitudinal and transverse-like phonon excitations. We suggest that in the very wide pressure range 5 MPa-500 MPa liquid helium near melting temperature is both solid-like and quantum.

Since their discovery in 1822, supercritical fluids have been of enduring interest, and have started to be deployed in many important applications. Theoretical understanding of the supercritical state is lacking, and is seen to limit further industrial deployment [31]. In Chapter V, we study thermodynamic properties of the supercritical state, and discover that specific heat shows a crossover between two different regimes, an unexpected result in view of currently perceived homogeneity of supercritical state in terms of physical properties. We subsequently formulate a theory of system thermodynamics above the crossover, and find good agreement between calculated and experimental specific heat by fitting only physically meaningful parameters. In this theory, energy and heat capacity are governed by the minimal length of the longitudinal mode in the system only, and do not explicitly depend on system-specific structure and interactions. Finally, we derive a power law in the system above the Frenkel line.

Despite the recent explosion of areas where supercritical fluids are used in industrial applications, further deployment is seen to be limited by the absence of solid theoretical guidance. In Chapter VI, we demonstrate that the supercritical state is not physically homogeneous as currently believed, but instead has a well-defined structural crossover. Evidenced by the qualitative changes of distribution functions of interatomic distances and angles, the crossover demarcates liquid-like and gas-like configurations and the presence of medium-range structural correlations. Importantly, the discovered structural crossover is closely related to both dynamic and thermodynamic crossovers operating in the supercritical state, providing new unexpected fundamental interlinks between the supercritical structure, dynamics and thermodynamics.

A fundamental task of statistical physics is to start with a microscopic Hamiltonian, predict the system's statistical properties and compare them with observable data. A notable current fundamental challenge is to analytically conclude whether and how an interacting Hamiltonian predicts different basic states of matter, including solid, liquid and gas phases. In Chapter VII, we propose a new idea that enables a unified description of all three states of matter. We introduce a generic form of an interacting phonon Hamiltonian with ground state configurations minimising the potential. Symmetry breaking SO(3) to SO(2), from the group of rotations in reciprocal space to its subgroup, leads to emergence of energy gaps of shear excitations as a consequence of the Goldstone theorem, and readily results in the emergence of energy spectra corresponding to solid, liquid and gas phases.

In Chapter VIII, we make a conclusion based on presented in thesis results.

Bibliography

[1] A. V. Granato, J. Non-Cryst. Sol. **307-310**, 376 (2002).

[2] B. Widom, J. Chem. Phys. **39**, 2808 (1963).

[3] E. Meeron, J. Chem. Phys. **27**, 1238 (1957).

[4] S. Alexander, P. M. Chaikin, P. Grant, G. J. Morales, P. Pincus, and D. Hone, J. Chem. Phys. **80**, 5776 (1984).

[5] P. Koehl, H. Orland, and M. Delarue, Phys. Rev. Lett. **102**, 087801 (2009).

[6] F. C. Santos and A. C. Tort, Eur. J. Phys. **25**, 859 (2004).

[7] M. M. Taddei, T. N. C. Mendes and C. Farina, Eur. J. Phys. **31**, 89 (2010).

[8] A. K. Jonscher, Appl. Phys. A **56**, 405 1993.

[9] R. R. Netz and H. Orland, Europhys. Lett. **45**, 726 (1999).

[10] A. R. Denton, J. Phys.: Condens. Matter **22**, 364108 (2010).

[11] P. Debye, E. Hückel, Phys. Z. **24**, 185 (1923).

[12] T. H. Gronwall, V. K. LaMer, K. Sandved, Phys. Z. **29**, 358 (1928).

[13] N. Bjerrum, Kgl. Danske Vidensk. Selskab. **9**, 7 (1926).

[14] L.W. Bahe, J. Phys. Chem. **76**, 1062 (1972).

[15] E. Waisman, J. L. Lebowitz, J. Chem. Phys. **52**, 4037 (1972).

[16] J. S. Høye, J. L. Lebowitz, G. Stell, J. Chem. Phys. **61**, 3253 (1974).

[17] H. C. Andersen, D. Chandler, J. Chem. Phys. **55**, 1497 (1971).

[18] A. R. Allnatt, Mol. Phys. **8**, 533 (1964).

[19] J. C. Rasaiah, H. L. Friedman, J. Chem. Phys. **48**, 2742 (1968).

[20] G. V. Efimov, E. A. Nogovitsin, Physica A **234**, 506 (1996).

[21] D. Bolmatov, J. Stat. Phys. **137**, 765 (2009).

[22] G. Grimvall, Physica Scripta **11**, 381 (1975).

[23] D. C. Wallace, Phys. Rev. E **57**, 1717 (1998).

[24] A. R. Dexter and A. J. Matheson, Trans. Faraday Soc. **64**, 2632 (1968).

[25] L. D. Landau and E. M. Lifshitz, Statistical Physics (Nauka, Moscow 1964).

[26] J. Frenkel, Kinetic Theory of Liquids (ed. R. H. Fowler, P. Kapitza, N. F. Mott, Oxford University Press, 1947).

[27] J. M. Ziman, Models of disorder (Cambridge University Press, 1979).

[28] N. H. March, Liquid Metals (Cambridge University Press, 1990).

[29] L. Brillouin, Tensors in Mechanics and Elasticity (Academic Press, 1964).

[30] M. Forsblom and G. Grimvall, Phys. Rev. B **72**, 132204 (2005).

[31] E. Kiran, P. G. Debenedetti and C. J. Peters, Supercritical Fluids: Fundamentals and Applications, NATO Science Series E: Applied Sciences 366 (Kluwer Academic Publishers, 2000).

CHAPTER 2

APPROACH TO LIQUIDS FROM SOLID PHASE

Among three basic states of matter (solid, liquid, gas), liquids are least understood from the theoretical point of view. The inter-atomic, or inter-molecular, interactions in a liquid are strong, and therefore strongly affect the liquid energy. At the same time, the interactions are system-specific, hence the calculation of liquid energy requires the explicit knowledge of the interactions. For this reason, it is argued [1] that no general expressions for liquid energy can be obtained, in contrast to gases and solids.

According to current theoretical understanding, liquids are strikingly different from both gases and solids. Indeed, small atomic displacements in a solid make it possible to expand the energy in terms of phonons and obtain general expressions for solid energy. On the other hand, this has largely considered to be impossible to do in liquids where atomic displacements are large. Similarly, small interactions in gases make it possible to treat interactions as a perturbation and obtain general expressions for the corrections to the system energy. On the other hand, this has not been useful for liquids with strong interactions and solid-like densities. An apt summary of this state of affairs, attributed to Landau, is that liquids "have no small parameter". Perhaps for this reason, liquid heat capacity is not, or is barely, mentioned in statistical physics textbooks as well as books dedicated to liquids [1–6]. This observation is shared by Granato [7], who further comments on the challenge faced by teachers to discuss liquid heat capacity in class.

The experimental behavior of liquid heat capacity is interesting. The heat capacity per atom *decreases* from approximately $3k_{\mathrm{B}}$ per atom at the melting point to about $2k_{\mathrm{B}}$ at high temperature, as witnessed by the data of many simple liquids [8, 9]. Similar behavior is also seen in complex liquids [10]. The decrease of heat capacity was observed in molecular dynamics simulations [11, 12]. Liquid heat capacity has also been discussed by considering liquid potential energy landscape with inter-valley motions [9].

Theoretically, liquids have been viewed to occupy an intermediate state between gases and solids. Liquids are fluid, and therefore might intuitively appear closer to gases in terms of their properties. On the other hand, unless they are close to critical point, liquids have solid-like densities and can support shear waves at high frequencies.

The question of how best to treat real dense liquids, i.e. approach them from the gas or solid state, has a long history [2].

Historically, liquids have predominantly been approached from the gas state, by developing schemes to calculate the interaction energy in addition to gas kinetic energy [1–6]. This approach relies on the knowledge of interatomic interactions as well as correlation functions [13, 14]. These are not generally available, apart from simple model systems, as discussed below in more detail. When they are available, it is not apparent how this approach explains the experimental decrease of heat capacity from $3k_{\mathrm{B}}$ to $2k_{\mathrm{B}}$ at high temperature.

An alternative approach to liquids was pioneered by Frenkel [2], and is based on liquid relaxation time τ. τ is the average time between two consecutive local structural rearrangements in a liquid at one point in space. In this picture, a liquid is approached from the solid state because locally, liquid structure remains unchanged, i.e. the same as in a solid, during time shorter than τ. An important advantage of this approach is that strong interactions are included in the consideration from the outset. This is in contrast to the approach from the gas state that attempts to calculate the interaction energy from correlation functions and interatomic interactions.

Frenkel noted that as τ continuously increases (if crystallization is avoided) beyond the experimental time scale, a liquid becomes a solid for practical purposes. Hence, a solid is different from a liquid only quantitatively but not qualitatively. Frenkel subsequently stated: "...the classification of condensed bodies into solids and liquids... has a relative meaning convenient for practical purposes but devoid of scientific value" [2]. Novel for that time, this view might perhaps come across as somewhat unusual even at present. We suggest that a possible reason for this is that solid-like properties of liquids have not become apparent in the traditional approach to liquids from the gas state. On the other hand, we propose here that as far as their energy and heat capacity are concerned, liquids can be understood on the basis of their solid-like properties, consistent with Frenkel's general idea.

It has been recently proposed how liquid energy can be calculated in Frenkel's approach, by relating liquid energy to τ [15]. A good agreement of liquid heat capacity between theoretical and experimental data for mercury was found. Two important questions subsequently arise. First, how well does the theory work for a larger number of liquids? Second, the proposed theory was harmonic. On other hand, anharmonic effects are known to be particularly large in liquids, where the coefficients of thermal expansion considerably exceed those in solids [15]. Hence, it is important to extend the theory to the anharmonic case and compare it with experiments.

In this Chapter, we propose how to include the anharmonic effects in the approach

to liquids from the solid state. We subsequently calculate heat capacity from both harmonic and anharmonic theory, and compare the results with experimental data for 5 commonly discussed liquids. We find good agreement between theoretical calculations and experimental data. Finally, we discuss and compare the proposed theory to the previous approaches to liquids.

2.1 Harmonic Theory

We begin our discussion with the work of Frenkel [2], who provided a microscopic description of Maxwell phenomenological viscoelastic theory of liquid flow [16], by introducing liquid relaxation time τ. As mentioned earlier, τ is the average time between two consecutive atomic jumps in a liquid at one point in space. Each jump can approximately be viewed as a jump of an atom from its neighboring cage into a new equilibrium position, with subsequent cage relaxation. These atomic jumps, or local relaxation events (LREs), give a liquid its ability to flow. τ is a fundamental flow property of a liquid, and is directly related to liquid viscosity η as $\eta = G_\infty \tau$ [2, 16], where G_∞ is the instantaneous shear modulus. On temperature decrease, τ increases by many orders of magnitude, reaching $10^2 - 10^3$ s at which point, by convention, a liquid forms a solid glass because LREs stop operating on a typical experimental time scale.

In Frenkel's theory, motion of an atom in a liquid consists of two types: vibrational motion around an equilibrium position as in a solid, with Debye vibration period of about $\tau_\mathrm{D} = 0.1$ ps ($\tau_\mathrm{D} = \frac{2\pi}{\omega_\mathrm{D}}$, where ω_D is the Debye frequency, the theoretical maximum frequency that atoms or molecules in the liquid can oscillate at) and diffusional motion between two neighboring positions during time τ. Therefore, if the observation time is smaller than τ, the local structure of a liquid does not change, and is the same as that of a solid glass. In this picture, Frenkel realized that a liquid should maintain solid-like shear waves [17, 18], similarly to those existing in a solid, at all frequencies ω larger than $\frac{1}{\tau}$ [2]. This prediction was later confirmed experimentally [19–23]. Longitudinal waves, associated with density fluctuations, are considered to be unaffected in this picture, apart from different dissipation laws for $\omega < \frac{1}{\tau}$ and $\omega > \frac{1}{\tau}$ [2].

Basing on the ability to support high-frequency shear waves, we have calculated liquid energy as follows [15]. In Frenkel's picture, liquid energy is

$$E = E_v + E_d \tag{2.1.1}$$

where E_v and E_d are the energies of vibration and diffusion, respectively.

The vibration energy consists of the energy of one longitudinal mode and two shear

modes with frequency $\omega > \frac{1}{\tau}$. Then, E_v can be written as $E_v = K_l + P_l + K_s(\omega > \frac{1}{\tau}) + P_s(\omega > \frac{1}{\tau})$ where K and P correspond to kinetic and potential terms, respectively. Here, the absence of shear modes with frequency $\omega < \frac{1}{\tau}$ is expressed as $K_s(\omega < \frac{1}{\tau}) = P_s(\omega < \frac{1}{\tau}) = 0$, implying the absence of restoring forces for low-frequency vibrations. Similarly, E_d can be written as $E_d = K_d + P_d$, where K_d and P_d are respective kinetic and potential terms, giving

$$E = K_l + P_l + K_s(\omega > \frac{1}{\tau}) + P_s(\omega > \frac{1}{\tau}) + K_d + P_d \tag{2.1.2}$$

We now approach a liquid from the solid state (glass) where diffusion is absent so that $E_d = 0$ and $E = E_v$. At certain temperature, shear waves with frequency $\omega < \frac{1}{\tau}$ disappear. The oscillatory motion at frequency smaller than $\omega < \frac{1}{\tau}$ is substituted by diffusional motion taking place during time τ. The latter motion can be thought of as a "slipping" motion at low frequency because the restoring force for low-frequency vibrations becomes small (see Figure 1). We note that forces experienced by diffusing atoms are of the same nature as those experienced by vibrating atoms, and are defined by interatomic interactions that give rise to both P_d and P_s. Therefore, the relative smallness of P_s at small frequency implies the smallness of P_d as compared to $P_s(\omega > \frac{1}{\tau})$ (as well as to P_l). In other words, if the interaction energy of diffusing atoms, P_d, were large and comparable to $P_s(\omega > \frac{1}{\tau})$, this would imply strong restoring forces and consequently the existence of low-frequency vibrations. Therefore, P_d can be neglected in Eq. (2.1.2). This is the only approximation in the theory [15]. We further note that the energy of diffusion becomes unimportant at low temperature [24]. Indeed, because the time that an atom spends in the transitory diffusing state is approximately τ_{D}, the relative number of diffusing atoms, $\frac{N_d}{N}$, is equal to the jump probability, $\frac{\tau_{\mathrm{D}}}{\tau}$, where N_d and N are the number of diffusing atoms and the total number of atoms, respectively. When τ significantly exceeds τ_{D}, the number of diffusing atoms and, therefore, diffusing energy, become small and can be ignored.

We now note that the sum of all kinetic terms in Eq. (2.1.2) gives the total kinetic energy of the liquid, K. Indeed, $K = \frac{3NT}{2}$ regardless of how the motion partitions into vibrational and diffusional motion. Then, Eq. (2.1.2) becomes

$$E = K + P_l + P_s(\omega > \frac{1}{\tau}) \tag{2.1.3}$$

It is convenient to re-write Eq. (2.1.3) using the equipartition theorem that implies $P_l = \frac{E_l}{2}$, $P_s(\omega > \frac{1}{\tau}) = \frac{E_l(\omega > \frac{1}{\tau})}{2}$ and $K = K_l + K_s = \frac{E_l}{2} + \frac{E_s}{2}$, where we noted that liquid kinetic energy is the same as in the solid ($K = \frac{3NT}{2}$), and can therefore be written as a sum of kinetic terms related to longitudinal and shear waves. Then, E in Eq. (2.1.3)

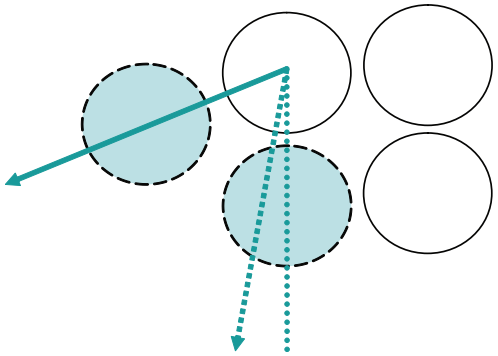

Figure 2.1: As temperature increases, the low-frequency oscillatory shear motion of the highlighted atom between the two dashed lines is lost, as the restoring force for low-frequency shear vibrations becomes weak. Instead, the atom "slips" and diffuses to another position defined by the solid arrow. Schematic illustration.

becomes $E = E_l + \frac{E_s}{2} + \frac{E_s(\omega > \frac{1}{\tau})}{2}$. For subsequent calculations, it is convenient to further write $E_s = E_s(\omega < \frac{1}{\tau}) + E_s(\omega > \frac{1}{\tau})$, where the two terms refer to their solid-state values. Then, E becomes finally

$$E = E_l + E_s(\omega > \frac{1}{\tau}) + \frac{E_s(\omega < 1/\tau)}{2} \tag{2.1.4}$$

The first two terms can be calculated in the same way as is done in the harmonic theory of solids [1], except we separate longitudinal and shear waves in the partition function and account for shear waves with frequency $\omega > \frac{1}{\tau}$ only. Let Z_2 be associated with the first two terms in Eq. (2.1.4). Then, Z_2 is:

$$\begin{aligned} Z_2 = (2\pi\hbar)^{-N'} \int \exp\left(-\frac{1}{2T}\sum_{i=1}^{N}(p_{li}^2 + \omega_{li}^2 q_{li}^2)\right) dpdq \\ \times \int \exp\left(-\frac{1}{2T}\sum_{\omega_{si}>\omega_F}^{2N}(p_{si}^2 + \omega_{si}^2 q_{si}^2)\right) dpdq \end{aligned} \tag{2.1.5}$$

where $\omega_{\mathrm{F}} = \frac{2\pi}{\tau}$ is the Frenkel frequency which puts a lower bound on the oscillation frequency of the atoms or molecules, ω_{li} and ω_{si} are frequencies of longitudinal and shear waves, p_i and q_i are the coordinates and momenta of the normal modes. N is the number of longitudinal modes, N_1 is the number of transverse modes with $\omega > \omega_{\mathrm{F}}$, therefore, $N' = N + N_1$ is the number of phonon states that include longitudinal waves and transverse waves with frequency $\omega > \frac{1}{\tau}$. Here and below, $k_{\mathrm{B}} = 1$.

Integrating, we find

$$Z_2 = T^N \left(\prod_{i=1}^{N} \hbar\omega_{li} \right)^{-1} T^{N_1} \left(\prod_{\omega_{si}>\omega_{\mathrm{F}}}^{2N} \hbar\omega_{si} \right)^{-1} \tag{2.1.6}$$

In the harmonic approximation, frequencies ω_{li} and ω_{ti} are considered to be temperature-independent, in contrast to anharmonic case discussed in the next section. Then, Eq. (2.1.6) gives the liquid energy in harmonic approximation $E = T^2 \frac{d}{dT} \ln Z = NT + N_1 T$. N_1 can be calculated using the quadratic density of states in the Debye model, as is done in solids [1]. The evidence for this comes from the quasilinear dispersion relationships measured by inelastic X-ray experiments [17, 18]. The density of states of shear modes is $g_s(\omega) = \frac{6N}{\omega_{ms}^3}\omega^2$, where ω_{ms} is Debye frequency of shear modes ($\omega_{ms} \approx \omega_{\mathrm{D}}$) and we have taken into account that the number of shear waves is $2N$. Then, $N_1 = \int_{\omega_{\mathrm{F}}}^{\omega_{ms}} g_s(\omega) d\omega = 2N \left(1 - \left(\frac{\omega_{\mathrm{F}}}{\omega_{ms}} \right)^3 \right)$.

To calculate the last term in Eq. (2.1.4), we note that similarly to $E_s(\omega > 1/\tau) = N_1 T$, $E_s(\omega < 1/\tau) = N_2 T$, where N_2 is the number of shear modes with $\omega < \omega_{\mathrm{F}}$. Because $N_2 = 2N - N_1$, $N_2 = 2N \left(\frac{\omega_{\mathrm{F}}}{\omega_{ms}} \right)^3$. Then, $E = (N + N_1 + \frac{N_2}{2})T$, giving finally

$$E = NT \left(3 - \left(\frac{\omega_{\mathrm{F}}}{\omega_{\mathrm{D}}} \right)^3 \right) \tag{2.1.7}$$

According to Eq. (2.1.7), the liquid energy is $3NT$ as in a solid when $\tau \gg \tau_{\mathrm{D}}$. This gives the heat capacity per atom, $c_v = \frac{1}{N}\frac{\mathrm{d}E}{\mathrm{d}T}$, $c_v = 3$, consistent with experimental results [8, 9]. When $\tau \to \tau_{\mathrm{D}}$ at high temperature, Eq. (2.1.7) predicts $c_v = 2$, as in the experimental data [8, 9].

2.2 Anharmonic Theory

In the harmonic approximation, temperature dependence of frequencies in Eq. (2.1.6) is ignored. This may be a good approximation for phonons in solids at either low temperature or in systems with small thermal expansion coefficient α. In liquids, on the other hand, anharmonicity and associated thermal expansion are large [26], and need to be taken into account. In this case, applying $E = T^2 \frac{d}{dT} \ln Z_2$ to Eq. (2.1.6) gives

$$E_2 = NT - T^2 \sum_{i=1}^{N} \frac{1}{\omega_{li}} \frac{\mathrm{d}\omega_{li}}{\mathrm{d}T} + N_1 T - T^2 \sum_{i=1}^{N_1} \frac{1}{\omega_{si}} \frac{\mathrm{d}\omega_{si}}{\mathrm{d}T} \tag{2.2.1}$$

which corresponds to the first two terms in Eq. (2.1.4).

The anharmonic effects lead to the decrease of frequencies with temperature, resulting in system softening [26]. We therefore need to calculate $\frac{\mathrm{d}\omega_{li}}{\mathrm{d}T}$ and $\frac{\mathrm{d}\omega_{si}}{\mathrm{d}T}$ in Eq. (2.2.1). These can be calculated in the Grüneisen approximation, by introducing the Grüneisen parameter $\gamma = -\frac{V}{\omega}\left(\frac{\partial\omega_i}{\partial V}\right)_T$, where ω_i are frequencies in harmonic approximation [24]. γ features in the phonon pressure $P_{ph} = -\left(\frac{\partial F}{\partial V}\right)_T$, where F is free energy in the harmonic approximation. $F = -T\ln Z$ can be calculated from Eq. (2.1.6), giving

$$F_2 = T\sum_{i=1}^{N}\ln\frac{\hbar\omega_{li}}{T} + T\sum_{i=1}^{N_1}\ln\frac{\hbar\omega_{si}}{T} \tag{2.2.2}$$

Calculating $P_{ph} = -\left(\frac{\partial F}{\partial V}\right)_T$ and introducing the above Grüneisen parameter gives $P_{ph} = \frac{\gamma T}{V}(N + N_1)$. Then, the bulk modulus due to the (negative) phonon pressure is $B_{ph} = V\frac{\partial P}{\partial V} = -\frac{\gamma T}{V}(N + N_1)$, giving $\left(\frac{\partial B_{ph}}{\partial T}\right)_v = -\frac{\gamma}{V}(N + N_1)$. We now use the macroscopic definition of γ, $\gamma = \frac{V\alpha B}{C_v}$ [26]. Here, $B = B_0 + B_{ph}$ is the total bulk modulus, B_0 is zero-temperature bulk modulus, α is the coefficient of thermal expansion and C_v is constant-volume heat capacity. For C_v, we use its harmonic value, $C_v = N + N_1$ from Eq. (2.2.1), because $\frac{\mathrm{d}\omega_{li}}{\mathrm{d}T}$ and $\frac{\mathrm{d}\omega_{si}}{\mathrm{d}T}$ in Eq. (2.2.1) already enter as quadratic anharmonic corrections. Then, $\left(\frac{\partial B_{ph}}{\partial T}\right)_v = -\alpha(B_0 + B_{ph})$. For small αT, as is often the case in experiments, this implies $B \propto -T$, consistent with the experimental data [26].

We note that experimentally, B linearly decreases with T at both constant volume and constant pressure [26]. The decrease of B with T at constant volume is due to the intrinsic anharmonicity related to the softening of interatomic potential at large vibrational amplitudes; the decrease of B at constant pressure has an additional contribution from thermal expansion.

Assuming $\omega^2 \propto B_0 + B_{ph}$ and combining it with $\left(\frac{\partial B_{ph}}{\partial T}\right)_v = -\alpha(B_0 + B_{ph})$ from above gives $\frac{1}{\omega}\frac{\mathrm{d}\omega}{\mathrm{d}T} = -\frac{\alpha}{2}$ [24] and it was also verified on the basis of Molecular Dynamics simulations [25]. Putting it in Eq. (2.2.1) gives:

$$E_2 = (N + N_1)\left(T + \frac{\alpha T^2}{2}\right) \tag{2.2.3}$$

The last term in Eq. (2.1.4), $\frac{E_s(\omega<1/\tau)}{2}$, can be calculated in the same way, giving $\frac{1}{2}N_2\left(T + \frac{\alpha}{2}T^2\right)$, where N_2 is the number of shear modes with $\omega < \omega_0$ defined in the previous section. Adding this term to Eq. (2.2.3) and using N_1 and N_2 calculated in the previous section gives the anharmonic liquid energy:

$$E = N\left(T + \frac{\alpha T^2}{2}\right)\left(3 - \left(\frac{\omega_{\mathrm{F}}}{\omega_{\mathrm{D}}}\right)^3\right) \tag{2.2.4}$$

At low temperature when τ exceeds $\tau_{\rm D}$, Eq. (2.2.4) gives $E = 3N(T + \frac{\alpha T^2}{2})$, and c_v is

$$c_v = 3(1 + \alpha T) \tag{2.2.5}$$

Eq. (2.2.5) explains why experimental c_v of liquids exceed the Dulong-Petit value just above the melting point [8, 9]. This result was verified on the basis of Molecular Dynamics simulations [25]. In the next section, we compare the calculated and experimental c_v in the entire temperature range.

2.3 Comparison with Experimental Data

We now compare the predictions of Eqs. (2.1.7) and (2.2.4) with the experimental c_v. Simple liquids [8, 9] offer a good test case for a number of reasons. First, they are frequently discussed in the literature. Consequently, the data of both c_v and viscosity are available for simple liquids, partially because their melting temperatures are fairly low, simplifying the measurements. Second, these liquids become low-viscous close to the melting point, in contrast to, for example, liquid B_2O_3, SiO_2 and so on. Consequently, the decrease of c_v, calculated from Eqs. (2.1.7) and (2.2.4) to operate around $\tau \approx \tau_{\rm D}$, can be observed in a convenient and accessible temperature range. Third, it is important to see that our theory works in a wide temperature range. We have taken experimental c_v for liquid Hg, In, Rb, Cs and Sn where c_v has been measured in a wide range of temperatures, from 200 to 1200 K.

To the best of our knowledge, apart from liquid Hg, this is the first attempt to analytically calculate c_v of the above liquids and compare them with experiments.

To calculate c_v from the theory, we write τ in terms of liquid viscosity using the Maxwell relationship $\tau = \frac{\eta}{G_\infty}$. Then, harmonic and anharmonic c_v in Eq. (2.1.7) and Eq. (2.2.4) are given by the two equations below:

$$c_v = \frac{\mathrm{d}}{\mathrm{d}T}\left(T\left(3 - \left(\frac{\tau_{\rm D} G_\infty}{\eta}\right)^3\right)\right) \tag{2.3.1}$$

$$c_v = \frac{\mathrm{d}}{\mathrm{d}T}\left(\left(T + \frac{\alpha T^2}{2}\right)\left(3 - \left(\frac{\tau_{\rm D} G_\infty}{\eta}\right)^3\right)\right) \tag{2.3.2}$$

We have taken viscosity data from Refs [28–30] and fitted them to the form of the Vogel-Fulcher-Tammann (VFT) law

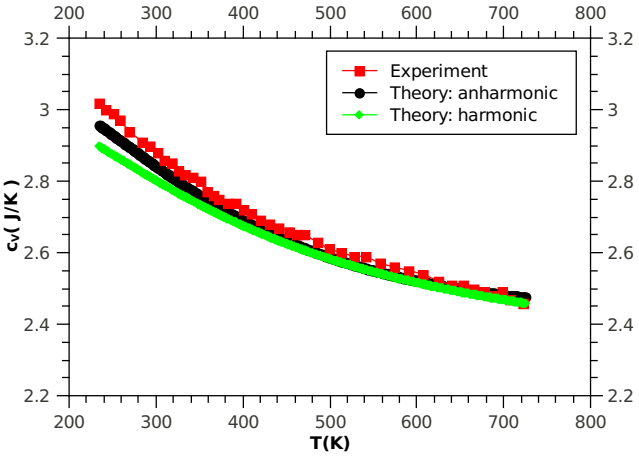

Figure 2.2: (Color online). Experimental and theoretical c_v for liquid Hg. Experimental c_v is shown in square symbols. Calculated harmonic and anharmonic c_v are shown in the bottom and thick black curve, respectively. $\tau_D G_\infty = 5.5 \cdot 10^{-4}$ Pa·s and $6.272 \cdot 10^{-4}$ Pa·s for theoretical harmonic and anharmonic c_v, respectively. $\alpha = 1.60 \cdot 10^{-4}$ K^{-1}. VFT parameters (see Eq.2.3.3): $\eta_0 = 0.6 \cdot 10^{-3}$, $A = 235.2$ K and $T_0 = 40.7$ K.

$$\eta = \eta_0 \exp\left(\frac{A}{T - T_0}\right) \tag{2.3.3}$$

Software package XMGR was used to determine η_0, A and T_0 in the Vogel-Fulcher-Tammann law (see Eq.2.3.3). The data were subsequently extrapolated on the temperature range of experimental c_v because the experimental c_v was measured in a wider temperature range than η, and used η in Eqs. (2.3.1,2.3.2) to calculate c_v. We note that c_v in Eqs. (2.3.1,2.3.2) depends on both η and $\frac{d\eta}{dT}$, and is therefore sensitive to the viscosity fit. We find that as long as the VFT fit has physical values of parameters (e.g. positive T_0), a reasonable agreement between the calculated and experimental c_v is found, as discussed below in more detail.

In practice the values of τ_D and G_∞ are not known precisely for all liquids. Therefore, we have varied $\tau_D G_\infty$ and α (the fitting was done by visual inspection) around their experimental values to fit the calculated c_v to the experimental data.

In Figures (2.2-2.6), we show the experimental c_v where the electronic contribution was subtracted [8, 9]. We also show c_v, calculated from both harmonic and anharmonic theory using Eqs. (2.3.1,2.3.2). Overall, Figures (2.2-2.6) show reasonably good agreement between the theoretical and experimental c_v.

The agreement is somewhat worse at low temperature, however the maximal difference between the calculated and experimental values is comparable with the ex-

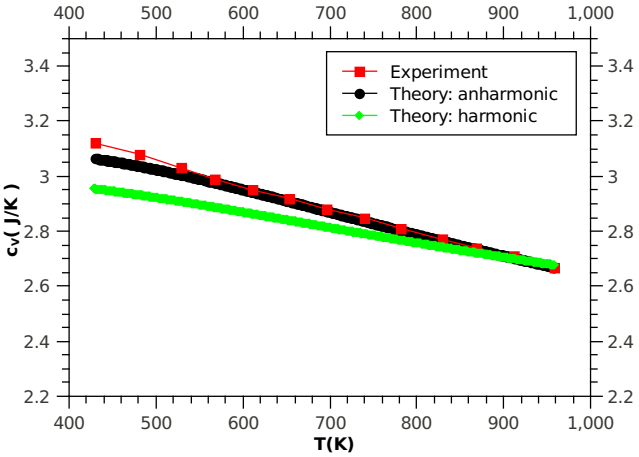

Figure 2.3: (Color online). Experimental and theoretical c_v for liquid In. Experimental c_v is shown in square symbols. Calculated harmonic and anharmonic c_v are shown in the bottom and thick black curve, respectively. $\tau_D G_\infty = 4.04 \cdot 10^{-4}$ Pa·s and $4.88 \cdot 10^{-4}$ Pa·s for theoretical harmonic and anharmonic c_v, respectively. $\alpha = 1.22 \cdot 10^{-4}$ K^{-1}. VFT parameters (see Eq.2.3.3): $\eta_0 = 0.4 \cdot 10^{-3}$, $A = 668$ K and $T_0 = -2.6$ K.

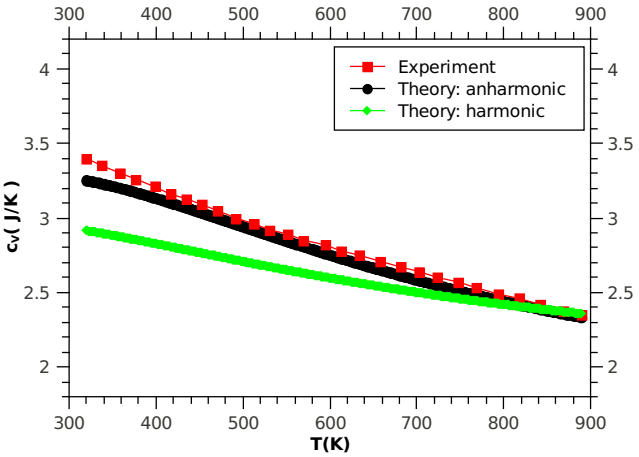

Figure 2.4: (Color online). Experimental and theoretical c_v for liquid Cs. Experimental c_v is shown in square symbols. Calculated harmonic and anharmonic c_v are shown in the bottom and thick black curve, respectively. $\tau_D G_\infty = 1.19 \cdot 10^{-4}$ Pa·s and $2.07 \cdot 10^{-4}$ Pa·s for theoretical harmonic and anharmonic c_v, respectively. $\alpha = 4.92 \cdot 10^{-4}$ K^{-1}. VFT parameters (see Eq.2.3.3): $\eta_0 = 0.9 \cdot 10^{-4}$, $A = 659.8$ K and $T_0 = -24.1$ K.

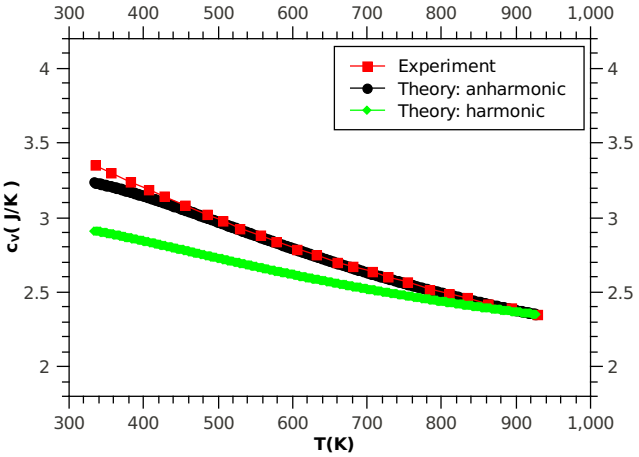

Figure 2.5: (Color online). Experimental and theoretical c_v for liquid Rb. Experimental c_v is shown in square symbols. Calculated harmonic and anharmonic c_v are shown in the bottom and thick black curve, respectively. $\tau_{\rm D} G_\infty = 1.46 \cdot 10^{-4}$ Pa·s and $1.914 \cdot 10^{-4}$ Pa·s for theoretical harmonic and anharmonic c_v, respectively. $\alpha = 4.52 \cdot 10^{-4}$ K^{-1}. VFT parameters (see Eq.2.3.3): $\eta_0 = 0.9 \cdot 10^{-4}$, $A = 604.1$ K and $T_0 = 4.1$ K.

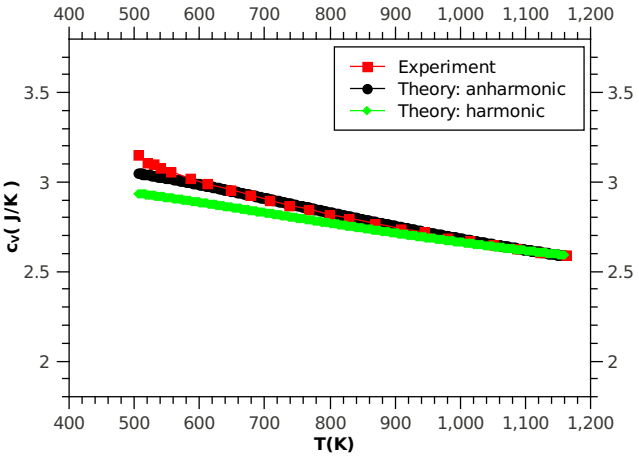

Figure 2.6: (Color online). Experimental and theoretical c_v for liquid Sn. Experimental c_v is shown in square symbols. Calculated harmonic and anharmonic c_v are shown in the bottom and thick black curve, respectively. $\tau_{\rm D} G_\infty = 4.67 \cdot 10^{-4}$ Pa·s and $5.67 \cdot 10^{-4}$ Pa·s for theoretical harmonic and anharmonic c_v, respectively. $\alpha = 1.11 \cdot 10^{-4}$ K^{-1}. VFT parameters (see Eq.2.3.3): $\eta_0 = 0.4 \cdot 10^{-3}$, $A = 949.9$ K and $T_0 = -30.6$ K.

perimental uncertainty of c_v of 0.1–0.2 J/K [8]. We note that $C_v = 3 - \left(\frac{\tau_D G_\infty}{\eta}\right)^3 + \frac{3T}{\eta}\left(\frac{\tau_D G_\infty}{\eta}\right)^3 \frac{d\eta}{dT}$ from Eq. (2.3.1), and similar $\propto \frac{d\eta}{dT}$ terms appear if Eq. (2.3.2) is used. Here, the second term is small at low temperature where $\tau \gg \tau_D$ and therefore $\eta \gg \tau_D G_\infty$. The last term depends on both η and $\frac{d\eta}{dT}$. $\frac{d\eta}{dT}$ is largest at low temperature, therefore the last term is most sensitive to the fitted slope of η at low temperature and its extrapolation, and is expected to contribute most to the difference between the calculated and experimental c_v.

Importantly, the theoretical curves in Figures (2.2-2.6) are calculated using physically sensible values of parameter $\tau_D G_\infty$ in the (1-6)$\cdot 10^{-4}$ Pa·s range (see captions in Figures (2.2-2.6)). For example, if G_∞ of Hg is about 5 GPa [27], the used values of $\tau_D G_\infty$ in Figure (2.2) imply τ_D of about 0.1 ps, a typical value of Debye vibrational period which is, furthermore, consistent with the experimental value [31]. Similarly, if G_∞ of Cs is 0.77 GPa [32], the used values of $\tau_D G_\infty$ in Figure (2.4) imply τ_D of about 0.1 ps, equally consistent with experiments [32]. We also note that the used value of $\tau_D G_\infty$ is close to that in other liquids [21].

Similarly to $\tau_D G_\infty$, the values of α used to calculate the anharmonic c_v (see captions to Figures (2.2-2.6)) are close to experimental ones. The experimental α for Hg, In, Rb, Cs and Sn are $1.8 \cdot 10^{-4}$ K^{-1}, 1.11$\cdot 10^{-4}$ K^{-1}, 3$\cdot 10^{-4}$ K^{-1}, 3$\cdot 10^{-4}$ K^{-1} and 0.87$\cdot 10^{-4}$ K^{-1}, respectively [9], in reasonably good agreement with the values used in Figures (2.2-2.6).

We observe that for all five liquids, harmonic c_v is systematically below the experimental value at low temperature. This is not surprising because the maximal low-temperature value of harmonic c_v is 3, according to Eq. (2.3.1). As Figures (2.2-2.6) show, the anharmonic contribution, calculated using Eq. (2.3.2), is important in order to reproduce the experimental behavior.

In summary, we find that overall, theoretical and experimental values of c_v agree reasonably well, using physically sensible values of parameters $\tau_D G_\infty$ and α.

We note that above we have discussed the behavior of c_v. The quantity that is frequently measured in the experiment is the constant-pressure heat capacity, C_p. For several low-viscous liquids, C_p weakly depends on temperature, in contrast to the constant-volume heat capacity, C_v [8, 11, 33]. On the other hand, for highly viscous liquids, C_p increases, approximately linearly, with temperature [34]. This behavior can be rationalized in the proposed picture as follows. We re-write the known relationship, $C_p = C_v + VT\alpha^2 B$ [1], as $c_p = c_v(1 + \gamma\alpha T)$, where $c_p = \frac{C_p}{N}$ and $\gamma = \frac{V\alpha B}{C_v}$ is the Grüneisen parameter, which is on the order of unity in various systems [26]. For highly viscous liquids where $\tau \gg \tau_D$, the last term in Eq. (2.2.4) representing the contribution

from the decreasing number of transverse waves, $\left(3-\left(\frac{\omega_0}{\omega_\mathrm{D}}\right)^3\right)$, can be neglected. Then, $c_v = 3(1+\alpha T)$, giving $c_p = 3(1+(\gamma+1)\alpha T)$, where we have neglected the square of the small parameter αT. This is consistent with the linear increase of experimental c_p [34]. On the other hand, in low-viscous liquids where τ approaches τ_D at high temperature, the contribution of the decreasing number of transverse modes in Eq. (2.2.4) can not be neglected. In this case, $c_p = c_v(1+\gamma\alpha T)$ is the product of temperature-decreasing c_v due to the decreasing contribution of transverse waves (see Figures (2.2-2.6)) and temperature-increasing term, $\propto \alpha T$. As a result, c_p is less sensitive to temperature, as is seen experimentally.

Bibliography

[1] L. D. Landau and E. M. Lifshitz, Statistical Physics (Nauka, Moscow 1964).

[2] J. Frenkel, Kinetic Theory of Liquids (ed. R. H. Fowler, P. Kapitza, N. F. Mott, Oxford University Press, 1947), pp. 188-249.

[3] J. M. Ziman, Models of disorder (Cambridge University Press, 1979).

[4] J. P. Boon and S. Yip, Molecular Hydrodynamics (Dover Publications, New York, 1980).

[5] N. H. March, Liquid Metals (Cambridge University Press, 1990).

[6] J. P. Hansen and I. R. McDonald, Theory of simple liquids (Elsevier, 2007).

[7] A. V. Granato, J. Non-Cryst. Sol. **307-310**, 376 (2002).

[8] G. Grimvall, Physica Scripta **11**, 381 (1975).

[9] D. C. Wallace, Phys. Rev. E **57**, 1717 (1998).

[10] A. R. Dexter and A. J. Matheson, Trans. Faraday Soc. **64**, 2632 (1968).

[11] B. Sadigh and G. Grimvall, Phys. Rev. B **54**, 15742 (1996).

[12] M. Forsblom and G. Grimvall, Phys. Rev. B **72**, 132204 (2005).

[13] M. Born and H. S. Green, Proc. Royal Soc. London A **188**, 10 (1946).

[14] D. Henderson, Ann. Rev. Phys. Chem. **15**, 31 (1964).

[15] K. Trachenko, Phys. Rev. B **78**, 104201 (2008).

[16] J. C. Maxwell, Phil. Trans. Royal Soc. London **157**, 49 (1867).

[17] V. M. Giordano, and G. Monaco, Proc. Natl. Acad. Sci. **107**, 21985 (2010).

[18] V. M. Giordano, and G. Monaco, Phys. Rev. B **84**, 052201 (2011).

[19] J. R. D. Copley and J. M. Rowe, Phys. Rev. Lett. **32**, 49 (1974).

[20] M. Grimsditch, R. Bhadra and L. M. Torell, Phys. Rev. Lett. **62**, 2616 (1989).

[21] W. C. Pilgrim, S. Hosokawa, H. Saggau, H. Sinn and E. Burkel, J. Non-Cryst. Sol. **250-252**, 96 (1999).

[22] E. Burkel, Rep. Prog. Phys. **63**, 171 (2000).

[23] W. C. Pilgrim and C. Morkel, J. Phys.: Cond. Matt. **18**, R585 (2006).

[24] K. Trachenko and V. V. Brazhkin, Phys. Rev. B **83**, 014201 (2011).

[25] E. I. Andritsos, E. Zarkadoula, A. E. Phillips, M. T. Dove, C. J. Walker, V. V. Brazhkin and K. Trachenko, J. Phys.: Cond. Matt. **25**, 235401 (2013).

[26] O. L. Anderson, Equations of State of Solids for Geophysics and Ceramic Science (Oxford University Press, 1995).

[27] D. C. Wallace, Phys. Rev. A **25**, 3290 (1982).

[28] C. M. Carlson, H. Eyring, and T. Ree, Proc. Natl. Acad. Sci. U.S.A. **46**, 649 (1960).

[29] E. N. da C. Andrade and E. R. Dobbs, Proc. Royal Soc. London A **211**, 12 (1952).

[30] M. F. Culpin, Proc. Phys. Soc. B **70**, 1069 (1957).

[31] S. Hosokawa, H. Sinn F. Hensel, A. Alatas, E. E. Alp, W. C. Pilgrim, J. Non-Cryst. Sol. **312-314**, 163 (2002).

[32] T. Bodensteiner, Chr. Morkel, W. Gläser and B. Dorner, Phys. Rev. A **45**, 5709 (1992).

[33] G. Pottlacher, E. Kaschnitz amd H. Jager, J. Non-Cryst. Sol. **156**, 374 (1993).

[34] S. L. Simon and G. B. McKenna, J. Non-Cryst. Sol. **355**, 672 (2009).

[35] D. Bolmatov, J. Stat. Phys. **137**, 765 (2009).

[36] M. V. Fernández-Serra and Emilio Artacho, Phys. Rev. Lett. **96**, 016404 (2006).

CHAPTER 3

THE PHONON THEORY OF LIQUIDS

The data from the experimental advances, together with theoretical understanding of the phonon states in a liquid due to Frenkel raise an important question of whether the phonon theory of liquids could be constructed, similar to the phonon theory of solids. Below we develop a phonon theory of liquids that covers both classical and quantum regimes. We find good agreement between calculated and experimental heat capacity for many liquids in a wide temperature and pressure range.

3.1 Theory

There are two types of atomic motion in a liquid: phonon motion that consists of one longitudinal mode and two transverse modes with frequency $\omega > \omega_{\mathrm{F}}$, where $\omega_{\mathrm{F}} = \frac{2\pi}{\tau}$ is Frenkel frequency, and the diffusional motion due to an atom jumping between two equilibrium positions. Hence, the phonon motion consists of kinetic and potential parts, giving the liquid energy as derived in Chapter II

$$E = K_l + P_l + K_s(\omega > \omega_{\mathrm{F}}) + P_s(\omega > \omega_{\mathrm{F}}) + K_d \tag{3.1.1}$$

where K_l and P_l are kinetic and potential components of the longitudinal phonon energy, $K_s(\omega > \omega_{\mathrm{F}})$ and $P_s(\omega > \omega_{\mathrm{F}})$ are kinetic and potential components of the energy of shear phonons with frequency $\omega > \omega_{\mathrm{F}}$, K_d is kinetic energy of diffusing atoms. The energy of longitudinal mode is the same as in a solid, albeit different dissipation laws apply at low and high frequency [1]. In the next paragraph, we re-write E in the form convenient for subsequent calculations.

Each term in Eq. (2.1.3) can be calculated using the phonon free energy, $F_{ph} = E_0 + T\sum\limits_i \ln\left(1 - \exp\left(-\frac{\hbar\omega_i}{T}\right)\right)$, where E_0 is the energy of zero-point vibrations [2]. The expression for F_{ph} implies that the phonon modes with frequencies ω_i are non-interacting, which is true for a harmonic solid, and which is assumed to be true in the proposed phonon theory of liquids. The anharmonic effects due to thermal expansion will be taken into account in the same way as it was done in the previous Section using Grüneisen approximation. In calculating the energy, $E_{ph} = F_{ph} - T\frac{dF_{ph}}{dT}$, we take into

account the effect of thermal expansion, important in liquids. This implies $\frac{d\omega_i}{dT} \neq 0$, contrary to the harmonic case, and gives

$$E_{ph} = E_0 + \hbar \sum_i \frac{\omega_i - T\frac{d\omega_i}{dT}}{\exp\left(\frac{\hbar\omega_i}{T}\right) - 1} \tag{3.1.2}$$

Using quasi-harmonic approximation Grüneisen approximation gives $\frac{\mathrm{d}\omega}{\mathrm{d}T} = -\frac{\alpha\omega}{2}$, where α is the coefficient of thermal expansion [3]. Putting it in Eq. (3.1.2) gives

$$E_{ph} = E_0 + \left(1 + \frac{\alpha T}{2}\right) \sum_i \frac{\hbar\omega_i}{\exp\left(\frac{\hbar\omega_i}{T}\right) - 1} \tag{3.1.3}$$

The energy of one longitudinal mode, the first term in Eq. (2.1.3), can be calculated by substituting the sum in Eq. (3.1.3), $\sum$, with Debye vibrational density of states for longitudinal phonons, $g(\omega) = \frac{3N}{\omega_\mathrm{D}^3}\omega^2$, where ω_D is Debye frequency. The normalization of $g(\omega)$ reflects the fact that the number of longitudinal modes is N. Integrating from 0 to ω_D gives $\sum = NTD\left(\frac{\hbar\omega_\mathrm{D}}{T}\right)$, where $D(x) = \frac{3}{x^3}\int_0^x \frac{z^3 \mathrm{d}z}{\exp(z)-1}$ is Debye function [2]. The energy of two shear modes with frequency $\omega > \omega_\mathrm{F}$, the second term in Eq. (2.1.3), can be similarly calculated by substituting $\sum$ with density of states $g(\omega) = \frac{6N}{\omega_\mathrm{D}^3}\omega^2$, where the normalization accounts for the number of shear modes of $2N$. Integrating from ω_F to ω_D gives $\sum = 2NTD\left(\frac{\hbar\omega_\mathrm{D}}{T}\right) - 2NT\left(\frac{\omega_\mathrm{F}}{\omega_\mathrm{D}}\right)^3 D\left(\frac{\hbar\omega_\mathrm{F}}{T}\right)$. $E_s(\omega < \omega_\mathrm{F})$ in the last term in Eq. (2.1.3) is obtained by integrating $\sum$ from 0 to ω_F with the same density of states, giving $\sum = 2NT\left(\frac{\omega_\mathrm{F}}{\omega_\mathrm{D}}\right)^3 D\left(\frac{\hbar\omega_\mathrm{F}}{T}\right)$. Putting all terms in Eq. (3.1.3) and then Eq. (2.1.3) gives finally the liquid energy

$$E = NT\left(1 + \frac{\alpha T}{2}\right)\left(3D\left(\frac{\hbar\omega_\mathrm{D}}{T}\right) - \left(\frac{\omega_\mathrm{F}}{\omega_\mathrm{D}}\right)^3 D\left(\frac{\hbar\omega_\mathrm{F}}{T}\right)\right) \tag{3.1.4}$$

where we have omitted E_0 that includes zero-point vibration energies because below we calculate the derivative of E.

Eq. (3.1.4) spans both classical and quantum regimes, an important feature for describing the behavior of liquids discussed below. At $\tau_\mathrm{D} \ll \tau$, $\frac{\hbar\omega_\mathrm{D}}{k_\mathrm{B}T} \ll 1$ we get Eq. 2.2.4 from the previous Chapter, because Debye function D becomes 1 in the classical limit.

We note that the presented phonon theory of liquids operates at the same level of approximation as Debye theory of solids, particularly relevant for disordered isotropic systems [2] such as glasses and liquids. The result for a harmonic solid follows from Eq. (3.1.4) when $\omega_\mathrm{F} = 0$, corresponding to infinite relaxation time, and $\alpha = 0$.

3.2 Comparison with Experimental Data

We now compare Eq. (3.1.4) to experimental data of heat capacity per atom, $c_v = \frac{1}{N}\frac{dE}{dt}$. We have used the National Institute of Standards and Technology (NIST) database [4] that contains c_v for many liquids, and have chosen monatomic nobel liquids, molecular liquids, as well as a hydrogen-bonded network liquids. We aimed to check our theoretical calculations in a wide range of temperature, and therefore selected the data at pressures exceeding the critical pressures of the above systems where they exist in a liquid form in the broad temperature range. As a result, the temperature range in which we calculate c_v is about 100–700 K for various liquids (see Figures 3.1–3.4). Experimental c_v of metallic liquids were taken from Refs. [5, 6] at ambient pressure (c_v of some of these were calculated previously in Ref. [7] on the basis of classical approach only). The total number of liquids considered is 21. Software package XMGR was used to determine η_0, A and T_0 in the Vogel-Fulcher-Tammann law (see Eq.2.3.3) and presented in Table 3.1.

To calculate c_v from Eq. (3.1.4), we have taken viscosity data from the NIST database at the same pressures as c_v and converted it to τ using the Maxwell relationship $\tau = \frac{\eta}{G_\infty}$, where η is viscosity and G_∞ is infinite-frequency shear modulus, giving $\omega_{\rm F} = \frac{2\pi}{\tau} = \frac{2\pi G_\infty}{\eta}$. Viscosities of liquid metals and F_2 were taken from Refs. [8–13] and Ref. [14], respectively.

We note that Debye model is not a good approximation in molecular and hydrogen-bonded systems where the frequency of intra-molecular vibrations considerably exceeds the rest of frequencies in the system (e.g. 2260 K in O_2, 3340 K in N_2, 3572 K in CO). However, the intra-molecular modes are not excited in the temperature range of experimental c_v (see Figures 3.1–3.4). Therefore, the contribution of intra-molecular motion to c_v is purely rotational, c^{rot}. Being classical, the rotational motion gives $c^{rot} = R$ for linear molecules such as CO, F_2, N_2 and O_2 and $c^{rot} = \frac{3R}{2}$ for molecules with three rotation axes such as CH_4, H_2S, H_2O and D_2O. Consequently, c_v for molecular liquids shown in Figures 3.1–3.4 correspond to heat capacities per molecule, with c^{rot} subtracted from the experimental data. In this case, N in Eq. (3.1.4) refers to the number of molecules.

We also note that in H_2O, approximately half of experimental c_v is the configurational contribution due to the temperature-induced structural change of the hydrogen-bonded network [15]. The change includes changing coordinations of H_2O molecules during the continuous transition between the low-density and high-density liquid in the wide temperature range [16]. Similarly to the phonon theory of solids, effects of this sort are not accounted for in the general theory presented here. Therefore, experimental c_v for H_2O and D_2O shows c_v with half subtracted from their values due to the

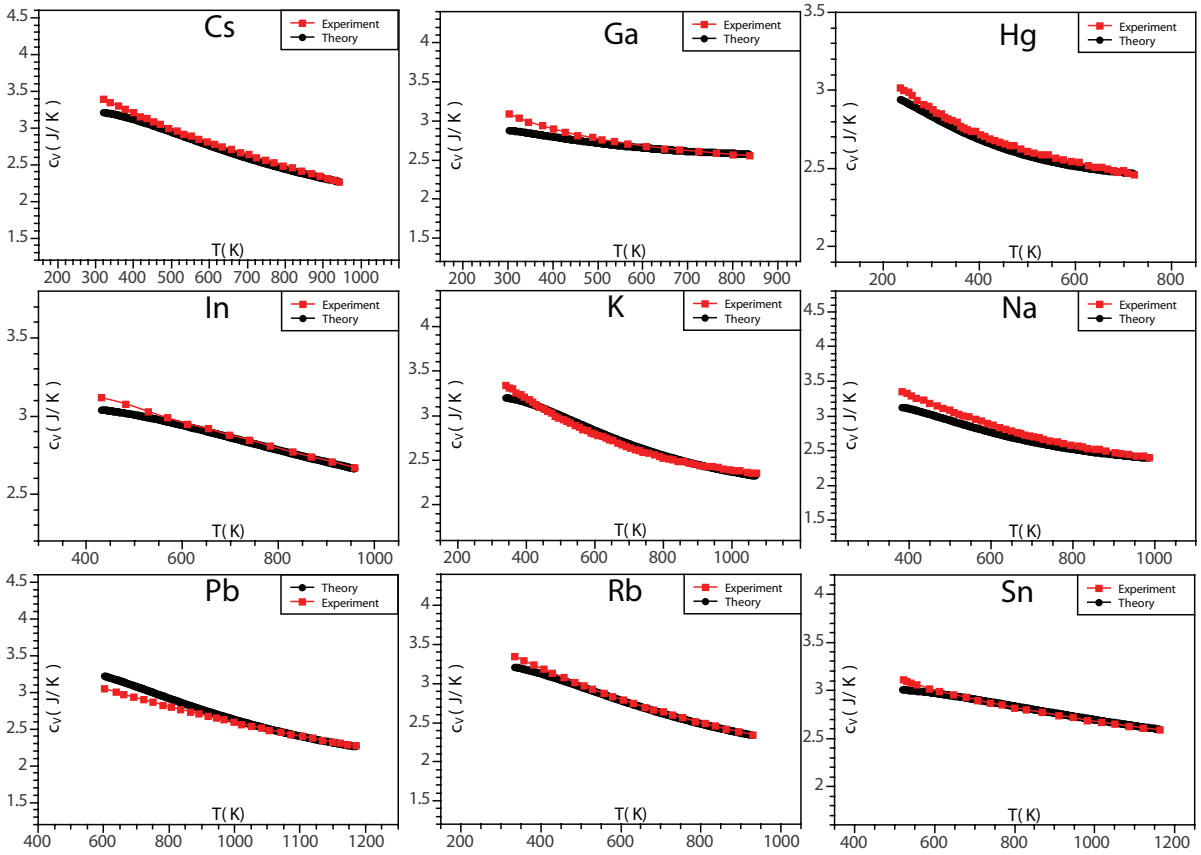

Figure 3.1: Experimental and calculated c_v for liquid metals. Experimental c_v are at ambient pressure, with electronic contribution subtracted [5, 6]. Values of τ_{D} used in the calculation are 0.95 ps (Cs), 0.27 ps (Ga), 0.49 ps (Hg), 0.31 ps (In), 0.57 ps (K), 0.42 ps (Na), 0.64 ps (Pb), 0.74 ps (Rb) and 0.18 ps (Sn). Values of G_∞ are 0.17 GPa (Cs), 2.39 GPa (Ga), 1.31 GPa (Hg), 1.58 GPa (In), 1.8 GPa (K), 3.6 GPa (Na), 1.42 GPa (Pb), 0.25 GPa (Rb) and 3 GPa (Sn). Experimental α (Ref. [6]) are $3 \cdot 10^{-4}$ K^{-1} (Cs), $1.2 \cdot 10^{-4}$ K^{-1} (Ga), $1.8 \cdot 10^{-4}$ K^{-1} (Hg), $1.11 \cdot 10^{-4}$ K^{-1} (In), $2.9 \cdot 10^{-4}$ K^{-1} (K), $2.57 \cdot 10^{-4}$ K^{-1} (Na), $3 \cdot 10^{-4}$ K^{-1} (Pb), $3 \cdot 10^{-4}$ K^{-1} (Rb) and $0.87 \cdot 10^{-4}$ K^{-1} (Sn). Values of α used in the calculation are $3.8 \cdot 10^{-4}$ K^{-1} (Cs), $1.2 \cdot 10^{-4}$ K^{-1} (Ga), $1.6 \cdot 10^{-4}$ K^{-1} (Hg), $1.25 \cdot 10^{-4}$ K^{-1} (In), $2.9 \cdot 10^{-4}$ K^{-1} (K), $2.57 \cdot 10^{-4}$ K^{-1} (Na), $3 \cdot 10^{-4}$ K^{-1} (Pb), $4.5 \cdot 10^{-4}$ K^{-1} (Rb) and $1.11 \cdot 10^{-4}$ K^{-1} (Sn).

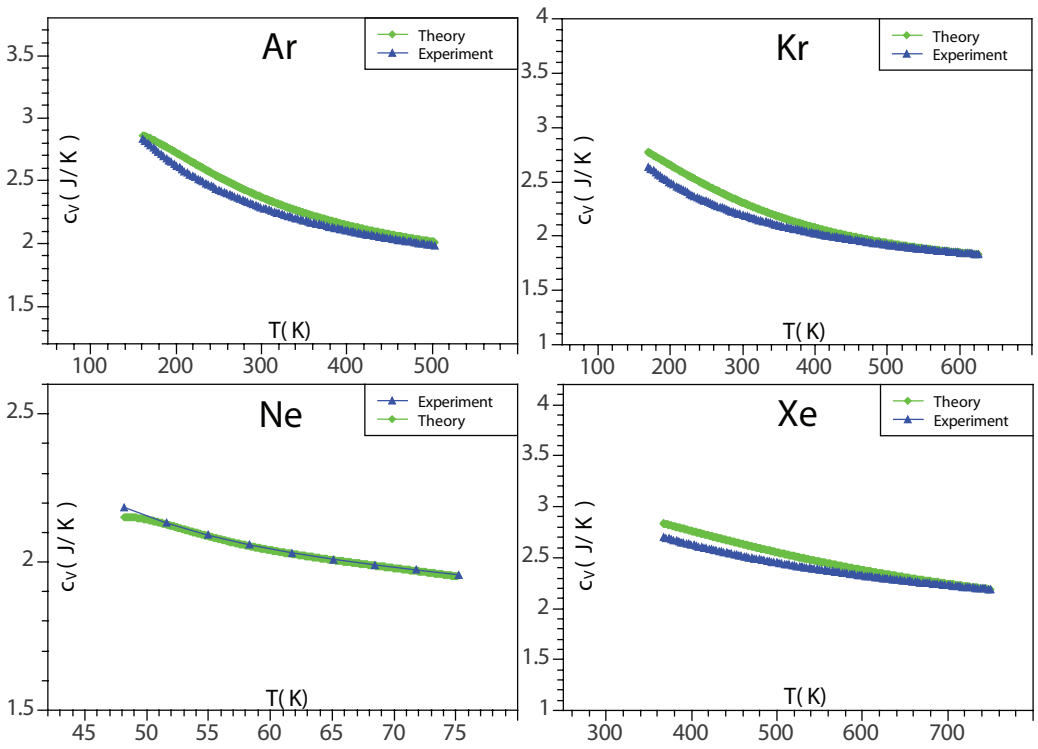

Figure 3.2: Experimental and calculated c_v for noble liquids. Experimental c_v and η are taken from the NIST database [4] at pressures 378 MPa (Ar), 200 MPa (Kr), 70 MPa (Ne), and 700 MPa (Xe). Values of τ_{D} used in the calculation are 0.5 ps (Ar), 0.67 ps (Kr), 0.31 ps (Ne) and 0.76 ps (Xe). Values of G_∞ are 0.18 GPa (Ar), 0.23 GPa (Kr), 0.12 GPa (Ne) and 0.45 GPa (Xe). Experimental values of α calculated from the NIST database at the corresponding pressures above are $3.6 \cdot 10^{-4}$ K^{-1} (Kr), $7.7 \cdot 10^{-3}$ K^{-1} (Ne) and $4.1 \cdot 10^{-4}$ K^{-1} (Xe). Values of α used in the calculation are $1.3 \cdot 10^{-3}$ K^{-1} (Kr), $6.8 \cdot 10^{-3}$ K^{-1} (Ne) and $3.6 \cdot 10^{-4}$ K^{-1} (Xe). For Ar, calculating c_v in harmonic approximation ($\alpha = 0$) gives good fit to experimental c_v.

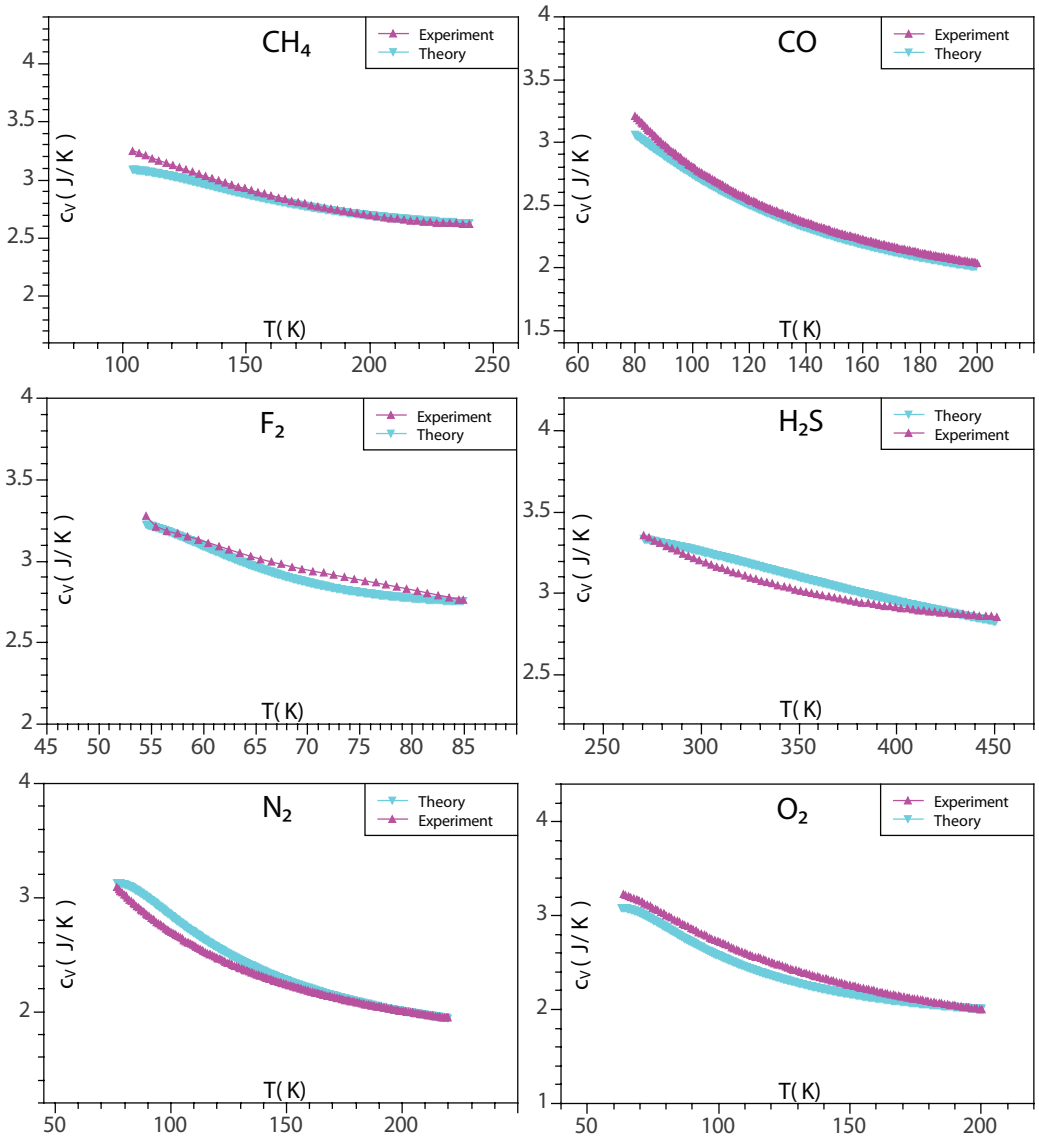

Figure 3.3: Experimental and calculated c_v for molecular liquids. Experimental c_v and η are taken from the NIST database [4] at pressures 50 MPa (CH_4), 55 MPa (CO), 0.1 MPa (F_2), and 170 MPa (H_2S), 65 MPa (N_2) and 45 MPa (O_2). Experimental η for F_2 is from Ref. [14]. Values of τ_D used in the calculation are 0.44 ps (CH_4), 0.55 ps (CO), 0.71 ps (F_2), 0.65 ps (H_2S), 0.38 ps (N_2) and 0.46 ps (O_2). Values of G_∞ are 0.1 GPa (CH_4), 0.11 GPa (CO), 0.23 GPa (F_2), 0.15 GPa (H_2S), 0.14 GPa (N_2) and 0.22 GPa (O_2). Experimental values of α calculated from the NIST database at the corresponding pressures above are $3.1 \cdot 10^{-3}$ K^{-1} (CH_4), $4.1 \cdot 10^{-3}$ K^{-1} (CO), $4.31 \cdot 10^{-3}$ K^{-1} (F_2), $1.2 \cdot 10^{-3}$ K^{-1} (H_2S), $3.9 \cdot 10^{-3}$ K^{-1} (N_2) and $4.4 \cdot 10^{-3}$ K^{-1} (O_2). Values of α used in the calculation are $1.4 \cdot 10^{-3}$ K^{-1} (CH_4), $5.5 \cdot 10^{-3}$ K^{-1} (CO), $4.31 \cdot 10^{-3}$ K^{-1} (F_2), $6.5 \cdot 10^{-4}$ K^{-1} (H_2S), $3.9 \cdot 10^{-3}$ K^{-1} (N_2) and $4.4 \cdot 10^{-3}$ K^{-1} (O_2).

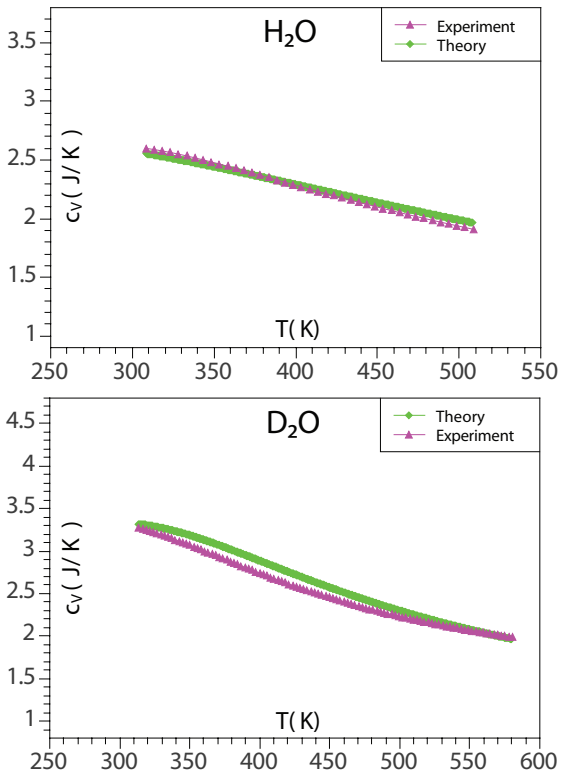

Figure 3.4: Experimental and calculated c_v for H_2O and D_2O. Experimental of c_v and η are taken from the NIST database [4] at pressures 150 MPa (H_2O) and 80 MPa (D_2O). Values of τ_D used in the calculation are 0.15 ps (H_2O) and 0.53 ps (D_2O). For D_2O, experimental α calculated from the NIST database at the corresponding pressure above is $9.4 \cdot 10^{-4}$ K^{-1}, and α used in the calculation is $1.1 \cdot 10^{-3}$ K^{-1}. For H_2O, calculating c_v in harmonic approximation ($\alpha = 0$) gives good fit to experimental c_v.

Liquid	η_0	A, K	T_0, K
Cs	$0.09 \cdot 10^{-3}$	659.8	-24
Ga	$0.66 \cdot 10^{-3}$	287	37
Hg	$0.6 \cdot 10^{-3}$	235	40
In	$0.4 \cdot 10^{-3}$	668	-2.6
K	$0.81 \cdot 10^{-3}$	427	112
Na	$1.3 \cdot 10^{-3}$	360	154
Pb	$0.67 \cdot 10^{-3}$	576	181
Rb	$0.09 \cdot 10^{-3}$	604	4
Sn	$0.4 \cdot 10^{-3}$	949.9	-30.6
Ar	$0.18 \cdot 10^{-3}$	260	42
Kr	$0.12 \cdot 10^{-3}$	170	2
Ne	$0.03 \cdot 10^{-3}$	24	36
Xe	$0.26 \cdot 10^{-3}$	330	20
CH_4	$0.05 \cdot 10^{-3}$	125	55
CO	$0.05 \cdot 10^{-3}$	46	36
F_2	$0.15 \cdot 10^{-3}$	23	43
H_2S	$0.08 \cdot 10^{-3}$	259	121
N_2	$0.04 \cdot 10^{-3}$	50	52
O_2	$0.07 \cdot 10^{-3}$	42	42
H_2O	$0.06 \cdot 10^{-3}$	308	69
D_2O	$0.07 \cdot 10^{-3}$	230	214

Table 3.1: VFT parameters (see Eq.2.3.3) of 21 liquids, including noble, metallic, molecular and hydrogen-bonded network liquids.

configurational term and $c^{rot} = \frac{3R}{2}$ subtracted further as discussed above. As for other molecular liquids above, the resulting c_v represents heat capacity per molecule. Due to the approximate way in which the configurational contribution is treated for H_2O and D_2O, the agreement between the experimental and calculated c_v should be viewed as qualitative, in contrast to the quantitative agreement for the rest of liquids considered.

Experimental and calculated c_v for 21 noble, metallic, molecular and hydrogen-bonded network liquids are shown in Figures 3.1–3.4. Figures 3.1–3.4 make one of the central points of this Chapter: the proposed phonon theory of liquids gives fairly good agreement with experimental data.

Importantly, calculated c_v depends on ω_{D}, α and G_∞ (see Eq. (3.1.4)) which are adjusted to fit the experimentally measured c_V. $\tau_{\mathrm{D}} = \frac{2\pi}{\omega_{\mathrm{D}}}$ used in the calculation (see the captions in Figures 3.1–3.4) are consistent with the known values that are typically in the 0.1–1 ps range [17, 18]. For monatomic liquids, τ_{D} were taken as experimental τ_{D} in corresponding solids. Similarly, the difference between experimental α and α used in the calculation is within 30% on average. Finally, G_∞ used in the calculation are on the order of GPa typically measured [17, 18].

3.3 Discussion

We first note that some of the considered liquids are in the quantum regime at low temperature. Taking T as the lowest temperature in Figures 3.1–3.4 and $\omega_{\rm D} = \frac{2\pi}{\tau_{\rm D}}$, where $\tau_{\rm D}$ are given in the caption of Figure 3.1–3.4, we find that $\frac{\hbar\omega_{\rm D}}{T}$ for various liquids varies in the range 0.1–3. Consequently, some liquids can be described by classical approximation fairly well, whereas others can not (for example, $\frac{\hbar\omega_{\rm D}}{T} > 1$ for Ne, O_2, N_2, F_2, CH_4 and CO), implying progressive phonon excitation with temperature increase.

We observe that c_v decreases with temperature in Figures 3.1–3.4. There are two main competing effects that contribute to c_v in Eq. (3.1.4). First, temperature increase results in the increase of $\omega_{\rm F} = \frac{2\pi}{\tau}$. Consequently, c_v decreases as a result of the decreasing number of shear waves that contribute to liquid energy and c_v. Second, c_v increases with temperature due to progressive phonon excitation as discussed above. The first effect dominates in the considered temperature range, and the net effect is the decrease of c_v with temperature seen in Figure 3.1. We further observe that c_v changes from approximately 3 to 2, showing a universal trend across a wide range of liquids. This can be understood by noting that at low temperature, $\left(\frac{\omega_{\rm F}}{\omega_{\rm D}}\right)^3$ and the second term in the last bracket in Eq. (3.1.4) are small, giving c_v close to 3 that includes the contribution from the anharmonic term. At high temperature when $\omega_{\rm F} \approx \omega_{\rm D}$ and Debye functions are close to 1, the term in the last bracket in Eq. (3.1.4) is 2, giving $c_v \approx 2$.

We note that on further temperature increase, c_v decreases from $2k_{\rm B}$ to its gas value of $1.5k_{\rm B}$ [4]. This is related to the progressive disappearance of longitudinal phonons.

The decrease of c_v seen in Figures 3.1–3.4 does not need to be generic. Indeed, when the phonon excitation dominates at low temperature, as in the case of strongly quantum liquids such as H_2 or He, c_v increases with temperature [4]. This will be discussed in the next Chapter.

Good agreement between theoretical and calculated c_v makes several important points. First, it is interesting to revisit the statement that liquid energy can not be calculated in general form because interactions are both strong and system-specific [2]. In the proposed phonon theory of liquids, this difficulty does not arise because strong interactions are treated from the outset as in the theory of solids.

Second, the proposed phonon theory of liquids has an advantage over the previous approach where liquid potential energy is calculated from correlation functions and interatomic interactions [2, 19–22]. Starting from the earlier proposals [23], this approach was developed in several directions (see, e.g., Refs. [2, 19, 24–27]), and can be used to calculate the energy of simple liquids where interactions are pair and short-ranged and correlations are two-body as is the case in, for example, noble liquids or hard-sphere

models. The calculations become intractable in general case [19, 26], particularly when interactions and correlations become complex (e.g., many-body) as in the liquids discussed above, precluding the calculation of c_v in this approach. On the other hand, if the phonon states of the liquid depend on τ only as proposed by Frenkel [1], the liquid energy and c_v depend implicitly on τ only, even though correlation functions and interatomic interactions may affect both c_v and τ in a complex way. Then, the relationship between c_v and τ becomes fairly simple (see Eq. (3.1.4)) and explains the experimental behavior of a wide class of liquids, both simple and complex.

The last assertion is important for a general outlook at liquids: despite their apparent complexity, understanding their thermodynamics may be easier than previously thought. Indeed, we have good understanding of thermodynamics and c_v in solids based on phonons no matter how complicated interactions or structural correlations in a solid are. Our current results suggest that the same can apply to liquids.

Bibliography

[1] J. Frenkel, Kinetic Theory of Liquids (ed. R. H. Fowler, P. Kapitza, N. F. Mott, Oxford University Press, 1947).

[2] L. D. Landau and E. M. Lifshitz, Statistical Physics (Nauka, Moscow 1964).

[3] K. Trachenko and V. V. Brazhkin, Phys. Rev. B **83**, 014201 (2011).

[4] http://webbook.nist.gov/chemistry/fluid.

[5] G. Grimvall, Phys. Scr. **11**, 381 (1975).

[6] D. C. Wallace, Phys. Rev. E **57**, 1717 (1998).

[7] D. Bolmatov and K. Trachenko, Phys. Rev. B **84**, 054106 (2011).

[8] C. M. Carlson, H. Eyring and H. Ree, Proc. Natl. Acad. Sci. USA **46**, 649 (1960).

[9] E. N. da C. Andrade and E. R. Dobbs, Proc. R. Soc. London, Ser. A **211**, 12 (1952).

[10] M. F. Culpin, Proc. Phys. Soc. B **70**, 1069 (1957).

[11] K. E. Spells, Proc. Phys. Soc. **48**, 299 (1936).

[12] A. V. Grosse, Science **147**, 1438 (1965).

[13] F. A. Kanda and R. P. Colburn, Physics and Chemistry of Liquids **1**, 159 (1968).

[14] G. W. Elverum and R. N. Doescher, J. Chem. Phys. **20**, 1834 (1952).

[15] D. Eisenberg and W. Kauzmann, The structure and properties of water (Oxford University Press, 2005).

[16] O. Mishima and H. E. Stanley, Nature **396**, 329 (1998).

[17] W. C. Pilgrim, S. Hosokawa, H. Saggau, H. Sinn and E. Burkel, J. Non-Cryst. Sol. **250-252**, 96 (1999).

[18] T. Bodensteiner, Chr. Morkel, W. Gläser and B. Dorner, Phys. Rev. A **45**, 5709 (1992).

[19] N. H. March, Liquid Metals (Cambridge University Press, Cambridge, UK, 1990).

[20] J. M. Ziman, Models of Disorder (Cambridge University Press, Cambridge, UK, 1979).

[21] J. L. Barrat and J. P. Hansen, Basic Concepts for Simple and Complex Liquids (Cambridge University Press, Cambridge, 2003) .

[22] J. P. Hansen and I. R. McDonald, Theory of Simple Liquids (Amsterdam, Boston, Elsevier, 2007).

[23] M. Born and H. S. Green, Proc. Royal Soc. London A **188**, 10-18 (1946).

[24] J. L. Lebowitz and J. K. Percus, J. Math. Phys. **4**, 116 (1963).

[25] W. A. Curtin and N. W. Ashcroft, Phys. Rev. A **32**, 2909 (1985).

[26] Y. Rosenfeld, Phys. Rev. A **33**, 2025 (1986).

[27] D. Bolmatov, J. Stat. Phys. **137**, 765-773 (2009).

CHAPTER 4

HELIUM AT ELEVATED PRESSURES: QUANTUM LIQUID WITH NON-STATIC SHEAR RIGIDITY

4.1 Liquid Helium

The liquid helium problem can be conveniently divided into two parts, a problem in statistical mechanics and a problem in hydrodynamics. The problem in statistical mechanics is essentially a many body problem, in which the interactions between the atoms can not be ignored and the symmetry of the wave-functions plays a dominate role. An analogous situation is encountered in heavy nuclei and has received so much attention in recent years [1]. In the case of liquid He^4, Landau has proposed a scheme of elementary excitations (or spectrum of energy levels) which is able to explain the thermodynamic properties, and Feynman has derived a wave-function which gives this scheme of excitations. We are therefore far advanced in our understanding of the thermodynamic nature of the liquid, and, although it is still necessary to justify our ideas by rigorous solution of the wave-mechanical problem of a large number of interacting helium atoms. On another hand, the detailed behaviour of the liquid helium at elevated pressures and temperatures is still not well understood, but the possible solution of the problem will lead to a better understanding of co-operative phenomena in general.

An interesting aspect of the situation is that He^3 differs from He^4 mainly because He^3 atoms require antisymmetric wave-functions. Experimentally, liquid He^3 shows none of the unusual properties of liquid He^4 and therefore presents a separate problem of its own.

Helium is the most difficult of all the permanent gases to liquefy. This is a consequence of the weakness of the attractive forces between helium atoms, for condensation into a liquid can occur only when the forces holding the liquid together are strong enough to overcome the disruptive influence of thermal agitation. This is the case for helium only if the temperature is within a few degrees of the absolute zero. The critical temperature is 5.20° K.

The He^4 atom is a particularly simple, stable and symmetrical structure. The nu-

cleus contains two protons and two neutrons and has no resultant angular momentum or magnetic moment. The two extra-nuclear electrons completely fill the innermost shell and, being so close to the nucleus, are firmly bound. The atom has no electric or magnetic dipole moment and its electric polarizability is very small. We might therefore expect the helium atom to be the nearest approximation to the hard spheres of classical kinetic theory and liquid helium might seem the simplest liquid to investigate in order to discover the fundamental properties of the theory of the liquid state. In actual fact the behaviour of liquid helium at elevated pressures and supercritical temperatures is so remarkable that it presents an intriguing problem which is unique in physical theory. The reason for this is almost certainly connected with the possibility that certain quantum effects are able to manifest themselves at such pressures and temperatures.

4.2 Thermodynamic Properties of Liquid ^{4}He

The investigation of the properties of helium has been one of the most prolific endeavors since its discovery (in 1868) [2–4]. Liquid helium is a quantum liquid at low temperatures and quantum effects play a crucial role. Considerable interest is still focused on the highly unusual properties of helium especially at low temperatures and the study of the properties of liquid ^{4}He continues to be an active area of condensed matter research [5–9].

Theory has been long drawn to study the condensed isotopes of helium and their mixtures because these liquids are model many-body systems but with fundamental quantum-statistical differences; they are fertile proving grounds for various quantum many-body formalisms. As Landau emphasized [10], these systems are amenable to theoretical attack because, when studied at relatively low temperatures, they are only weakly excited from their ground states. A description in terms of weakly interacting elementary excitations is then appropriate. The heat capacity of liquid helium has been discussed on just such a basis of elementary excitations and to describe it below the critical temperature Landau suggested two classes of elementary excitations, phonons or quanta of longitudinal compressional waves and rotons [10]. The latter are still not completely well understood. The consideration of non-static shear phonon contributions to the energy spectrum of liquid helium has been largely ignored simply because it was not clear whether liquids are actually capable of supporting transverse or shear modes. But according to Frenkel's proposition a liquid should support transverse modes provided the frequency ω is larger than the Frenkel frequency ω_{F}.

Nevertheless the idea that at least longitudinal phonons could be excited below 0.5 K has traditionally been taken as the explanation for the observation that the heat capacity of liquid helium varies as T^3 [11]. In most cases investigations have been limited

to narrow ranges of temperature and pressure which were of immediate concern in early experiments. Therefore, it is interesting to examine the thermodynamic properties of liquid helium both at elevated pressures, but still in a liquid phase, and also in wider ranges of temperature.

Accordingly in this Chapter we present the heat capacity of bosonic liquid helium as determined within in the framework of a phonon theory of liquids. The physical picture of elementary excitations is clarified by means of a study of phonon contributions, both longitudinal-like and transverse-like, to the energy spectrum of liquid helium at elevated pressures. From the analysis of experimental data of viscosity and heat capacity [12] and theoretical calculations, we find that liquid helium remains quantum at elevated pressures for a broad temperature range, yet is able to maintain solid-like shear waves.

4.3 The Phonon Theory of Liquid ^{4}He

The phonon theory of liquids allows us to calculate liquid internal energy in general form which can be compactly presented as

$$E = NT\left(1+\frac{\alpha T}{2}\right)\left(3D\left(\frac{\hbar\omega_{\mathrm{D}}}{T}\right)-\left(\frac{\omega_{\mathrm{F}}}{\omega_{\mathrm{D}}}\right)^3 D\left(\frac{\hbar\omega_{\mathrm{F}}}{T}\right)\right) \tag{4.3.1}$$

where $D(x) = \frac{3}{x^3}\int\limits_0^x \frac{z^3 \mathrm{d}z}{\exp(z)-1}$ is the Debye function [13], α is the thermal expansion coefficient, N is the number of phonon states, T is the temperature, and ω_D and ω_F are Debye and Frenkel frequencies correspondingly.

Eq.(4.3.1) accounts for longitudinal and also for two high-frequency shear modes with frequency $\omega > \frac{1}{\tau}$. It originates at the same level of approximation as Debye's phonon theory of solids by using the quadratic density of states. The result for a harmonic solid follows from Eq.(4.3.1) when $\omega_F = 0$, corresponding to infinite relaxation time, and thermal expansion coefficient $\alpha = 0$. This theory of liquids incorporates the effects of anharmonicity and thermal expansion, which is very important not only for classical liquids such as Hg and Rb [14], but also for liquid helium as we can see further.

4.4 Heat Capacity of Liquid ^{4}He

Accordingly we now take a derivative of energy E (Eq.(4.3.1)) with respect to temperature T at constant volume and compare it to experimental data of heat capacity per atom: $c_V = \frac{1}{N}\frac{dE}{dT}$. We have used the National Institute of Standards and Technology (NIST) database [12] that contains data for many chemical and physical quantities,

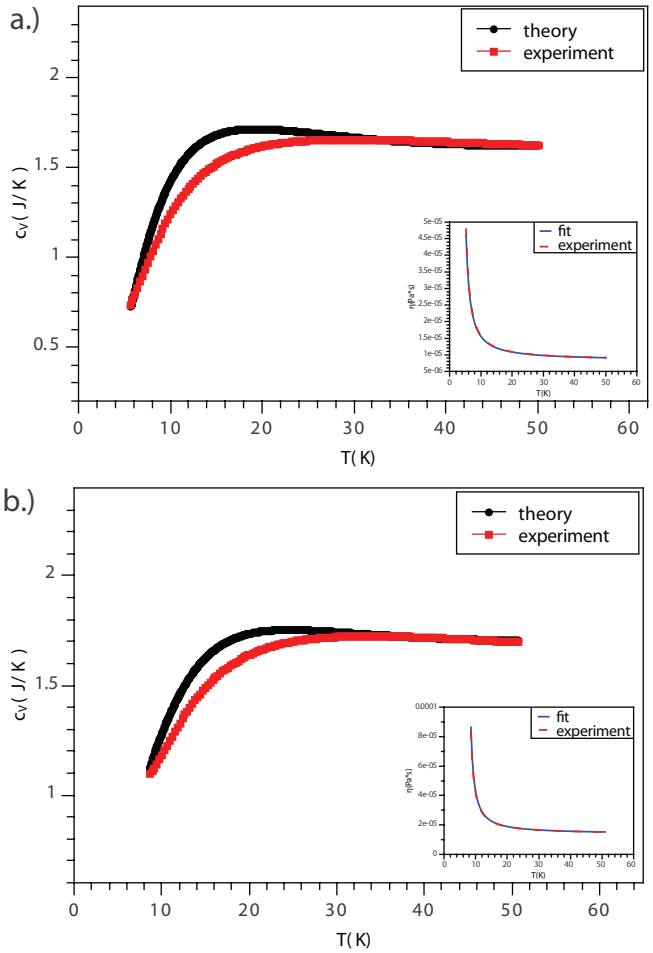

Figure 4.1: Experimental and calculated c_v, experimental and interpolated η (insets) for liquid helium. Experimental c_V and η are taken from the NIST database at pressures 20 MPa (Fig. 4.a) and 45 MPa (Fig. 4.b). Values of τ_D used in the calculation are 1.41 ps (^{4}He at 20 MPa) and 1.40 ps (^{4}He at 45 MPa). Values of G_∞ are 0.0070 GPa and 0.0074 GPa. Experimental values of α calculated from the NIST database at the corresponding pressures above are $8.7 \cdot 10^{-3}$ K^{-1} and $8.3 \cdot 10^{-3}$ K^{-1}. Values of α used in the calculation are $3 \cdot 10^{-3}$ K^{-1} and $2.8 \cdot 10^{-3}$ K^{-1}. The uncertainty of both experimental heat capacities and viscosities is about 5-10% [12]. VFT parameters (see Eq.2.3.3):a. P=20 MPa, $\eta_0 = 8.2 \cdot 10^{-5}$, $A = 4.8$ K and $T_0 = 2.5$ K; b. P=45 MPa, $\eta_0 = 0.07 \cdot 10^{-5}$, $A = 5.6$ K and $T_0 = 6$ K.. Insets also show viscosity fits.

including c_V for liquid helium. We aimed to check our theoretical calculations in a wider range of temperature, and therefore selected the data at pressures significantly exceeding the critical temperature and pressure of liquid helium ($T_c = 5.1953$ K and $P_c = 0.22746$ MPa) where it exists in a liquid form in the broader temperature range. As a result, the temperature range in which we calculate c_V is about 40-45 K. Viscosity data was taken from the same database [12], and fitted in order to use in Eq.(4.3.1) to calculate c_V. We used the Vogel-Fulcher-Tammann (VFT) expression to fit the viscosity data: $\eta = \eta_0 \exp A/(T - T_0)$. To calculate c_V from Eq.(4.3.1), we have taken viscosity data at the same pressures as c_V and converted it to τ using the Maxwell relationship $\tau = \frac{\eta}{G_\infty}$, where the Frenkel frequency can be conveniently expressed as $\omega_F = \frac{2\pi}{\tau} = \frac{2\pi G_\infty}{\eta}$.

Eq.(4.3.1) has no non-physical parameters, because the parameters ω_D, α and G_∞ are fixed by system properties. Values of these parameters used in Eq.(4.3.1) are in a good agreement with typical experimental values. There is a difference between the experimental α and the α used in the calculation. At each pressure the experimental α was estimated from the formula $\alpha = \frac{1}{V}\frac{\Delta V}{\Delta T}$. Experimentally, V$\propto$T only approximately. Consequently, we approximated V=V(T) by a linear dependence (an approximation results in somewhat different α used in Eq.(4.3.1)). Further, $\tau_D = \frac{2\pi}{\omega_D}$ used in the calculation (see the caption in Fig. 4.1) is consistent with the known values for low temperature liquid helium under pressure that are typically in the 1-2 ps range [15]. The uncertainty of both experimental heat capacities and viscosities is about 5-10% [12].

4.5 Discussion

As noted earlier, there are two basic analytical approaches to calculate liquid energy and heat capacity: from the gas phase and from the solid. The approach from the classical gas phase has two main contributions to liquid energy; kinetic and potential parts and can be presented as

$$E = K + \int gU dV \tag{4.5.1}$$

where K is kinetic energy, g is normalized correlation function and U is the interatomic energy. Generally the expression in Eq.(4.5.1) is difficult to evaluate for a many-body systems and it is not clear how to rigorously incorporate quantum effects at elevated temperatures (say tens of Kelvins for He) into Eq.(4.5.1). To describe the behaviour of c_V on the basis of Bose-Einstein condensation (BEC) in liquid helium at low temperatures was originally initiated by F. London [16]. The heat capacity of BEC varies

as $T^{3/2}$ at low temperatures and must pass through a maximum. This maximum has the character of a cusp which appears at critical temperature T_c and it has nothing to do with a subsidiary maximum which liquid helium possesses at elevated pressures and higher temperatures (see Fig. 4.1).

The odd behaviour of the heat capacity of liquid helium at elevated pressures can now be explained in the framework of the phonon theory of liquids. When we calculate liquid energy and heat capacity in this theory the problem of strong interactions is avoided from outset because it is included in the phonon energy.

On the basis of agreement of Eq. 4.3.1 and experimental c_V we predict that transverse waves exist in liquid helium at high pressures. This prediction can be verified in a future high-pressure experimental work. The experimental data for heat capacity and viscosity of liquid helium confirms our hypothesis [12]. At elevated pressures liquid helium persists at temperatures which are 3-5 times lower than Debye's temperature (see Fig.4.1). As the temperature is raised in liquid helium, more longitudinal and transverse-like phonons become progressively excited and therefore the heat capacity rapidly grows, which is very abnormal for ordinary liquids studied earlier [17]. Thus liquid helium at this P-T region persists as a quantum liquid and also as a solid-like liquid with non-static shear rigidity, similar to classical liquids. When the Debye and the Frenkel temperatures become roughly comparable, c_V of liquid helium enters the saturation region ('hump'). Further increase of temperature then leads to the dissipation of transverse-like waves and c_V of liquid helium becomes shallow (see Fig.4.1), implying that at very high temperatures c_V reaches its asymptotic value 3/2.

The results just presented appear to be fairly accurate over the temperature range of experimental importance, despite the fact that the formal expression for liquid internal energy is quite trivial (see Eq.(4.3.1)). The agreement is somewhat worse at intermediate part (the slight maximum or 'hump' region mentioned earlier) of the c_V curve, however the maximal difference between the calculated and experimental values is actually comparable to the experimental uncertainty of c_V, namely of 0.1-0.2 J/K [12]. But this can also be attributed to an oversimplified form of the Debye spectrum of phonon-like states used in our analysis.

Liquid helium in its normal state and at atmospheric pressure is actually above the conditions of the Frenkel line (see the diagram [18]) and barely supports transverse-like elementary excitations. At significant pressures (around 10 GPa) liquid helium quite resembles the other noble-gas liquids; there are transverse-like excitations but at its melting temperature almost all phonons are already excited. This state of liquid helium is rigid but not quantum. Here we are suggesting an interesting intermediate pressure range of 5 MPa-500 MPa where liquid helium near melting temperature is

already solid-like but is still significantly quantum.

Bibliography

[1] M. Warda, M. Centelles, X. Vinas, X. R.-Maza, Acta Phys. Polonica B **43** 2012.

[2] H. N. V. Temperley, Proc. Phys. Soc. A **65**, 619 (1952).

[3] I. Prigogine, Adv. Phys. **3**, 131 (1954).

[4] A. D. B. Woods and R. A. Cowley, Rep. Prog. Phys. **36**, 1135 (1973).

[5] P. M. Platzman, M. I. Dykman, Science **284**, 1967 (1999).

[6] K. Nauta, R. E. Miller, Science **287**, 293 (2000).

[7] G. P. Bewley, D. P. Lathrop and K. R. Sreenivasan, Nature **441**, 588 (2006).

[8] D. Konstantinov, K. Kono, Phys. Rev. Lett. **103**, 266808 (2009).

[9] J. M. McMahon, M. A. Morales, C. Pierleoni, and D. M. Ceperley, Rev. Mod. Phys. **84**, 1607 (2012).

[10] L. Landau, J. Phys. U.S.S.R. **5**, 71 (1941).

[11] R. P. Feynman, Phys. Rev. **91**, 1301 (1953).

[12] http://webbook.nist.gov/chemistry/fluid.

[13] L. D. Landau and E. M. Lifshitz, Statistical Physics (Nauka, Moscow 1964).

[14] D. Bolmatov and K. Trachenko, Phys. Rev. B **84**, 054106 (2011).

[15] H. J. Maris and S. Balibar, J. Low Temp. Phys. **147**, 539 (2007).

[16] F. London, Nature **141**, 643 (1938).

[17] D. Bolmatov, V. V. Brazhkin, and K. Trachenko, Sci. Rep. **2**, 421 (2012).

[18] V. V. Brazhkin, Yu. D. Fomin, A. G. Lyapin, V. N. Ryzhov, and K. Trachenko, Phys. Rev. E **85**, 031203 (2012).

CHAPTER 5

THERMODYNAMIC BEHAVIOUR OF SUPERCRITICAL MATTER

5.1 Supercritical State

The discovery of what we now call the critical point came about with Cagniard de la Tour's experiments with Papin's digester. In 1822, in the context of his interests in acoustics, he placed a flint ball in a digester partially filled with liquid. Upon rolling the device, a splashing sound was generated as the solid ball penetrated the liquid-vapour interface [1]. Cagniard de la Tour noticed that upon heating the system the splashing sound ceased above a certain temperature and pressure. This marks the discovery of the supercritical fluid phase. In this phase there is no surface tension as there is no liquid-gas phase boundary. The supercritical fluid can dissolve matter like a liquid and can diffuse through solids like a gas.

Although the properties of supercritical fluids are well known, they are as yet not fully exploited for industrial applications. The density of a pure supercritical fluid is easily changed by relatively small variations in pressure and temperature. In many cases, release of pressure drastically decreases temperature owing to the Joule-Thomson effect, which induces effects on phase behavior that can be the basis for many practical applications. The surface tension of a supercritical fluid is essentially non-existent. Diffusivity is high, which in combination with low viscosity induces interesting transport phenomena in condensed phases.

When very near to the critical point, fluids exhibit substantial deviations from normal behavior. Making use of these phenomena is difficult because control of process conditions to 1 °C or 0.1 MPa is not easy to maintain. Furthermore, supercritical fluids are generally applied with other components to create at least a binary system that is far from the binary critical point. Supercritical fluids influence the properties of components with which they are mixed. Supercritical fluids dissolve substantially in condensed phases and are able to dissolve compounds far beyond their vapor pressure. Solubility in gaseous and condensed phases is one of the main useful supercritical fluid properties. The surface tension of liquids also decreases drastically with the amount of dissolved supercritical fluid, which enables mixtures containing supercritical fluids to

move freely in small pores and tiny structures.

Well-known industrial applications of supercritical fluids to the extraction of natural materials include the decaffeination of coffee and tea, the defatting of cacao, and the production of extracts from hops, fruits, spices, nuts, and other natural materials; these processes are well documented elsewhere [2]. Although the development of supercritical fluid chromatography for production on the preparative scale was successful, its transfer to industrial processes has not yet been reported. Enhanced oil recovery with carbon dioxide has been a promising application for 35 years and may contribute to carbon capture and storage.

5.2 Computer Simulations

5.2.1 Methods of computer simulations

In the past decades, computer "experiments" have come to play a major role in liquid state physics. Their importance, from the theorist's point of view, rests on the fact that they provide essentially exact, quasi-experimental data on well-defined models. As there is no uncertainty about the form of the interaction potential, theoretical results can be tested unambiguously in a manner that is generally impossible with data obtained in experiments on real liquids. It is also possible to obtain information on quantities of theoretical importance that are not readily measurable in the laboratory. In this section, we give a brief account of how a computer simulation can be carried out, and discuss some of the limitations as well as the advantages of the method.

The behaviour of liquids, solids and dense gases can be simulated at the molecular level in different ways, by Molecular Dynamics or by Monte Carlo method. In a conventional Molecular Dynamics calculation, a system of N particles (atoms, molecules or ions) is placed within a cell of fixed volume, frequently cubic in shape. A set of velocities is also assigned, usually drawn from a Maxwell-Boltzmann distribution appropriate to the temperature of interest and selected in such a way as to make the net linear momentum equal to zero. The subsequent trajectories of the particles are then calculated by integration of the classical equation of motion. The particles are assumed to interact through some prescribed force law and the bulk of the computational labour is concerned with the calculation at every step of the forces acting on each particle. The coordinates and momenta of the particles are usually on the computer cluster for later analysis, and thermodynamic and other properties are obtained as time averages over the dynamical history of the system.

5.2.2 Molecular dynamics simulations

Molecular Dynamics simulations, first introduced by Alder and Wainright in 1956, is a standard simulation method in computational statistical physics. By solving the classical equations of motion for a system of big number of molecules numerically on a computer, the phase space trajectory of the system is generated over many thousands, up to millions, of time steps. These time periods correspond to some picoseconds up to some microseconds of real time. At every simulated time step, the instantaneous properties of the system are calculated by their corresponding molecular expressions and stored on a hard disk. Subsequently, macroscopic properties of the system are calculated by analyzing the stored data. This chapter describes the implementation of the simulation software and details of the simulations carried out in this work. Furthermore, the influence of the simulation parameters on the results is discussed and results for thermodynamic state variables of the Lennard-Jones model fluid are presented. Detailed descriptions of the molecular simulation methodology are given in the books.

In this Chapter, we have used DL-POLY molecular dynamics simulation code [3] to run the system with 64000 atoms in the constant-volume (nve) ensemble at different temperatures. We have used 3000 processors of the high-throughput cluster to simulate 500 temperature points in the temperature range of about 0–12000 K shown in Figure 7.1. We have used the model Lennard-Jones potential [4] to simulate model liquids. Each structure was equilibrated for 25 ps, and the system energy and other properties were averaged for the following 25 ps of the production run. The timestep of 0.001 ps was used.

5.3 Thermodynamics of Supercritical Phase

In recent years, a significant effort has been devoted to investigation of various properties of supercritical fluids [5–9]. This has been an exciting field with a long history since 1822 when Baron Charles Cagniard de la Tour discovered supercritical fluids while conducting experiments involving the discontinuities of the sound in a sealed cannon barrel filled with various fluids at high temperature [10]. More recently, supercritical fluids have started to be deployed in several important applications. Much of the excitement and interest of the past decade is due to the enormous progress made in increasing the power of relevant experimental tools [11–14]. The development of new experimental methods and improvement of existing ones continues to play a important role in this field [16–20, 22], with recent research focusing on dynamic properties of fluids [22–26].

High density and high thermal motion are two main properties responsible for ef-

ficient cleaning, dissolving and extracting abilities of supercritical fluids in the above industrial applications. From the point of view of practical applications, supercritical fluids have got the best of both worlds: high density comparable to ordinary liquids and solids and high thermal motion and diffusivity approaching that of gases. Notably, it is this very combination that presents a formidable problem to the theory: high density and strong interactions mean that theories and approximations used for dilute gases do not apply [27]. Early Enskog and related kinetic approaches to gases were followed by more extensive developments, yet they do not adequately describe dense systems with strong interactions and many-body correlations [27] such as supercritical fluids. One general issue with extending gas-like approaches to fluids was noted earlier: in a system with strong interactions, the system energy strongly depends on the type of interactions, and is therefore system-specific, ruling out the possibility to develop a theory universally applicable to many fluids, in contrast to gases and solids [1].

In addition to theoretical challenges, the lack of fundamental understanding is seen as an obstacle towards wider deployment of supercritical fluids in industrial applications, primarily due to the absence of guidance regarding pressure and temperature at which the desired properties are optimized as well as the possibility to use new systems [8].

In this Chapter, we focus on the thermodynamic properties of the supercritical state. On the basis of molecular dynamics simulations, we find that specific heat shows a crossover between two different dynamic regimes of the low-temperature rigid liquid and high-temperature non-rigid gas-like fluid. The crossover challenges the currently held belief that no difference can be made between a gas and a liquid above the critical point and that the supercritical state is homogeneous in terms of physical properties [1]. We subsequently formulate a theory of system thermodynamics and heat capacity above the crossover. In this theory, energy and heat capacity are governed by the minimal length of the longitudinal mode in the system only, and do not depend on system-specific structure and interactions.

5.3.1 Frenkel Line

Standard ways to distinguish two phases of matter show no difference at high pressures and temperatures because it is believed that no differences between gases and liquids exist above the critical point. But a look at a medium's microscopic behaviour makes it possible to discriminate between liquid and gas everywhere on a phase diagram. Along with solids, liquids and gases are the most common aggregate states of matter. It does not take a scientist to distinguish among them and, in particular, to tell the difference between a liquid and a gas; it is enough to point to partially filled and empty glasses. And yet an attempt to introduce a rigorous physical distinction between the

two phases raises subtle issues.

At first glance, it seems that numerous quantitative distinctions separate gases from liquids. To name just two, gas densities and viscosities are many times smaller than those of liquids. Those and other distinctions, however, depend strongly on temperature and pressure, and the quantitative distinctions cease to hold near the critical point, the abrupt terminus of the line separating liquid and gas. Indeed, as illustrated in Figure 5.1, the system can be continuously changed from liquid to gas along a phase-space path that goes around the critical point, but quantitative properties would not reveal just where the change from one phase to the other takes place. For that reason textbooks may report that distinguishing between liquid and gas beyond the critical point is impossible. But it is possible as it can be seen further.

A typical (T ,P) diagram (see Fig. 5.1) implies that a liquid is separated from a gas by the boiling line ending at the critical point. The diagram further implies that only one single state, customarily called "supercritical fluid", exists for all pressures and temperatures above the critical point. On the other hand, an important qualitative change in a fluid behavior takes place on crossing the Frenkel line (see Fig. 1) [31]. Importantly, this dynamical line extends for arbitrary values of pressure and temperature above the critical point.

Frenkel provided a microscopic description of Maxwell phenomenological visco-elastic theory of liquid flow by introducing liquid relaxation time τ: τ is the average time between two consecutive atomic jumps in a liquid at one point in space. Each jump can approximately be viewed as a jump of an atom from its neighboring cage into a new equilibrium position with subsequent cage relaxation. These atomic jumps give a liquid its ability to flow. The relaxation time τ is a fundamental flow property of a liquid, and it defines liquid viscosity η and diffusion coefficient D. This implies that the motion of an atom in a liquid consists of two types: quasiharmonic vibrational motion around an equilibrium position as in a solid and diffusive motion between two neighboring positions where typical diffusion distances exceed vibrational distances by about a factor of 5-10. Therefore, atomic motion in a liquid combines both elements of the short-amplitude vibrational motion as in a solid and the large-amplitude ballistic-collisional motion as in a gas. One should mention that Frenkel's ideas were discussed and used for the past 20 years by Wallace [3] and Chisolm and Wallace [4] to calculate the thermodynamic and dynamic properties of a liquid.

The value of τ decreases with temperature increase, spanning many orders of magnitude. On the other hand, the minimal (Debye) vibration period, τ_0 ($\tau_0 \approx$0.1-1 ps), is weakly temperature dependent and is mostly defined by interactions in a given system. At certain high temperatures, the solid-like vibration character ceases. This point is

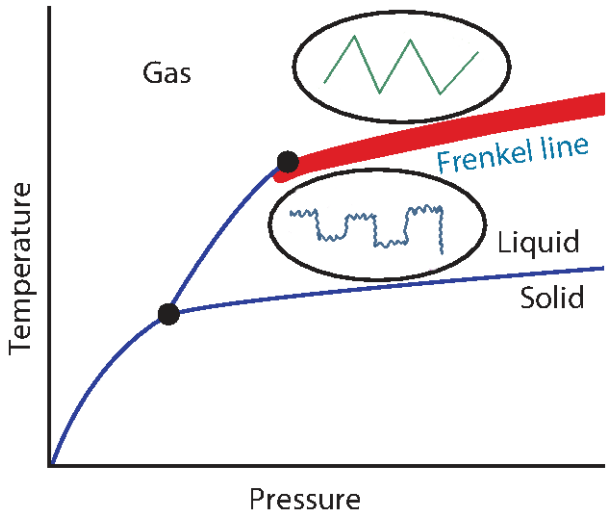

Figure 5.1: The Frenkel line separates systems with liquid-like and gas-like properties. The two inset plots show particle position as a function of time. The particle motion in the liquid below the line combines both small-amplitude vibrational motion as in a solid and large-amplitude, ballistic-collisional motion as in a gas. As illustrated above the Frenkel line, particle motion in a gas is purely ballistic–collisional.

reached when τ becomes comparable to τ_0: $\tau \approx \tau_0$. The sign of the approximate equality means that the values can differ by tens of percent. In the following discussion, we consider τ as the average time it takes an atom to move the average inter-particle distance d. Then, τ quantifies the motion envisaged by Frenkel where an atom jumps distance a during time τ between two equilibrium positions at low temperatures as well as the motion at high temperatures where two equilibrium positions are absent altogether and the motion between collisions is ballistic as in a gas.

The Frenkel line separates a rigid liquid where solid-like shear waves exist and the diffusion regime is jump-like and is activated as in a solid from a non-rigid gas-like fluid where no shear modes exist and diffusion is collisional as in a gas [31].

When a system is brought across the Frenkel line, many of its key properties are altered. But those changes lack the sharp, thermodynamically anomalous character of the changes in a system traversing the liquid-gas phase transition line. The ability of liquids to flow, which is associated with their zero shear rigidity distinguishes liquids from solids. Liquids, however, actually have zero rigidity only at small frequency; if a shear stress is applied at high enough frequency, a liquid will support that stress. But above the Frenkel line, the system simply cannot sustain rigidity at any frequency: it behaves like a gas. The loss of rigidity is accompanied by a reduction of the constant-volume specific heat to $2k_{\mathrm{B}}$ per particle; that reduction corresponds to the potential energy of shear modes becoming zero. Furthermore, viscosity, the speed of sound, and

thermal conductivity all decrease with increasing temperature below the Frenkel line, as in liquids, but increase with temperature sufficiently above the line, as in gases. The behavior of the diffusion constant crosses over from exponential temperature dependence below the Frenkel line, as in liquids, to power-law dependence above the line, as in gases.

Considerations of particle dynamics do more than help distinguish liquids from gases. They also shed light on why liquids are so difficult to describe theoretically. The dynamics suggest that solids and gases are pure states of matter in the sense that dynamics in solids are purely oscillatory and dynamics in gases are purely ballistic and collisional. Physically, the different behaviors arise because in solids the kinetic energy of particles is much smaller than the energy barriers between various potential minima and in gases it is the other way around. The dynamics of a liquid, on the other hand, involves both oscillations and ballistic motions, and the relative contributions of the two types of motion gradually change in response to external parameters. To a large degree, it is this mixed dynamical state that has been responsible for the difficulty in constructing a theory of liquids.

5.3.2 Dynamic crossover of the specific heat

We start with molecular dynamics simulations of a model liquid. Our primary aim here is to show that specific heat, c_V, shows a crossover in the supercritical region of the phase diagram. This result is unexpected in view of currently perceived homogeneity of supercritical state in terms of physical properties.

Using molecular dynamics simulations, we have simulated the binary (two types of atoms have been used in the system) Lennard-Jones (LJ) fluid. We have simulated the system with 64000 atoms using constant-volume (nve) ensemble in the wide temperature range (see Fig.5.2) well extending into the supercritical region. Indeed, the temperature range in Figure 5.2 is between about $2\mathrm{T_c}$ and $70\mathrm{T_c}$, where $\mathrm{T_c}$ is the critical temperature of Ar, $\mathrm{T_c} \approx 150$ K; the simulated density, 2072 kg m^{-3}, corresponds to approximately four times the critical density of Ar. From the energy of the system E at each temperature, we calculate constant-volume specific heat, c_V, as $c_V = \frac{1}{N}\frac{dE}{dT}$ ($k_\mathrm{B} = 1$).

We observe that c_V decreases steeply from the solid-state value of about $3k_\mathrm{B}$ at low temperature to approximately $2k_\mathrm{B}$ around 2000 K. The steep decrease is followed by crossing over to a considerably weaker temperature dependence. This crossover is a new effect not reported in previous MD simulations. We further observe that the crossover takes place around $c_V \approx 2k_\mathrm{B}$. This value of c_V, $c_V = 2k_\mathrm{B}$ is non-coincidental, and corresponds to the crossover taking place across the Frenkel line [30, 31] as discussed below.

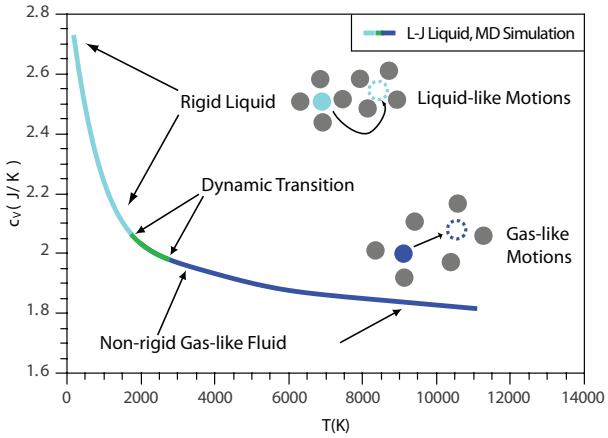

Figure 5.2: **Heat capacity of binary Lennard-Jones fluid**. Calculated c_V showing the crossover and continuous dynamical transition around $c_V \approx 2$, ($k_B = 1$). The crossover takes place between different dynamical regimes of the rigid liquid and non-rigid supercritical fluid.

Crossing the Frenkel line corresponds to the qualitative change of atomic dynamics in a liquid. In liquids, atomic motion has two components: a solid-like, quasi-harmonic vibrational motion about equilibrium locations and diffusive gas-like jumps between neighboring equilibrium positions. As the temperature increases, a particle spends less time vibrating and more time diffusing. Eventually, the solid-like oscillating component of motion disappears; all that remains is the gas-like ballistic motion. That disappearance, a qualitative change in particle dynamics, corresponds to crossing the Frenkel line, the transition of the substance from the liquid dynamics to the gas dynamics. This transition takes place when liquid relaxation time τ (τ is liquid relaxation time, the average time between consecutive atomic jumps at one point in space [5]) approaches its minimal value, τ_D, the Debye vibration period. As recently discussed [30, 31], crossing the Frenkel line is accompanied by qualitative changes of most important properties of the system, including diffusion, viscosity, thermal conductivity and dispersion curves [30, 31]. One of these properties is the crossover of the speed of sound and appearance of the high-frequency "fast" sound [14, 33–35]. At the microscopic level, the Frenkel line can be identified by the loss of oscillations in the velocity autocorrelation function [31], a point studied in detail elsewhere.

Fig. 5.2 implies that in addition to the dynamic properties discussed above, the thermodynamics of the system changes at the Frenkel line too. This is an important general insight regarding the behavior of the supercritical state.

The initial steep decrease of c_V from about $3k_B$ to $2k_B$ can be quantitatively explained by the progressive loss of two transverse waves with frequency $\omega > 1/\tau$ [36–38].

Physically, this picture is based on Frenkel's prediction that on time scale shorter than τ, liquid is a solid, and therefore supports rigidity and solid-like transverse waves at short times, or at frequency larger than $\omega > 1/\tau$ [39]. When τ approaches its maximal value, τ_{D}, the liquid can not sustain transverse waves at any frequency [40]. Consequently, the potential energy of the system is due to the longitudinal mode only, giving the total energy of $2NT$ and specific heat of $2k_{\mathrm{B}}$ [36, 38]. Hence, the decrease of c_V from about $3k_{\mathrm{B}}$ to $2k_{\mathrm{B}}$ corresponds to the region of a "rigid" liquid where short-time solid-like rigidity and high-frequency transverse waves exist. On the other hand, the liquid is unable to sustain transverse waves at any available frequency above the Frenkel line. Instead, the liquid enters a new dynamic "non-rigid" gas-like regime where oscillatory component of particles is lost and the motion becomes purely collisional as in a gas.

We therefore need to develop a new theory capable of describing thermodynamics of supercritical matter above the Frenkel line where the system enters the new dynamic regime and where c_V falls below $2k_{\mathrm{B}}$ and approaches the ideal-gas value of $3/2k_{\mathrm{B}}$ at high temperature (see Fig. 5.2).

5.3.3 Thermodynamics of supercritical state above Frenkel line

We now focus on the theory of the non-rigid gas-like liquid above the Frenkel line, and add a new proposal regarding how the system energy can be evaluated. As temperature rises in the ballistic gas-like regime and kinetic energy increases, the mean free path l, the average distance between particle collisions, increases at the constant pressure. At the Frenkel line where the ballistic regime starts, l is comparable to interatomic separation. In the limit of high temperature where the particle's kinetic energy is much larger than potential energy, l tends to infinity as in the non-interacting ideal gas. Our proposal is that l determines the shortest wavelength of the longitudinal mode that exists in the system, λ, because below this length the motion is purely ballistic and therefore can not be oscillatory: $\lambda = l$. On the other hand, the longitudinal modes with larger wavelength are supported, and represent the excitations existing in the supercritical system.

We note that the existence of long-wavelength longitudinal waves in a gas, sound, is well-known. What is new here is that we propose that the contribution of the longitudinal waves to the energy of the gas-like supercritical system starts from very short wavelengths comparable with interatomic separation a. In this sense, we are extending the solid state concepts (e.g. short-wavelength solid-like phonons with Debye density of states, see below) to the new area of gas-like supercritical state where these ideas have not been hitherto contemplated. Indeed, it is well established experimentally that dynamics in sub-critical liquids shows solid-like character, in that liquids can sustain high-frequency propagating modes down to wavelengths on the atomic scale, with solid-

like dispersion relations [40]. Importantly, recent experimental evidence shows that the same applies to supercritical fluids [14, 41].

Here and elsewhere, our discussion of liquid vibrational states includes an important point. Namely, a disordered system such glass or liquid supports non-decaying collective excitations obtainable from the secular equation involving the force matrix constructed from the amorphous glass or liquid structure. Harmonic plane waves naturally decay in liquids as in any non-crystalline systems, yet importantly they are clearly seen in fluids experimentally as quasi-linear solid-like dispersion relations even in low-viscous liquids [22, 23, 40], leading to the quadratic density of states $g(\omega) \propto \omega^2$. A detailed discussion of this point is forthcoming.

In the proposed theory, the energy of the non-rigid supercritical fluid per particle includes the contribution from the kinetic energy, $K = \frac{3}{2}k_{\mathrm{B}}T$ and the potential energy of the longitudinal phonons with wavelengths larger than l. Using the equipartition theorem $\langle P_l \rangle = \frac{\langle E_l \rangle}{2}$, where $\langle E_l \rangle$ is the energy of the longitudinal phonons, we write

$$E = \frac{3}{2}k_{\mathrm{B}}T + \frac{1}{2}\int_0^{\omega_0} \varepsilon(\omega, T)g(\omega)d\omega + E_{anh} \tag{5.3.1}$$

where the upper integration limit ω_0 is given by the shortest wavelength in the system, λ: $\omega_0 = \frac{2\pi}{\lambda}c$, c is the speed of sound, $\varepsilon(\omega, T)$ is the mean energy of harmonic oscillator, $\varepsilon(\omega, T) = \frac{\hbar\omega}{2} + \frac{\hbar\omega}{e^{\hbar\omega/T}-1}$, or $\varepsilon(T) = k_{\mathrm{B}}T$ in the classical case, and E_{anh} is the anharmonic contribution to the phonon energy.

The second term in Eq. (5.3.2) can be calculated using the Debye density of states, $g(\omega) \equiv \frac{3}{\omega_{\mathrm{D}}^3}\omega^2$, giving $k_{\mathrm{B}}T\frac{\omega^3}{\omega_{\mathrm{D}}^3}$, or $k_{\mathrm{B}}T\frac{a^3}{\lambda^3}$, where a is the interatomic separation. The use of the quadratic density of states is supported by the experimental evidence showing solid-like quasi-linear dispersion relationships in supercritical fluids [14, 41] similar to the subcritical liquids. E_{anh} can be evaluated in the Grüneisen approximation from the softening of phonon frequencies with temperature, with the result that the energy is modified as $E \to E\left(1 + \frac{\alpha T}{2}\right)$, where α is the coefficient of thermal expansion [37, 38]. Then, the energy of non-rigid gas-like supercritical fluid becomes:

$$E = \frac{3}{2}k_{\mathrm{B}}T + \left(1 + \frac{1}{2}\alpha T\right)\frac{1}{2}k_{\mathrm{B}}T\frac{a^3}{\lambda^3} \tag{5.3.2}$$

We observe that when $\lambda \approx a$ at the Frenkel line, Eq. (5.3.2) gives $E = 2k_{\mathrm{B}}T$ and the specific heat of 2 (here we neglect the small term $\propto \alpha T$). This corresponds to the crossover of c_V in Figure 5.2 to the gas-like regime as discussed above. When λ increases

on temperature increase in the gas-like regime, Eq. (5.3.2) predicts that c_V tends to $\frac{3}{2}$, the ideal-gas value as expected.

5.3.4 Comparison with experimental data

As discussed above, λ is given by the particle mean free path in the non-rigid gas-like regime, and can therefore be calculated from $\eta = \frac{1}{3}\rho\bar{u}\lambda$, where η is viscosity, ρ is density and $\bar{u}$ is average velocity. Therefore, Eq. (5.3.2) provides an important relationship between the energy of the non-rigid supercritical liquid and its gas-like viscosity. We now check this relationship experimentally, by comparing the specific heat $c_V = \frac{dE}{dT}$ calculated from Eq. (5.3.2) and the experimental c_V.

We have used the National Institute of Standards and Technology (NIST Chemistry WebBook, http://webbook.nist.gov/chemistry/fluid) database. We aimed to check our theoretical calculations and selected the isochoric data of several supercritical noble and molecular liquids in a wide range of temperature and density. We note that λ in Eq. (5.3.2) changes in response to both temperature and density: λ increases with temperature and decreases with density. Practically, the range of isochoric data in the NIST database is fairly narrow in terms of density compared to the range of temperature. We therefore analyze the temperature behavior of c_v and η along several isochores. Our choice of liquids is dictated by the availability of isochoric data in the supercritical region. For each density, we fit experimental viscosity, using software package XMGR, to

$$\eta = A_0 + A_1 T^{A_2} \tag{5.3.3}$$

and calculate λ from $\eta = \frac{1}{3}\rho\bar{u}\lambda$ and subsequently use λ in Eq. (5.3.2) to calculate c_V. Parameters ρ, $\bar{u}$, a, A_0, A_1 and A_2 we summarized in Table 5.1.

We note that Debye model is not a good approximation in molecular liquids where the frequency of intra-molecular vibrations considerably exceeds the rest of frequencies in the system (3340 K in N_2 and 3572 K in CO). However, the intra-molecular modes are not excited in the temperature range of experimental c_V (see Figures 5.4–5.5). Therefore, the contribution of intra-molecular motion to cv is purely rotational, c^{rot}. On the other hand, the rotational motion is excited in the considered temperature range, and is therefore classical, giving $c^{rot} = R$ for linear molecules in N_2 and CO. Consequently, c_V for molecular liquids shown in Figure 5.5 correspond to heat capacities per molecule, with c^{rot} subtracted from the experimental data.

We also note that experimental isochoric c_V is affected by lambda-like critical anoma-

Fluid	ρ, kg/m^3	a, $\mathring{A}$	$\bar{u}$, m/s	A_0,	A_1,	A_2
Ne	550	4.2	500	9.18×10^{-6}	8.76×10^{-7}	0.47
Ne	700	4.1	516	1.72×10^{-5}	7.01×10^{-7}	0.49
Ar	700	5.8	400	1.3×10^{-5}	1.8×10^{-6}	0.52
Ar	900	5.1	415	4.1×10^{-5}	7.9×10^{-7}	0.61
Kr	1000	4.1	470	1.4×10^{-5}	1.5×10^{-6}	0.57
Kr	1200	4.7	485	2.7×10^{-5}	1.3×10^{-6}	0.58
Xe	1300	5.2	435	1.3×10^{-5}	2.9×10^{-6}	0.49
Xe	1700	5.3	450	7.4×10^{-6}	1.5×10^{-5}	0.29
CO	350	6.1	400	2.3×10^{-5}	1.1×10^{-7}	0.83
N_2	320	4.6	420	5.4×10^{-6}	8.0×10^{-7}	0.59

Table 5.1: Viscosity parameters A_0, A_1 and A_2 used in Eq. 5.3.3. Parameters ρ and $\bar{u}$ were taken from NIST database to calculate energy in Eq. 5.3.2. We have varied interatomic separation parameter a around its experimental values to fit experimental c_V.

lies (see Figs. 5.2, 5.3) because the isochoric NIST data do not extend far above the critical point. Here, we do not consider critical effects related to phase transitions, and therefore fit the data at temperatures that are high enough not to be affected by the lambda-anomaly at the phase transition. In Figures 5.3 and 5.4 we observe good agreement between experimental and fitted c_V, in view of (a) 2-5% uncertainty of experimental c_V and η (see NIST Chemistry WebBook), (b) approximations introduced by the Debye model and (c) increased curvature of c_V at low temperature due to proximity of lambda-anomalies that are not taken into account by the theory.

5.3.5 Power law

Here, we study supercritical exponents of specific heat and viscosity. If η in the non-rigid gas-like supercritical region can be approximated as a power law, $\eta \propto T^{\gamma}$, then Eq. (5.3.2) makes two relationships. First, E and c_V should also follow power laws. Second, Eq. (5.3.2) provides a specific relationship between the scaling exponents of η on one hand and E and c_V on the other hand.

Studying the supercritical scaling exponents is interesting in the wider context of scaling behavior of physical properties. In the area of phase transitions, the scaling behavior idea has been a crucial element in the subject of liquids and other systems from the nineteenth century onwards [43]. Critical points occur in a great variety of systems [11, 44, 45, 47], yet there is a considerable degree of similarity in the way in which systems approach the critical point [48].

Temperature dependences of η, $\bar{u}$, E and c_V can be fairly well approximated by the

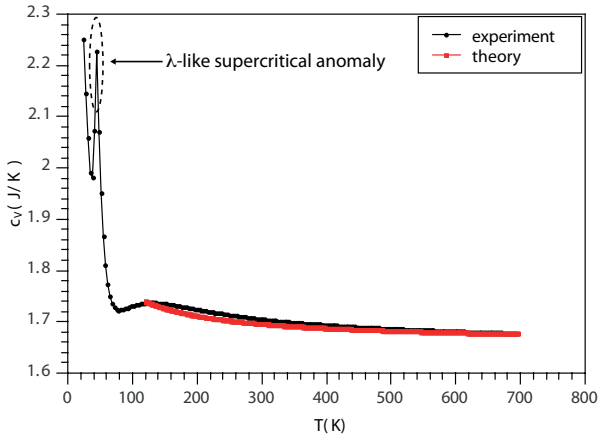

Figure 5.3: **Heat capacity of liquid Ne**. Experimental and calculated c_V ($k_\mathrm{B} = 1$) for non-rigid supercritical fluid Neon. Experimental c_V and η are taken from the NIST database at density 700 kg m^{-3}. Value of α used in the calculation is 3.5×10^{-3} K^{-1}.

power law above the Frenkel line. Therefore, we use the following power-law relationships:

$$\eta = const \times T^{\gamma} \tag{5.3.4}$$

$$\bar{u} = const \times T^{\frac{1}{2}} \tag{5.3.5}$$

$$E = 1.5 \times T + const \times T^{\delta} \tag{5.3.6}$$

$$c_V = 1.5 + \frac{const}{T^{\xi}} \tag{5.3.7}$$

From $\eta = \frac{1}{3}\rho\bar{u}\lambda$ ($k_\mathrm{B} = 1$), $\lambda = const \times T^{\gamma - 0.5}$. Using λ in Eq. (5.3.2) gives for the energy (neglecting the small $\propto \alpha T$ term):

$$E \propto T^{2.5-3\gamma} \tag{5.3.8}$$

and specific heat:

$$c_V \propto (2.5 - 3\gamma)T^{1.5-3\gamma} \tag{5.3.9}$$

Then, from Eqs. (5.3.4), (2.1.2) and (5.3.9) we find the following relationships between the power-law scaling exponents:

$$2.5 - 3\gamma = \delta \tag{5.3.10}$$

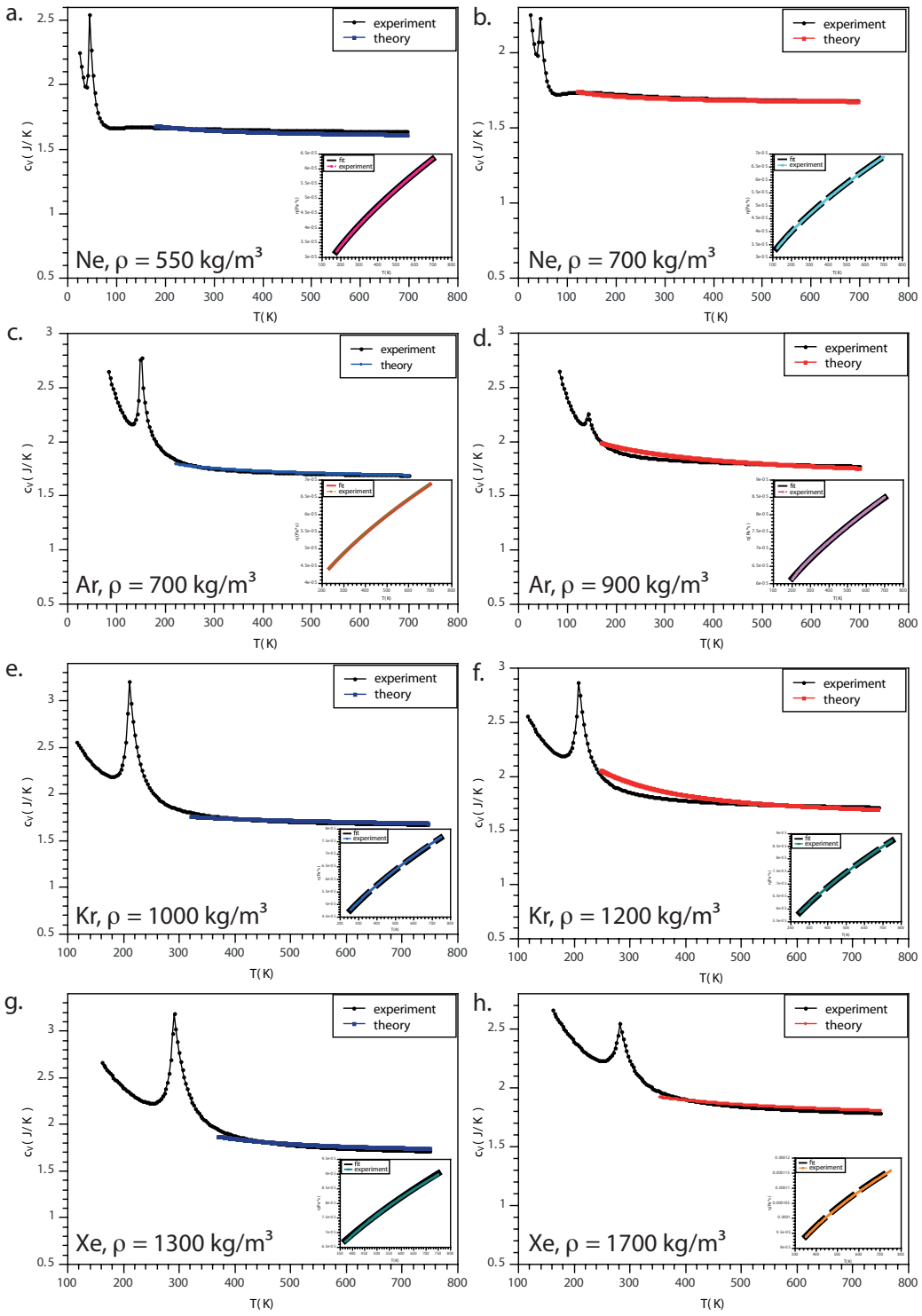

Figure 5.4: **Heat capacity of noble gas liquids**. Experimental and calculated c_V ($k_B = 1$) for noble non-rigid supercritical fluids. Experimental c_V and η are taken from the NIST database at different densities as shown in the Figure. Values of α used in the calculation are 3.5×10^{-3} K^{-1} (Ne), 3.3×10^{-3} K^{-1} (Ar), 1.8×10^{-3} K^{-1} (Kr) and 8.2×10^{-4} K^{-1} (Xe). The uncertainty of both experimental heat capacities and viscosities is about 2-5%. Insets show viscosity fits.

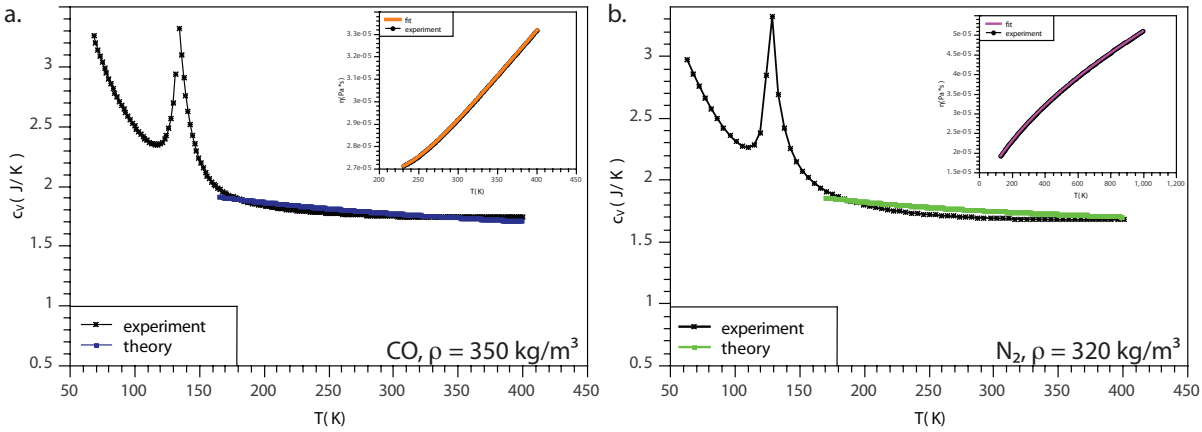

Figure 5.5: **Heat capacity of molecular liquids**. Experimental and calculated c_V ($k_B = 1$) for molecular non-rigid supercritical fluids. Experimental c_V and η are taken from the NIST database. Values of α used in the calculation are 6.5×10^{-3} K^{-1} (CO) and 8.5×10^{-3} K^{-1} (N_2). The uncertainty of both experimental heat capacities and viscosities is about 2-5%. Insets show viscosity fits.

$$3\gamma - 1.5 = \xi \tag{5.3.11}$$

We note that Eqs. (2.1.2) and (5.3.9), together with the general requirement for c_V to be positive and the experimental requirement for c_V to decrease with temperature, imply that γ should be in the range $\frac{1}{2} < \gamma < \frac{5}{6}$. We also note that $\gamma = \frac{1}{2}$ corresponds to the non-interacting ideal gas and $\eta \propto T^{0.5}$. Additionally, we note that the derived power laws for the supercritical region are valid for those systems where the term αT in expression for the total energy (see Eq. 5.3.2) can be ignored.

5.4 Discussion

Our first important observation in this work is that contrary to the current belief, the thermodynamic properties of the supercritical state are not homogeneous. Instead, the specific heat shows a crossover related to the change of particle dynamics, which we attributed to the recently introduced Frenkel line [31].

We have subsequently focused on thermodynamic properties of supercritical fluids above the Frenkel line. Here, we faced the problem of strong interactions, the long-persisting challenge in condensed matter physics. Indeed, strong interactions imply that approximations used for dilute gases do not apply to real dense liquids [27]. If we consider realistic strong interactions (assuming that interactions are known and can be represented in analytical form, the assumption that is valid for a relatively small

number of simple systems only) and structural correlations that often include those beyond two-body correlations, we quickly find that the problem becomes intractable. Further, strong interactions, coupled with their specificity in different systems, have been suggested to preclude the calculation of energy and heat capacity in general form from the outset [1].

In this Chapter, we addressed the problem in a different way, by substituting all potentially complicated effects of interactions and structural correlations by one physical quantity, the minimal wavelength of the longitudinal mode in the system λ. This has enabled us to rationalize the experimental behavior of c_V as well as provide the relationship between different physical properties and experimental outcomes (e.g. relationship between c_V and η). Notably, our approach unveils similarity of thermodynamics of supercritical state in the following sense. First, c_V does not explicitly depend on system details such as structure and interactions but on λ only. Fluids may have very different structure and interactions, yet our theory predicts the similarity of their thermodynamic behavior as long as λ behaves similarly in those systems. Second, and more specifically, our approach predicts that supercritical scaling of thermodynamic properties such as heat capacity is governed by viscosity scaling. Consequently, similar temperature scaling of viscosity gives similar temperature scaling of thermodynamic properties.

We note here that we have mostly dealt with systems with fairly simple interatomic interactions whereas the found similarity of thermodynamic behavior may not hold in systems with the hierarchy of interactions and non-trivial structural transformations such as water [49].

Bibliography

[1] G. Brunner, Annu. Rev. Chem. Biomol. Eng. **1**, 321 (2010).

[2] E. Kiran, P. G. Debenedetti and C. J. Peters, Supercritical Fluids: Fundamentals and Applications, NATO Science Series E: Applied Sciences 366 (Kluwer Academic Publishers, 2000).

[3] I. T. Todorov, B. Smith, M. T. Dove and K. Trachenko, DL-POLY-3: new dimensions in molecular dynamics simulations via massive parallelism. J. Mater. Chem. **16**, 1911 (2006).

[4] W. Kob and H. C. Andersen, Phys. Rev. Lett. **73**, 1376 (1994).

[5] J. Cowan and J. Cann, Nature **333**, 259 (1988).

[6] C. A. Eckert, B. L. Knutson and P. G. Debenedetti, Nature **383**, 313 (1996).

[7] R. Kessel, M. W. Schmidt, P. Ulmer and T. Pettke, Nature **437**, 724 (2005).

[8] E. Kiran, P. G. Debenedetti and C. J. Peters, Supercritical Fluids: Fundamentals and Applications, NATO Science Series E: Applied Sciences 366 (Kluwer Academic Publishers, 2000).

[9] J. McHardy and S. P. Sawan, Supercritical Fluid Cleaning: Fundamentals, Technology and Applications (Noyes Publications, 1998).

[10] B. Berche, M. Henkel, R. Kenna, J. Phys. Studies **13**, 3201 (2009).

[11] J. M. De Simone, Science **296**, 799 (2002).

[12] R. A. Pai, R. Humayun, M. T. Schulberg, A. Sengupta, J.-N. Sun, J. J. Watkins, Science **303**, 507 (2004).

[13] K. P. Johnston, P. S. Shah, Science **303**, 482 (2004).

[14] G. G. Simeoni, T. Bryk, F. A. Gorelli, M. Krisch, G. Ruocco, M. Santoro and T. Scopigno, Nat. Phys. **6**, 503 (2010).

[15] F. Sette, M. H. Krisch, C. Masciovecchio, G. Ruocco, G. Monaco, Science **280**, 1550 (1998).

[16] C. J. Fecko, J. D. Eaves, J. J. Loparo, A. Tokmakoff, P. L. Geissler, Science **301**, 1698 (2003).

[17] B. J. Siwick, J. R. Dwyer, R. E. Jordan, R. J. D. Miller, Science **302**, 1382 (2003).

[18] G. M. Whitesides, Nature **442**, 368 (2006).

[19] P. F. McMillan and H. E. Stanley, Nat. Phys. **6**, 479 (2010).

[20] P. S. Salmon, R. A. Martin, P. E. Mason, and G. J. Cuello, Nature **435**, 75 (2005).

[21] V. M. Giordano, G. Monaco, Proc. Natl. Acad. Sci. **107**, 21985 (2010).

[22] C. Fradin, A. Braslau, D. Luzet, D. Smilgies, M. Alba, N. Boudet, K. Mecke and J. Daillant, Nature **403**, 871 (2000).

[23] L. Berthier, G. Biroli, J.-P. Bouchaud, L. Cipelletti, D. El Masri, D. L'Hote, F. Ladieu, M. Pierno, Science **310**, 1797 (2005).

[24] C. P. Royall, D. G. A. L. Aarts and H. Tanaka, Nat. Phys. **3**, 636 (2007).

[25] S. Karmakar, S. Dasgupta and S. Sastry, Proc. Natl. Acad. Sci. **106**, 3675 (2009).

[26] E. Flenner and G. Szamel, Nat. Phys. **8**, 696 (2012).

[27] S. Chapman and T. G. Enskog, The mathematical theory of non-uniform gases (Cambridge University Press, 1995).

[28] L. D. Landau and E. M. Lifshitz, *Statistical Physics* (Nauka, Moscow 1964).

[29] J. L. Barrat and J. P. Hansen, Basic concepts for simple and complex liquids (Cambridge University Press, 2003).

[30] V. V. Brazhkin and K. Trachenko, Physics Today **65**(11), 68 (2012).

[31] V. V. Brazhkin, Yu. D. Fomin, A. G. Lyapin, V. N. Ryzhov and K. Trachenko, Phys. Rev. E **85**, 031203 (2012).

[32] J. Frenkel, Kinetic Theory of Liquids (ed. R. H. Fowler, P. Kapitza, N. F. Mott, Oxford University Press, 1947).

[33] F. Gorelli, et al. Phys. Rev. Lett. **97**, 245702 (2006).

[34] F. Bencivenga, et al., Phys. Rev. Lett. **98**, 085501 (2007).

[35] F. Bencivenga, et al., Europhys. Lett. **75**, 70 (2006).

[36] D. Bolmatov, V. V. Brazhkin and K. Trachenko, Sci. Rep. **2**, 421 (2012).

[37] K. Trachenko and V. V. Brazhkin, Phys. Rev. B **83**, 014201 (2011).

[38] D. Bolmatov and K. Trachenko, Phys. Rev B **84**, 054106 (2011).

[39] D. Bolmatov, V. V. Brazhkin and K. Trachenko, J. Appl. Phys. **113**, 103514 (2013).

[40] W. C. Pilgrim and C. Morkel, J. Phys.: Condens. Matter **18**, R585 (2006).

[41] H. E. Cunsolo, et al., J. Chem. Phys. **114**, 2259 (2001).

[42] S. Hosokawa, M. Inui, Y. Kajihara, et al., Phys. Rev. Lett. **102**, 105502 (2009).

[43] H. E. Stanley, Rev. Mod. Phys. **71**, S358 (1999).

[44] O. Mishima and Y. Suzuki, Nature **419**, 599 (2002).

[45] T. Senthil, A. Vishwanath, L. Balents, S. Sachdev, M. P. A. Fisher, Science **303**, 1490 (2004).

[46] Y. S. Elmatad, R. L. Jack, D. Chandler and J. P. Garrahan, Proc. Natl. Acad. Sci. **107**, 12793 (2010).

[47] H. Tanaka, T. Kawasaki, H. Shintani and K. Watanabe, Nat. Mat. **9**, 324 (2010).

[48] V. Holten and M. A. Anisimov, Sci. Rep. **2**, 713 (2012).

[49] L. B. Skinner, C. Huang, D. Schlesinger, L. G. M. Pettersson, A. Nilsson and C. J. Benmore, J. Chem. Phys. **138**, 074506 (2013).

CHAPTER 6

STRUCTURAL CROSSOVER IN THE SUPERCRITICAL MATTER

6.1 Introduction

It is currently believed that supercritical state is physically homogeneous, in the sense that moving along any path on a pressure and temperature phase diagram above the critical point does not involve any marked physical and structural changes but only monotonic variations of density, between the gas density and the density of the subcritical liquids [1–3]. The recent explosion of the new ways and applications where supercritical fluids are deployed has called for better fundamental understanding of the supercritical state of matter [2, 3]. This call is consistent with the ongoing effort in elucidating and understanding the structure and properties of disordered matter such as liquids and glasses [4–15].

The understanding of the liquid structure is crucial for all aspects of chemical physics, solution chemistry and the functioning of biological macromolecules. As well as being of inherent scientific interest, the link between the microscopic interactions, between small numbers of molecules, and the macroscopic properties of the bulk system comprising them is of great industrial relevance. Despite the great accuracy of the existing sophisticated approaches based on the solution of field equations or the generalised OZ equations, they are usually purely formal and give smooth temperature dependencies thus unable to predict the structural transformations or crossovers in fluids. The same was seen in extensive Molecular Dynamics (MD) simulations [16].

Debye first demonstrated that in the discussion of X-ray diffraction in liquids, one had to consider two atoms whose scattered rays interfere with one another, and as a result an interference pattern is obtained which depends crucially on the relative separation of the two atoms, or the Radial Distribution Function (RDF, $g(r)$) introduced below. While, in principle, $g(r)$ could be calculated from statistical mechanics, and hence the X-ray intensity patterns predicted, the major progress in understanding the structure of liquids has come from analysis of the X-ray (or neutron) data, to yield g(r).

In this Chapter, we demonstrate that the supercritical state is not structurally homogeneous as is currently believed, but that there is a well-defined structural crossover

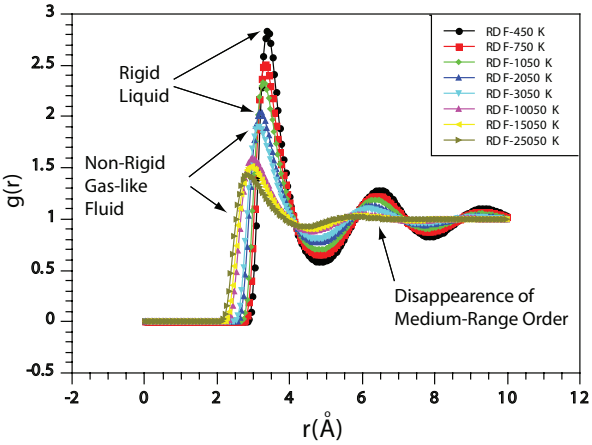

Figure 6.1: The radial distribution functions $g(r)$ of simulated one-component Lennard-Jones (LJ) supercritical fluid at different temperatures showing the disappearance of the medium-range order at high temperature.

instead. Our detailed analysis reveals the crossover between the structure with well-defined short- and medium-range order as in liquids and the random gas-like structure. We explain the origin of this crossover, and relate its origin to the change of dynamic and thermodynamics properties of the supercritical state above the Frenkel Line.

Using Molecular Dynamics (MD) simulations [17], we have simulated one-component Lennard-Jones (LJ) fluid fitted to Ar properties [18]. We have simulated the system with 32000 atoms using constant-volume (nve) ensemble in the very wide temperature range (see Figs. 6.1–6.3) well extending into the supercritical region. The temperature range in Figs.6.1–6.3 is between about $3T_c$ and $167T_c$, where T_c is the critical temperature of Ar, $T_c \simeq$150 K; the simulated density, 1880 kg/m^3, corresponds to approximately three times the critical density of Ar. A typical MD simulation lasted about 50 ps, and the properties were averaged over the last 20 ps of simulation, preceded by 30 ps of equilibration. The simulations at different temperature included 500 temperature points simulated on the high-throughput computing cluster. We calculate radial distribution function (RDF), average it over the last 20 ps of the simulation, and show its temperature evolution in Figure 6.2. We observe the decrease of the first peak of the RDF, and the near disappearance of the second and third peaks of RDFs, implying that the medium-range structure is no longer visible at high temperature.

6.2 Structural crossover in the supercritical region

To analyze temperature changes of RDF in more detail, we calculate the heights of the first and second peak of RDF, and plot these in Figure 6.3 as a function of

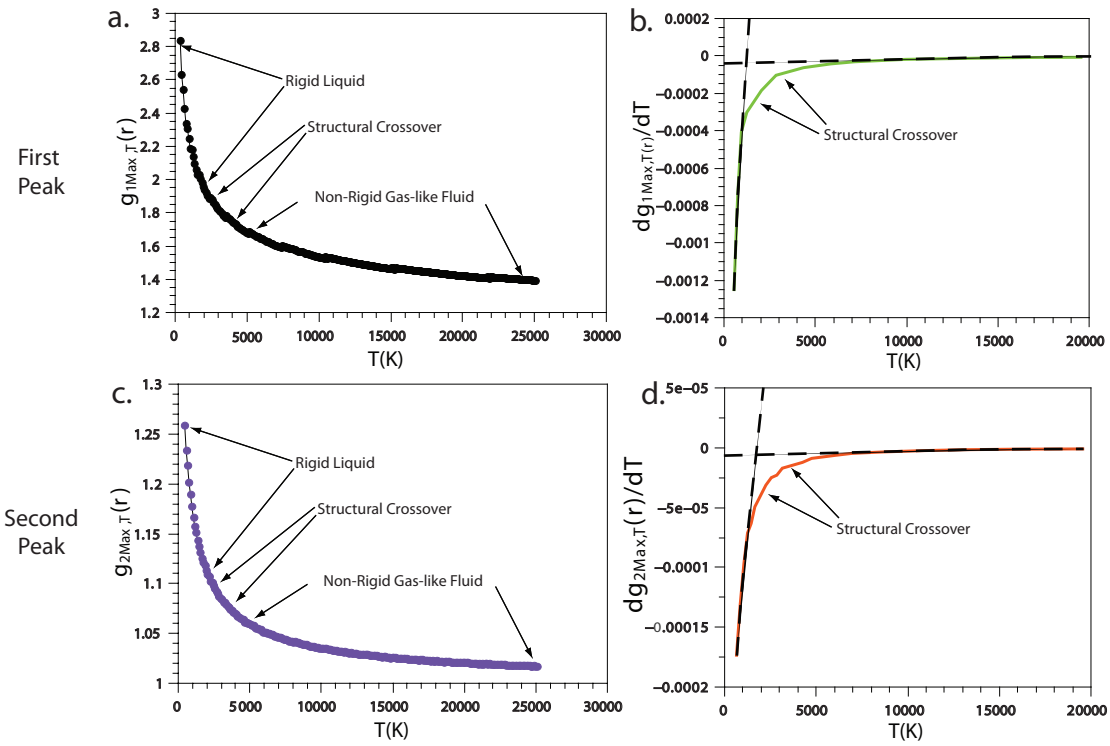

Figure 6.2: Evolution of the first and second peaks of RDF of the supercritical state with temperature (a,c) and their derivatives (b,d).

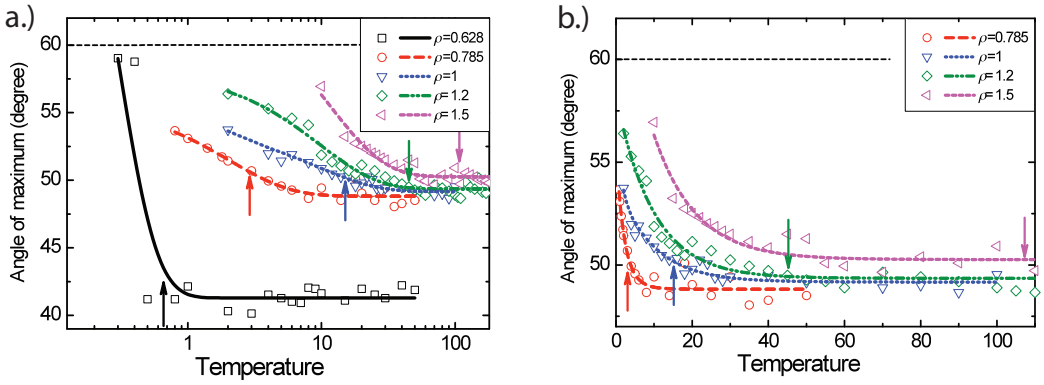

Figure 6.3: Evolution of α_m with temperature for different densities in the supercritical state. Density and temperature are in LJ units where $\rho = 1$ corresponds to 1880 kg/m^3 and $T = 1$ to 115 K for Ar.

temperature. We observe the steep decrease of both peaks at low temperature, followed by their flattening at high temperature, with the crossover between the two regimes taking place around 3000 K. To make the crossover more visible, in Figures 6.3.b and 6.3.d we plot the temperature derivative of the heights of both peaks. These plots clearly show two regimes corresponding to the fast and slow change of RDF peaks [27].

The structural crossover is further evidenced by the calculation of the bond angles. For each atom, we calculate the angle α_m between the "bonds" joining the atom with its two nearest neighbor atoms which, in turn, are the nearest neighbors of each other. For a range of different densities, we calculate α_m at different temperatures, and subsequently average it over time and different local configurations. In Figure 6.4, it is shown the temperature dependence of averaged α_m in re-scaled units of both density and temperature in order to compare the simulations at different density in one plot. Figure 6.4 shows the same trend as the heights of the RDF peaks above: the steep initial decrease of α_m from about 60 degrees (the characteristic angle in the face-centred cubic lattice), followed by flattening and constancy at high temperature.

We have repeated the same simulations in the constant pressure ensemble at various pressures, and have found the same crossover as the one shown in Figures 6.2–6.3, except the crossover temperature decreases. For example, at 3 GPa, the crossover operates in the temperature range of about 1500–2500 K. This is an important insight with regard of future experimental detection of the structural crossover in the supercritical state.

The structural crossover in the supercritical state is the new effect not hitherto anticipated, in view of the currently perceived homogeneity of the supercritical state [1–3]. We now address the origin of this crossover, and relate this origin to the changes of both dynamics and thermodynamics of the supercritical state.

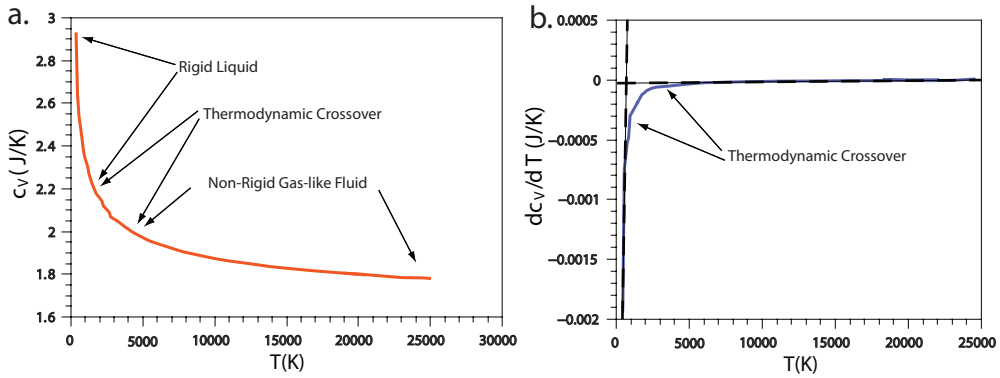

Figure 6.4: Calculated c_V showing the crossover and continuous thermodynamic transition around $c_V \simeq 2$, ($k_B = 1$). The crossover takes place between different dynamic regimes of the rigid liquid and non-rigid supercritical fluid. The thermodynamic crossover undergoes within 2000 K-4000 K temperature range granting the relationship between thermodynamic, dynamic and the structural crossover (see Figs. 6.2–6.4) correspondingly.

The structural crossover seen in Figures 6.3–6.4 can now be explained as follows. In the regime where $\tau \gg \tau_D$, particles oscillate for long time before jumping to the neighbouring quasi-equilibrium sites. This means that the short- and medium-range order similar to that present in amorphous systems such as glasses or viscous liquids is maintained during time τ. Consequently, the calculated RDF shows the correlations due to atomic packing in several spheres that extend beyond the short-range order as in subcritical liquids, as is seen in Figure 6.2 at low temperature. When τ approaches its minimal value of approximately τ_D, the oscillatory component of the motion is lost, and the dynamics becomes ballistic as in a gas. The gas-like configuration has qualitatively different structure with notably less constraints and structural correlations in the medium range, as is seen in Figure 6.2. As a result, the structural crossover witnessed by the RDF peaks is intimately related to the dynamic crossover at the Frenkel line.

Importantly, RDF peaks on both sides of the crossover are predicted to change differently with temperature in this picture. Indeed, in the rigid liquid regime, RDF peaks decrease rapidly due to the fast exponential decrease of τ and the accompanied decrease of particles located at similar distances. On the other hand, in the gas-like regime where the oscillatory motion and the medium-range order are no longer present, structural correlations are less sensitive to temperature increase because the dynamics is already randomized by ballistic motions as in a gas. The temperature dependence shown in Figure 6.3 is consistent with this picture. Taken together, the evidence presented in Figures 6.3–6.5 constitutes the relationship between the *structure and dynamics* of the supercritical state.

Phase	Structure	Dynamics
Solid	Medium and/or Long-Range Order	1-L+2-S Phonon Modes
Liquid	Medium and/or Short-Range Order	1-L+2-S ($\omega_s > \frac{1}{\tau}$) Phonon Modes
Ideal Gas	No Order	No Phonon Modes
Rigid Liquid	Medium-Range Order	1-L+2-S ($\omega_s > \frac{1}{\tau}$) Phonon Modes
Non-Rigid Gas-like Fluid	Short-Range Order	1-L Mode

Table 6.1: Structural and Dynamic properties of solids, liquids and gases, followed by two states in the supercritical region: Rigid Liquid and Non-Rigid Gas-like Fluid. L and S letters refer to longitudinal and shear modes.

Phase	$< E_{kin} >$, $k_{\mathrm{B}}NT$	$< E_{pot} >$, $k_{\mathrm{B}}NT$	C_V, $k_{\mathrm{B}}N$
Solid	$\frac{3}{2}$	$\frac{3}{2}$	3
Liquid	$\frac{3}{2}$	$\frac{3}{2} \rightarrow \frac{1}{2}$	$3 \rightarrow 2$
Ideal Gas	$\frac{3}{2}$	0	$\frac{3}{2}$
Rigid Liquid	$\frac{3}{2}$	$\frac{3}{2} \rightarrow \frac{1}{2}$	$3 \rightarrow 2$
Non-Rigid Gas-like Fluid	$\frac{3}{2}$	$\frac{1}{2} \rightarrow 0$	$2 \rightarrow \frac{3}{2}$

Table 6.2: Thermodynamic properties of solids, liquids and gases, followed by two states in the supercritical region: Rigid Liquid and Non-Rigid Gas-like Fluid.

In addition to the relationship between structural and dynamic crossovers discussed above, there is also an important link between structural and thermodynamic crossovers of the supercritical system. In Figure 6.5, we show the calculated constant-volume specific heat, $c_v = \frac{1}{N}\frac{dE}{dT}$, of the simulated system as a function of temperature using the same interatomic LJ potential. We observe a crossover of c_v around 3000 K, an effect that is also clearly seen in Figure 6.5.b where the temperature derivative of c_v is shown. Importantly, the crossover of c_v takes place at the same temperature as the crossover of RDF peaks in Figure 6.3. This provides the quantitative evidence for the close relationship between the *structural and thermodynamic* properties and their crossover in the supercritical system, the relationship we explore below.

6.3 Discussion

We first note that the crossover of c_v in Figure 6.5, $c_v \approx 2k_{\mathrm{B}}$, is non-coincidental. We have recently provided the quantitative theory of liquid c_v [24–27]. This was discussed

in Chapters I-IV in detail. In this theory, the reduction of heat capacity from $3k_{\mathrm{B}}$ to $2k_{\mathrm{B}}$ is due to the progressive loss of two shear modes with frequency $\omega > \frac{1}{\tau}$. When all shear modes are lost at the Frenkel line as discussed above, only the remaining longitudinal mode with the potential energy of $\frac{1}{2}Nk_{\mathrm{B}}T$ contributes to the total system energy. Together with $\frac{3}{2}Nk_{\mathrm{B}}T$ given by kinetic energy, the total energy is $2Nk_{\mathrm{B}}T$, giving $c_v = 2k_{\mathrm{B}}$ [24–27]. On further temperature increase when c_v decreases from $c_v = 2k_{\mathrm{B}}$ to its ideal-gas value of $c_v = 2k_{\mathrm{B}}$, another mechanism kicks in: the disappearance of the remaining longitudinal mode with the wavelength smaller than the mean-free path of particles [27]. The two mechanisms naturally give a crossover of c_v at $c_v = 2k_{\mathrm{B}}$.

In addition to the evidence from MD simulations, the relationship between the crossover of structure and thermodynamics in the supercritical states can also be discussed on the basis of the general relationship between the system energy, E, and $g(r)$:

$$E = \frac{3}{2}Nk_{\mathrm{B}}T + 2\pi N\rho \int_0^\infty r^2 u(r)g(r)dr \tag{6.3.1}$$

where N is the number of particles, ρ is the density and $u(r)$ is the interatomic potential.

According to Eq. (6.3.1), the crossover of $g(r)$ necessarily implies the crossover of energy and c_v and vice versa, consistent with our observation that the crossovers of RDFs seen in Figure 6.3 is accompanied by the crossover of c_v in Figure 6.5. Physically, these crossovers are related as follows. In the rigid-liquid supercritical regime when $\tau \gg \tau_{\mathrm{D}}$, the initial steep decrease of c_v from $3k_{\mathrm{B}}$ to $2k_{\mathrm{B}}$ is due to the fast loss of two shear modes as discussed above. This decrease is fast because τ exponentially decreases with temperature, giving fast decrease of c_v seen in Figure 6.5. At the same time, $\tau \gg \tau_{\mathrm{D}}$ implies that solid-like structures persist during time τ and hence give rise to the correlations in the medium range as seen in Figure 6.2, correlations that decrease steeply in Figure 6.3. In the non-rigid gas-like supercritical regime, c_v decreases slowly due to the slow disappearance of the remaining longitudinal mode in the gas-like state [27], which via Eq. (6.3.1) implies slowly decaying behavior of $g(r)$, consistent with Figure 6.3. The two effects explain why both c_v and $g(r)$ undergo a crossover simultaneously, as Eq. (6.3.1) demands.

We note that the relationship between structure and dynamics have always fascinated scientists in condensed matter physics, with the recognition that such a relationship may exist in some classes of systems but not in others [18, 28]. Here, we find that not only the supercritical state is not homogeneous as previously viewed, it is also universally amenable to supporting fundamental interlinks between all three fundamental system properties: structure, dynamics and thermodynamics. This is summarized in Tables 6.1-6.2.

In summary, we presented the evidence for the existence of the structural crossover in the supercritical state of matter, and discussed the relationship between the structure, dynamics and thermodynamics of the supercritical state. The existence of this crossover has not been hitherto anticipated, in view of the common belief that the supercritical state is structurally homogeneous. Our results therefore call for the experiments (neutron, X-ray scattering experiments) to detect the crossover.

Bibliography

[1] J. L. Barrat, and J. P. Hansen, Basic concepts for simple and complex liquids (Cambridge University Press, 2003).

[2] E. Kiran, P. G. Debenedetti, and C. J. Peters, Supercritical Fluids: Fundamentals and Applications, NATO Science Series E: Applied Sciences 366 (Kluwer Academic Publishers, 2000).

[3] J. McHardy, and S. P. Sawan, Supercritical Fluid Cleaning: Fundamentals, Technology and Applications (Noyes Publications, 1998).

[4] S. J. L. Billinge, I. Levin, Science **316**, 561 (2007).

[5] J. C. Dyre, Rev. Mod. Phys. **78**, 953 (2006).

[6] A. Widmer-Cooper, H. Perry, P. Harrowell and D. R. Reichman, Nat. Phys. **4**, 711 (2008).

[7] G. Biroli, J.-P. Bouchaud, A. Cavagna, T. S. Grigera and P. Verrocchio, Nat. Phys. **4**, 771 (2008).

[8] J. R. Errington and P. G. Debenedetti, Nature **409**, 318 (2001).

[9] P. Wernet, D. Nordlund, U. Bergmann, M. Cavalleri, M. Odelius, H. Ogasawara, L. Å. Näslund, T. K. Hirsch, L. Ojamäe, P. Glatzel, L. G. M. Pettersson, A. Nilsson, Science **304**, 995 (2004).

[10] P. S. Salmon, R. A. Martin, P. E. Mason and G. J. Cuello, Nature **435**, 75 (2005).

[11] D. Chandler, Nature **437**, 640 (2005).

[12] H. W. Sheng, W. K. Luo, F. M. Alamgir, J. M. Bai and E. Ma, Nature **439**, 419 (2006).

[13] C. Huang, et.al., Phys. Chem. Chem. Phys. **13**, 19997 (2011).

[14] E. B. Moore and M. Molinero, Nature **479**, 506 (2011).

[15] S. Wei, F. Yang, J. Bednarcik, I. Kaban, O. Shuleshova, Nat. Commun. **4**, 2083 (2013).

[16] J. VandeVondele, F. Mohamed, M. Krack, J. Hutter, M. Sprik, and M. Parrinello, J. Chem. Phys. **122**, 014515 (2005).

[17] I. T. Todorov , B. Smith, M. T. Dove and K. Trachenko, DL-POLY-3: new dimensions in molecular dynamics simulations via massive parallelism. J. Mater. Chem. **16**, 1911 (2006).

[18] M. T. Dove, Structure and Dynamics: An Atomic View of Materials (Oxford Master Series in Condensed Matter Physics, 2003).

[19] V. V. Brazhkin and K. Trachenko, Physics Today **65**(11), 68 (2012).

[20] V. V. Brazhkin, Yu. D. Fomin, A. G. Lyapin, V. N. Ryzhov and K. Trachenko, Phys. Rev. E **85**, 031203 (2012).

[21] J. Frenkel, Kinetic Theory of Liquids (ed. R. H. Fowler, P. Kapitza, N. F. Mott, Oxford University Press, 1947).

[22] F. Sette, M. H. Krisch, C. Masciovecchio, G. Ruocco, G. Monaco, Science **280**, 1550 (1998).

[23] S. Hosokawa, M. Inui, Y. Kajihara, et al., Phys. Rev. Lett. **102**, 105502 (2009).

[24] K. Trachenko, Phys. Rev. B **78**, 104201 (2008).

[25] D. Bolmatov and K. Trachenko, Phys. Rev. B **84**, 054106 (2011).

[26] D. Bolmatov, V. V. Brazhkin and K. Trachenko, Sci. Rep. **2**, 421 (2012).

[27] D. Bolmatov, V. V. Brazhkin and K. Trachenko, Nat. Commun. **4**, 2331 (2013).

[28] A. Kitaigorodsky, Molecular crystals and Molecules (Elsevier, 1973).

CHAPTER 7

SYMMETRY BREAKING GIVES RISE TO ENERGY SPECTRA OF THREE STATES OF MATTER

7.1 Quantum Field Theory

Quantum field theory is the most complete microscopic theory we have today describing the physics of energy and matter. It has been successfully applied to explain phenomena ranging over many orders of magnitude, from the study of elementary particles on the sub-nucleonic scale to the study of neutron stars and other astrophysical objects on the cosmological scale. At the same time, statistical mechanics is a formalism which aims at explaining the physical properties of matter in bulk on the basis of the dynamical behavior of its microscopic constituents. The scope of the formalism is almost as unlimited as the very range of the natural phenomena, for in principle it is applicable to matter in any state whatsoever. It has, in fact, been applied, with considerable success, to the study of matter in the solid state, the liquid state or the gaseous state, matter composed of several phases and/or several components, matter under extreme conditions of density and temperature, matter in equilibrium with radiation as in astrophysics.

The main general premise of statistical physics is that observable properties of a macroscopic system can be calculated and explained on the basis of a microscopic Hamiltonian with many degrees of freedom. This has been implemented as a successful program that, notably, has been applied to each of the three states of matter (solids, gases, liquids) *individually* [1]. For example, the model Hamiltonian of a solid enforces oscillations around fixed equilibrium positions [2, 3], resulting in the marked restriction on the sampled volume of phase space. On the other hand, a gas state is approached by starting with free particles, switching interactions on and predominantly viewing these as small perturbations. The third state of matter, liquids, occupy an interesting intermediate state with a combination of strong interactions and cohesive state as in solids and large flow-enabling particle displacements as in gases. This combination is believed to preclude the calculation of thermodynamic properties of liquids in general form [1].

The general problem represented by liquids is well-known [1, 4], yet here we begin with asking an even more fundamental question. The question bears on some deep issues that were recognized long ago [5] yet remain unsolved, those of operating in restricted phase space rather full phase space. As in the example above, most model Hamiltonians of solids impose restrictions on the phase space where atoms never leave their equilibrium sites. Even with anharmonicity of interactions properly introduced, modern statistical physics can not predict whether and under what conditions a given Hamiltonian corresponds to a solid, a liquid or a gas. This is often illustrated as a story of some best physicists who are gathered on an island, given a Hamiltonian and failed to analytically find which state of matter it corresponds to, despite being surrounded by water [6].

Here, we ask whether a Hamiltonian can be proposed that demonstrably describes energy spectra corresponding to solid, liquid and gas phases. To address this challenge we operate in terms of the phonon Hamiltonian. Ground state configuration breaks the symmetry and the Hamiltonian readily describes energy spectra corresponding to solids, liquids and gases (both interacting and ideal). In this picture, the energy gaps of shear excitations naturally emerge as a consequence of the Goldstone theorem. The group of rotations in reciprocal space $SO(3)$ is spontaneously broken to its subgroup $SO(2)$. Consequently, different choices of couplings of fields correspond to energy spectra of distinct states of matter and it is reassuring that our proposed general approach captures the experimental findings. Phase transitions are common occurrences observed in nature [7, 8] and the description of phase transitions in the framework of the proposed formalism (solid/liquid, liquid/gas and solid/gas) is another remaining challenging task, we discuss it below.

7.2 Symmetry Breaking in Phonon Interactions

We start with the Hamiltonian describing the dynamics of the phonon field in harmonic approximation [9]

$$H_0 = \frac{1}{2} \sum_{\omega_k < \omega_{\mathrm{D}}} \left[\Pi_k^\alpha \Pi_{-k}^\alpha + \mu\, \omega_k^2 Q_k^\alpha Q_{-k}^\alpha \right]. \tag{7.2.1}$$

Here the small Greek indices run from 1 to 3 labelling three space directions and k is a multiindex $\{k_1, k_2, k_3\}$ that denotes the wave vector of the corresponding harmonics and ω_{D} is the Debye frequency. The parameter μ that takes values 1 or 0 was introduced for further convenience. Summation over the repeated space indices is always implied and the metric has the signature $\{+, +, +\}$. The collective canonical coordinates Π_k^α

and Q_k^α are introduced as

$$\begin{aligned} Q_k^\alpha &= \sqrt{m}\sum_{j=1}^{N} e^{\mathtt{i}Lj\cdot k} x_j^\alpha, \\ \Pi_k^\alpha &= \dot{Q}_k^\alpha, \end{aligned} \tag{7.2.2}$$

where x_j^α are 3 coordinates of the j-th atom of the lattice, L is the lattice spacing , N is the total number of atoms, $\mathtt{i}$ is the imaginary unit ($\mathtt{i}^2 = -1$) and m is the mass of an atom in the lattice. The coefficient ω_k^2 gives dispersion relation of a phonon. Normal modes satisfy $Q_k^\alpha = {Q_{-k}^\alpha}^*$ since coordinates of atoms x_j^α are real, where star denotes the complex conjugation.

The Hamiltonian (7.2.1) that is quadratic in fields defines a free theory with no interactions between phonons. To introduce an interaction one adds a term H_{int} that is of higher order in fields which leads to spontaneous symmetry breaking [10]

$$\begin{aligned} H_{int} &= \sum_{\omega_k<\omega_\mathrm{D}} \left[-\frac{g}{2}\left(Q_k^\alpha Q_{-k}^\alpha\right)^2 + \frac{\lambda}{6}\left(Q_k^\alpha Q_{-k}^\alpha\right)^3 \right] \\ &= \sum_{\omega_k<\omega_\mathrm{D}} \left[-\frac{g}{2}|Q_k^\alpha|^4 + \frac{\lambda}{6}|Q_k^\alpha|^6 \right], \end{aligned} \tag{7.2.3}$$

where $g, \lambda \in \mathbb{R}^+$ are some real non-negative coupling constants (see discussions in conclusions) and $|Q_k^\alpha| = (Q_k^\alpha Q_{-k}^\alpha)^{1/2}$. The total Hamiltonian $H = H_0 + H_{int}$ is invariant under the following transformations

$$\begin{aligned} Q_k^\alpha &\to R^\alpha{}_\beta Q_k^\beta, \\ \Pi_k^\alpha &\to R^\alpha{}_\beta \Pi_k^\beta, \end{aligned} \tag{7.2.4}$$

for any $||R^\alpha{}_\beta|| \in SO(3)$.

The configurations $\bar{Q}_k^\alpha$ and $\bar{\Pi}_k^\alpha$ that minimise energy of the system, break the $SO(3)$ symmetry to $SO(2)$ for a certain range of frequency ω_k. The kinetic energy is minimal at configurations $\bar{\Pi}_k^\alpha = 0$ and the minimum of the potential term can be found in the usual way

$$\frac{\delta V[Q_k^\alpha]}{\delta Q_l^\beta} = 0, \tag{7.2.5}$$

where the potential $V[Q_k^\alpha]$ is defined as

$$V[Q_k^\alpha] = \sum_{\omega_k<\omega_\mathrm{D}} \left[\frac{\mu}{2}\omega_k^2 |Q_k^\alpha|^2 - \frac{g}{2}|Q_k^\alpha|^4 + \frac{\lambda}{6}|Q_k^\alpha|^6 \right]. \tag{7.2.6}$$

The equation (7.2.5) is of the fifth order in $|Q_k^\alpha|$ and therefore has five solutions. We

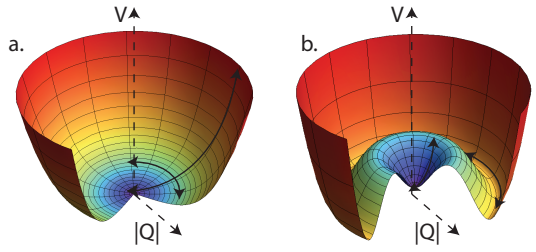

Figure 7.1: When $\omega_k > \omega_{\rm F}$, the global minimum is given by $|Q_k^\alpha| = 0$ (a). For $\omega_k < \omega_{\rm F}$, the global minimum of the potential is provided by the family of solutions $|Q_k^\alpha|_+$ that breaks the symmetry $SO(3) \to SO(2)$ (b).

choose only non-negative roots

$$\begin{aligned} |Q_k^\alpha|_\pm &= \left(\frac{g}{\lambda} \pm \sqrt{\frac{\omega_{\rm F}^2 - \omega_k^2}{\lambda}} \right)^{1/2}, \\ |Q_k^\alpha|_0 &= 0, \\ \omega_{\rm F}^2 &\equiv \frac{g^2}{\lambda}. \end{aligned} \tag{7.2.7}$$

The factor μ was omitted here since it takes value 1 for non-trivial cases (see next section). The solution (7.2.7) behave quite differently when $\omega_k > \omega_{\rm F}$ and $\omega_k < \omega_{\rm F}$. Namely, for the frequencies $\omega_k > \omega_{\rm F}$ all three roots coincide and the potential has only one minimum $|Q_k^\alpha| = 0$ that is invariant under the $SO(3)$ transformations. However, for $\omega_k < \omega_{\rm F}$ the global minimum of the potential is provided by the family of solutions $|Q_k^\alpha|_+$ that is not invariant under $SO(3)$ and spontaneously breaks the symmetry to $SO(2)$.

When $\omega_k < \omega_{\rm F}$ the solution $|Q_k^\alpha|_0 = 0$ represents the local metastable minimum. Indeed, two roots $|Q_k^\alpha|_\pm$ correspond to two extrema of the potential, one of which (with the minus sign) is a local maximum (see Fig.7.1). This means that the pseudo-vacuum state $|Q_k^\alpha| = 0$ is stable on the classical level, but becomes metastable if quantum effects are taken into account. This leads to quantum tunneling of the state $|Q_k^\alpha| = 0$ to the true vacuum state given by $|\bar{Q}_k^\alpha| \equiv |Q_k^\alpha|_+$ and symmetry breaking.

According to the Goldstone theorem this leads to two massless modes $\varphi_k^{2,3}$, one for each broken symmetry generator, and one massive mode φ_k^1 [11, 12]. Excitations of the phonon field around the ground state $\bar{Q}_k^\alpha$ can be written as

$$Q_k^\alpha = \bar{Q}_k^\alpha + \varphi_k^\alpha. \tag{7.2.8}$$

For a particularly chosen vacuum $\bar{Q}_k^\alpha = \delta_1^\alpha |\bar{Q}_k|$ we obtain the following Hamiltonian:

$$\begin{aligned} H[\varphi_k^\alpha] = \frac{1}{2} \sum_{\omega_k<\omega_{\rm D}} \pi_k^\alpha \pi_{-k}^\alpha + \sum_{\omega_k<\omega_{\rm D}} \left[\frac{\Omega_k^2}{2} \varphi_k^1 \varphi_{-k}^1 \right] + \\ + \sum_{\omega_{\rm F}<\omega_k<\omega_{\rm D}} \left[\frac{\mu\omega_k^2}{2} (\varphi_k^2 \varphi_{-k}^2 + \varphi_k^3 \varphi_{-k}^3) \right] + \\ + V_{int}[\varphi_k^\alpha] + V_0. \end{aligned} \tag{7.2.9}$$

Here φ_k^α are small excitations around the vacuum state and $\pi_k^\alpha = \dot{\varphi}_k^\alpha$ are corresponding canonical momenta. The term V_{int} denotes all higher order interactions and includes all three modes φ_k^α while the last term is an irrelevant shift of the total energy of the system

$$V_0 = \sum_{\omega_k<\omega_{\rm F}} \left(\frac{\mu\omega_k^2}{2} |\bar{Q}_k|^2 - \frac{g}{2} |\bar{Q}_k|^4 + \frac{\lambda}{6} |\bar{Q}_k|^6 \right). \tag{7.2.10}$$

Here the cutoff $\omega_k < \omega_{\rm F}$ reflects the fact that for $\omega_k > \omega_{\rm F}$ we have $|\bar{Q}_k| = 0$ and the corresponding potential becomes zero.

One should note that the frequency Ω_k^2 of the longitudinal mode φ_k^1 defined as

$$\Omega_k^2 = \begin{cases} 4\left(\omega_{\rm F}^2 - \omega_k^2\right) + 4\omega_{\rm F}\sqrt{\omega_{\rm F}^2 - \omega_k^2} > 0, & \omega_k < \omega_{\rm F}, \\ \omega_k^2, & \omega_k > \omega_{\rm F}, \end{cases} \tag{7.2.11}$$

is non-continuous at the point $\omega_k = \omega_{\rm F}$ and μ is again set to 1. Since the symmetry is broken and the system is in the true ground state $|Q_k^\alpha| \neq 0$ the plus sign in (7.2.7) should be chosen.

At the same time, the Goldstone theorem asserts that the transverse modes φ_k^2 and φ_k^3 do not contribute to the energy of the system at the quadratic level for $\omega_k \leq \omega_{\rm F}$. The term V_{int} that encodes interactions between all three modes involves all frequencies $\omega_k \in (0, \omega_D)$. The detailed analysis of the physical consequences of these facts is given in the next section.

Finally, it is worth mentioning that the direction of $\bar{Q}_k^\alpha$ is chosen spontaneously and the form of the resulting Hamiltonian does not depend on this choice.

7.3 Regimes of the Theory

Identifying the field φ_k^1 with longitudinal normal mode and the fields $\varphi_k^{2,3}$ with transverse shear modes one can write energy of the theory defined by the Hamiltonian

(7.2.9) as

$$E = K + P_l + P_s(\omega_k > \omega_{\rm F}) + E_{int} \tag{7.3.1}$$

where K is the total kinetic energy and P_l and P_s are the potential energies of longitudinal and shear modes, respectively, and E_{int} corresponds to higher-order terms such as an anharmonicity. The Eq. (7.3.1) implies that contributions of transverse modes with frequencies $\omega < \omega_F$ to linearised energy vanish. This means, that we do not have free propagating transverse modes with such frequencies.

According to Eq. (7.3.1), the system supports one longitudinal mode and two shear modes with frequency larger than ω_F. Our theory therefore predicts a non-trivial and a non-anticipated effect of the frequency cutoff of shear modes. Remarkably, such a cutoff was earlier discussed on purely dynamic grounds by Frenkel as discussed in Chapters I-IV. Here, we note that our symmetry breaking approach essentially captures this earlier dynamic idea [5].

The most intriguing feature of the proposed formalism is albeit the energy (7.3.1) can be interpreted as the energy of a liquid, in fact it describes all three phases of matter depending on the parameters g, λ and μ. This is summarized in Table 7.1.

Phase	Coupling constants	Normal modes
Ideal Gas	$\mu = 0, \quad g \to 0,$ $\lambda \to 0, \quad \frac{g^2}{\lambda} \to 0.$	$\lvert\bar{Q}\rvert = 0$ no modes
Interacting Gas	$\mu = 1, \quad g \neq 0,$ $\lambda \neq 0, \quad \frac{g^2}{\lambda} = \omega_{\rm D}.$	$\lvert\bar{Q}\rvert \neq 0,$ φ_k^1
Liquid	$\mu = 1, \quad g \neq 0,$ $\lambda \neq 0, \quad \frac{g^2}{\lambda} \neq 0.$	$\lvert\bar{Q}\rvert \neq 0,$ $\varphi_k^{1,2,3}\left(\omega_k^{s,s} > \frac{1}{\tau}\right)$
Solid	$\mu = 1, \quad g \ll \lambda,$ $\lambda \neq 0, \quad \frac{g^2}{\lambda} \to 0.$	$\lvert\bar{Q}\rvert \neq 0,$ $\varphi_k^{1,2,3}$

Table 7.1: States of Matter. **Ideal Gas**: no elementary excitations; **Interacting Gas**: only longitudinal excitations $0 \leq \omega_k^l \leq \omega_{\rm D}$; **Liquid**: both longitudinal ($0 \leq \omega_k^l \leq \omega_{\rm D}$) and shear ($\omega_{\rm F} \leq \omega_k^{s,s} \leq \omega_{\rm D}$) modes; and **Solid**: all modes are supported ($0 \leq \omega_k^{l,s,s} \leq \omega_{\rm D}$).

As follows from the Table 7.1, the parameter μ is used to distinguish the phase of

the ideal gas when the potential energy is zero. In contrast, the couplings g and λ are model dependent and can be, for example, derived from the experiment (see discussion in the next section). As summarized in the Table 7.1, our theory readily gives rise to the different states of matter as follows:

Ideal gas. The quartic coupling g and the sextic coupling λ are set to be zero as well as the parameter μ. This leaves only the kinetic term in the Hamiltonian. Both longitudinal and transverse modes are non-interacting and massless which corresponds to the ideal gas.

Interacting gas. The Frenkel frequency $\omega_{\rm F}$ becomes equal to the Debye frequency $\omega_{\rm D}$ which eliminates all transverse shear modes. However, in contrast to the case of the ideal gas the longitudinal mode φ^1_k is massive and has non-zero couplings.

Liquid. Transverse shear modes $\varphi^{2,3}_k$ with frequencies $\omega_k < \omega_{\rm F}$ do not contribute to the Hamiltonian at quadratic level while the longitudinal mode φ^1_k does not feel the bound $\omega_k = \omega_{\rm F}$ since its couplings are continuous.

Notably, our Eq. (7.3.1) essentially captures the earlier idea of J. Frenkel that as far as propagating modes are concerned, the only difference between a solid and a liquid is that the liquid does not support shear waves at all frequencies as the solid does, but only those with frequency $\omega_k > \omega_F = \frac{2\pi}{\tau}$ [5]. Here, τ is liquid relaxation time, the average time between two consecutive atomic jumps in one point in space. With a remarkable physical insight, the argument about the liquid vibrational states was developed as follows. At times shorter than τ, a liquid is a solid, and therefore supports one longitudinal mode and two transverse modes, whereas at times longer than τ, liquid flows and loses its ability to support shear stress, and therefore supports the longitudinal mode only as any elastic medium (in a dense liquid, the wavelength of this mode extends to the shortest wavelength comparable to interatomic separations). Derived on purely theoretical grounds, this idea was later experimentally confirmed, although with a significant time lag (for review, see, e.g. Ref. [13]).

We therefore find that the ability of liquids to support high-frequency shear modes with $\omega_{\rm F}$ as a lower frequency cutoff originates in our general approach based on symmetry breaking. This is an unexpected and a highly non-trivial result. For viscous liquids such as B_2O_3, the experimental evidence was available some time ago [16]. For low-viscous liquids such as Na and Ga, the experimental evidence came about fairly recently when powerful synchrotron radiation sources started to be deployed that mapped dispersion curves in these systems [17, 18]. The proposed approach captures the experimental findings [13, 19–21].

We therefore find that the ability of liquids to support high-frequency shear modes with $\omega_{\rm F}$ as a lower frequency cutoff originates in our general approach based on sym-

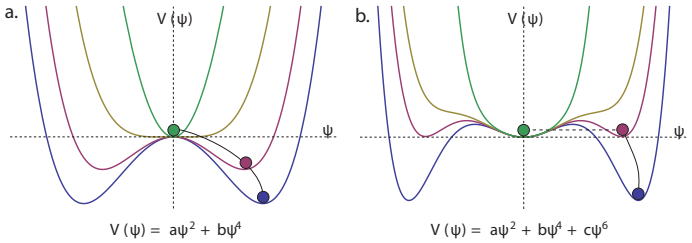

Figure 7.2: Schematic illustration of ground state behaviour for different potentials. Flow of coefficients changes the form of the corresponding potentials and leads to descriptions of different types of phase transitions. The global minimum of the potential on Figure 7.2.a can be continuously translated to local metastable state and in general describes continuous second-order phase transitions. The translation of the global minimum of the potential on Figure 7.2.b to local metastable state is discontinuous and in general describes discontinuous first-order phase transitions.

metry breaking. This is an unexpected and a highly non-trivial result. It is reassuring and gratifying that our proposed general approach captures the experimental findings [13].

Taking the inverse Fourier transform of both sides of (7.2.8), we find

$$x^\alpha(t) = \bar{x}^\alpha + \xi^\alpha(t) \tag{7.3.2}$$

If we associate $\xi^\alpha(t)$ with oscillations around equilibrium positions and $\bar{x}^\alpha$ with translations, the symmetry breaking $SO(3) \to SO(2)$ acquires a microscopic meaning in real space. Namely, no symmetry breaking takes place in solids where atoms do not jump, giving $\bar{x}^\alpha = 0$. In liquids and gases, on the other hand, symmetry breaking is due to particle jumps, i.e. spontaneous translations with amplitudes $\bar{x}^\alpha$.

Glass has been widely viewed as not a separate state of matter but as a slowly flowing liquid, with relaxation time tau exceeding observation time. When τ exceeds experimental time scale, the liquid forms glass [22]. Therefore, the glass state in our classification scheme originates when τ reaches a certain large value.

Solid. All normal modes are supported and $\omega_{\rm F}$ is equal to zero, reflecting the fact that solids are not able to flow. There is no the described symmetry breaking in phonon interactions [3].

The Hamiltonian (7.2.9) describes solid, liquid and gas states depending on the choice of coupling constants g and λ, that in general may depend on wavenumber k. The transverse shear modes $\varphi_k^{2,3}$ for $\omega_k < \omega_{\rm F}$ do not contribute to the Hamiltonian on the quadratic level in the liquid regime. In the coordinate space it may correspond to atomic jumps with characteristic time $\tau \sim 1/\omega_{\rm F}$.

We now discuss two interesting directions for future work. Identification of the physical meaning of the couplings g and λ from the experiment is an important task. In general these constants may depend on the wavenumber k and have to predict known experimental observables such as, for example, melting and boiling temperature.

The form of the potential in particular can be justified by the following observation. The potential on Figure 7.2.a in general describes continuous phase transitions. In contrast, the potential on Figure 7.2.b [15], that was used in the suggested formalism, can be associated with discontinuous phase transitions such as melting (or freezing) . Hence, an intriguing question is a dynamic description of the switch from the liquid to the solid phase regime by investigating the RG flow of the couplings g and λ [14]. The description of phase transitions (solid/liquid, liquid/gas and solid/gas) are another remaining challenging tasks. These ideas need more rigorous explanation and connection to the experiment.

Bibliography

[1] L. D. Landau and E. M. Lifshitz, Statistical physics,(Nauka, Moscow, 1964).

[2] A. Einstein, Die Plancksche Theorie der Strahlung und die Theorie der spezifischen Warme [Planck's theory of radiation and the theory of specific heat]. Ann. Phys. (Berlin) **22**, 180 (1907).

[3] P. Debye, Zur Theorie der spezifischen Waerme [On the theory of specific heat,]. Ann. Phys. (Berlin) **39**(4), 789 (1912).

[4] M. Born and H. S. Green, Nature **159**, 251 (1947).

[5] J. Frenkel, Kinetic Theory of Liquids, eds R. H. Fowler, P. Kapitza, N. F. Mott, (Oxford University Press,1947).

[6] N. W. Ashcroft, (private communication).

[7] V. Nicosia, P. E. Vertes, W. R. Schafer, V. Latora, E. T. Bullmore, Proc. Natl. Acad. Sci. **110**, 7880 (2013).

[8] D. L. Donoho, M. Gavish, A. Montanari, Proc. Natl. Acad. Sci. **110**, 8405 (2013).

[9] C. Kittel, Quantum Theory of Solids, (Wiley, New York, 1963).

[10] V. Rubakov and S. S. Wilson, Classical Theory of Gauge Fields, (Princeton University Press,2009).

[11] J. Goldstone, Nuovo Cimento **19**, 154 (1961).

[12] F. Strocchi, Phys. Lett. A **267**, 40 (2000).

[13] D. Bolmatov, V. V. Brazhkin and K. Trachenko, Sci. Rep. **2**, 421 (2012).

[14] K. Wilson, J. B. Kogut, Phys.Rept. **12**, 75 (1974).

[15] J. J. Binnet, N. J. Dowrick, A. J. Fisher and M. E. J. Newman, The theory of critical phenomena, (Clarendon Press, Oxford, 1992).

[16] M. Grimsditch, R. Bhadra and L. M. Torell, Phys. Rev. Lett. **62**, 2616 (1989).

[17] V. M. Giordano and G. Monaco, Proc. Natl. Acad. Sci. **107**, 21985 (2010).

[18] V. M. Giordano and G. Monaco, Phys. Rev. B **84**, 052201 (2011).

[19] D. Bolmatov, V. V. Brazhkin and K. Trachenko, Nat. Commun. **4**, 2331 (2013).

[20] D. Bolmatov and K. Trachenko, Phys. Rev. B **84**, 054106 (2011).

[21] D. Bolmatov, V. V. Brazhkin and K. Trachenko, J. Appl. Phys. **113**, 103514 (2013).

[22] J. C. Dyre, Rev. Mod. Phys. **78**, 953 (2006).

CHAPTER 8

CONCLUSION

To conclude, we briefly review the results presented in this thesis and note possible directions of further research.

In Chapter II, which follows the Introduction in Chapter I, we start from introducing the classical harmonic approach to liquids from solid phase. This approach was developed by accounting for the contribution of anharmonicity and thermal expansion, and by relating liquid energy and heat capacity to relaxation time τ. We subsequently compared theoretical calculations to the experiments results of 5 commonly discussed liquids, and found a good agreement.

In Chapter III, we derived an expression for the energy of a liquid in terms of its temperature and three parameters – the liquid's coefficient of expansion, and its Debye and Frenkel frequencies. The Debye frequency is the theoretical maximum frequency that atoms or molecules in the liquid can oscillate at and can be derived from the speed of sound in the liquid. The Frenkel frequency puts a lower bound on the oscillation frequency of the atoms or molecules and can be derived from the viscosity and shear modulus of the liquid. The phonon theory of liquids covers both the classical and quantum regimes and agrees with experiment over a wide range of temperatures and pressures. In the framework of the theory we successfully fitted the heat capacity of 21 different liquids ranging from metals to noble and molecular liquids. In all 21 liquids studied, the theory was able to reproduce the observed drop in heat capacity as temperature increases. We explained this drop in terms of an increase in the Frenkel frequency as a function of temperature. As the liquid gets hotter, there are fewer shear phonon modes available to transport heat and therefore the heat capacity drops.

In Chapter IV, we presented the heat capacity of bosonic liquid helium as determined within in the framework of a phonon theory of liquids. The physical picture of elementary excitations is clarified by means of a study of phonon contributions, both longitudinal-like and transverse-like, to the energy spectrum of liquid helium at elevated pressures. Liquid helium in its normal state and at atmospheric pressure supports transverse-like elementary excitations. At significant pressures (around 10 GPa) liquid helium strongly resembles the other noble-gas liquids; there are transverse-like excitations but at its melting temperature almost all phonons are already excited. This

state of liquid helium is rigid but not quantum. In the thesis, we suggested an interesting intermediate pressure range of 5 MPa-500 MPa where liquid helium near melting temperature is already solid-like but is still significantly quantum.

In Chapter V, we studied thermodynamic properties of the supercritical state. We discovered that specific heat shows a crossover between two different regimes, an unexpected result in view of currently perceived homogeneity of supercritical state in terms of physical properties. We subsequently formulated a theory of system thermodynamics above the crossover, and found good agreement between fitted and experimental specific heat. In this theory, energy and heat capacity are governed by the minimal length of the longitudinal mode in the system only, and do not explicitly depend on system-specific structure and interactions. We derived a power law in the supercritical region above the Frenkel line.

In the Chapter VI, we demonstrated that the supercritical state is not structurally homogeneous as is currently believed, but that there is a well-defined structural crossover instead. Using Molecular Dynamics simulations, we simulated one-component Lennard-Jones fluid fitted to Ar properties. We calculated radial distribution function, and showed its temperature evolution. We observed the decrease of the first peak of the RDF, and the near disappearance of the second and third peaks of RDFs, implying that the medium-range structure is no longer visible at high temperature. Evidenced by the qualitative changes of distribution functions of interatomic distances and angles, the crossover demarcates liquid-like and gas-like configurations and the presence of medium-range structural correlations. Importantly, the discovered structural crossover is closely related to both dynamic and thermodynamic crossovers operating in the supercritical state, providing new unexpected fundamental interlinks between the supercritical structure, dynamics and thermodynamics.

In Chapter VII, we proposed a new idea that enables a unified description of all three states of matter. We introduced a generic form of an interacting phonon Hamiltonian with ground state configurations minimising the potential. Symmetry breaking SO(3) to SO(2), from the group of rotations in reciprocal space to its subgroup, leads to emergence of energy gaps of shear excitations as a consequence of the Goldstone theorem, and readily results in the emergence of energy spectra corresponding to solid, liquid and gas phases. Nevertheless, these ideas need more rigorous explanation and connection to the experiment.